

**THEORETICAL INVESTIGATION OF THE EFFECT OF
NITROGEN ON OPTICAL AND ELECTRONIC
PROPERTIES OF GAINASN SEMICONDUCTORS**

Ph.D. Thesis
in
Engineering of Physics
University of Gaziantep

Supervisor
Prof. Dr. Beşire GÖNÜL

By
Koray KÖKSAL
September 2009

T.C.
GAZİANTEP UNIVERSITY
GRADUATE SCHOOL OF
NATURAL AND APPLIED SCIENCES
ENGINEERING OF PHYSICS

Name of the Thesis : Theoretical investigation of the effect of nitrogen on optical and electronic properties of GaInAsN semi-conductors
Name of the Student : Koray KÖKSAL
Exam Date : 25.9.2009

Approval of the Graduate School of Natural and Applied Sciences.

Prof. Dr. Ramazan KOÇ
Director

I certify that this thesis satisfies all the requirements as a thesis for the degree of Doctor of Philosophy.

Prof. Dr. Ramazan KOÇ
Head of Department

This is to certify that we have read this thesis and that in our opinion it is fully adequate, in scope and quality, as a thesis for the degree of Doctor of Philosophy.

Prof. Dr. Beşire GÖNÜL
Co-Supervisor

Prof. Dr. Beşire GÖNÜL
Major Supervisor

Examining Committee Members:

Prof. Dr. Rauf SÜLEYMANOV	_____
Prof. Dr. Beşire GÖNÜL	_____
Assoc. Prof. Dr. Mustafa ÖZTAŞ	_____
Assoc. Prof. Dr. Mehmet ŞAHİN	_____
Assoc. Prof. Dr. Hayriye TÛTÛNCÜLER	_____

ABSTRACT

THEORETICAL INVESTIGATION OF THE EFFECT OF NITROGEN ON OPTICAL AND ELECTRONIC PROPERTIES OF GAINASN SEMICONDUCTORS

KÖKSAL, Koray

Ph.D. in Engineering of Physics

Supervisor: Prof. Dr. Beşire GÖNÜL

Co-Supervisor: Prof. Dr. Beşire GÖNÜL

September 2009, 95 pages

Nitrogen incorporated III-V semiconductor alloys which have striking fundamental properties, play very important role in technology. Recently, because of their different band structure compared with other III-V's, III-N-V semiconductors have been produced by modern thin film techniques and there is an increased number of scientific studies about this subject. One of the most important and interesting characteristics of III-N-V's is the splitting of conduction band and the rapid reduction of the band gap due to nitrogen impurities. While usual impurities causes insignificant perturbation in band structure of III-V semiconductors, little fraction of nitrogen impurities results in significant changes in band structure because of the big difference in electronegativity, atomic size and ionization energy between N and V group elements. This anomalous characteristics of III-N-V compound semiconductors provides opportunity to produce different devices.

The aim of this thesis is to investigate profounds of nitrogen containing III-V semiconductors in fundamental properties proven experimentally and device applications and to propose new device materials. In this thesis, we have presented an overview of the fundamental properties of nitrogen incorporated GaInAs semiconductor and the physics behind of unusual characteristics of GaInAsN.

GaInAsN has been proposed to improve quantum well lasers which can produce the laser beam in wavelength of $1.3 \mu\text{m}$, $1.55 \mu\text{m}$ and $2.3 \mu\text{m}$ and are needed in telecommunication and satellite technology. As indicated by a great number of studies in literature, GaInAsN is ideal as a well layer in QW lasers. As experimentally proven, GaInAsN based QW's have efficient confinement of electrons and light, and high temperature performance. Therefore, we have compared the

band alignments of the nitrogen-free and nitrogen-included laser devices on GaAs and InP substrates. We have seen that the band alignment of strained GaInAsN QW laser systems on InP is better than that of the GaAs substrate and both substrates provide deeper conduction wells and the introduction of opposite strain to the barrier results in deep electron wells which is essential to have good high temperature characteristics. Furthermore, our calculations show that the band alignment of conventionally strained GaInAsN/InP QW laser systems with high indium concentration (beyond 53%) compete with the ideal band alignment of GaInAsN / GaAs lasers.

We have presented the calculations to investigate the role of N and Sb on the critical thickness(h_c) of strained GaInAsNSb QWs on GaAs and InP substrate for (001) and (111) orientations. These calculations have shown that the limitation of h_c is eliminated by means of using the compressive GaInAs/InP wells. The addition of Sb and In atoms into the system has similar effects on h_c . The use GaAs_xSb_{1-x} QW instead of In_xGa_{1-x}As brings an advantage from the point of view of h_c . We have shown that the growth of indium rich GaInAsN QW is possible on InP substrates due to the improved critical layer thickness. Although GaInAsNSb has still the constraint of critical layer thickness, its growth on InP brings improvements in critical thickness.

We have presented a new analytical method to investigate the effect of nitrogen on intrinsic carrier density, screening parameter, effective Bohr radius and binding energy of shallow donors in GaAsN alloys. We have investigated the relation between the binding energy of hydrogenic shallow donor in bulk GaAsN alloys for different screening parameter and nitrogen concentrations. Furthermore, we have noticed that an increase of screening parameter appearing in our work causes a decrease in binding energy.

Optical mode confinement is one of the basic ingredients while designing the semiconductor quantum well lasers. We have investigated the refractive indices and the corresponding optical confinement factors of the proposed GaInAsN laser material systems on GaAs substrate. We have compared conventional and N-based quantum well laser systems to find which has better optical confinement.

Key words: GaInNAs(Sb), nitrides, optical confinement, electron confinement, critical thickness, band offsets, donor binding energy.

ÖZET

NİTROGEN'İN GAINASN YARIİLETKENLERİN OPTİKSEL VE ELEKTRONİK ÖZELLİKLERİ ÜZERİNDEKİ ETKİLERİNİN TEORİK ANALİZİ

KÖKSAL, Koray

Doktora Tezi, Fiz. Müh.

Tez Yöneticisi: Prof. Dr. Beşire GÖNÜL

Tez Yönetici Yardımcısı: Prof. Dr. Beşire GÖNÜL

Eylül 2009, 95 sayfa

Nitrojen katkılı III-V yarıiletken malzemeler ilginç temel özellikler taşımakla birlikte, teknolojik olarak büyük bir önem arz etmektedir. Son yıllarda, band yapılarının III-V'lere göre farklı özellikler göstermesinden dolayı, III-N-V yarıiletkenler ileri ince film büyütme teknikleri sayesinde sorunsuz bir şekilde üretilmiş ve yapılan bilimsel araştırmalar yoğunlaşmıştır. Bu malzemelerin en önemli ve dikkate değer özelliklerinden biri, iletim bandının az miktarda nitrojen safsızlıklardan dolayı ikiye bölünmesi ve band aralığının hızlı bir şekilde azalmasıdır. Az miktardaki sıradan safsızlığın band yapısında meydana getirdiği değişiklik az iken, nitrojen ve V. grup elementleri arasındaki yüksek elektronegatiflik, iyonlaşma ve büyüklük farkı yüzünden, az miktardaki nitrojen katkısı çok büyük değişikliklere sebep olmaktadır. Bu özelliğinden dolayı III-N-V bileşik yarıiletken malzemeler teknolojiye farklı cihazların üretilme yolunu açmıştır. Mesela, GaInAsN'lar telekomünikasyonda ve uydu iletişim teknolojisinde kullanılan 1,3; 1,55 ve 2,3 μm dalga boylarında lazer üretebilen kuantum kuyu lazerleri geliştirmek için önerilen bir malzemedir. Literatürdeki bir çok çalışmada belirtildiği gibi, InGaAsN yarıiletkenleri kuantum kuyu lazerleri için ideal bir kuyu malzemesidir. Yine deneysel olarak kanıtlanmıştır ki, bu malzemeler bilinen malzemelere göre elektronları ve ışığı daha fazla hapsedebilmekte ve yüksek sıcaklıklarda elektron sızıntısına izin vermemektedir.

Bu tezin amacı, nitrojen katkılı III-V yarıiletken bileşiklerin deneysel olarak gösterilmiş temel özellikleri ve cihaz uygulamaları ile ilgili üstünlüklerini teorik olarak incelemek, yorumlamak ve bu konuda yapılabilecek farklı çalışmalara bir kapı açmak için yeni malzemeler önermektir. Bu tezde, nitrojen katkılı GaInAs yarıiletkeninin temel özellikleri ve sıradışı karakteristiğinin altında yatan fizik üzerinde duruldu.

GaInAsN, uydu ve iletişim teknolojisinde kullanılan 1,3 μm , 1,55 μm ve 2,3 μm dalgaboylarında lazer ışını üretebilen kuantum kuyu lazerlerinin geliştirilmesi için önerilmiş bir malzemedir. Literatürde mevcut bulunan çok sayıda çalışmada da ifade edildiği gibi, GaInAsN kuantum kuyu lazerlerinde kuyu malzemesi olarak oldukça idealdir. Deneysel olarak da gösterilmiştir ki, GaInAsN bazlı kuantum kuyularında, elektron ve ışık etkin bir biçimde hapsedilebilir ve yüksek sıcaklıklarda iyi bir performans gözlenir. Bu bilgiler doğrultusunda, biz de nitrojen içeren ve içermeyen GaAs veya InP üzerine büyütülmüş lazer cihazlarının band hizalanmasını inceledik. Sonuçta görüldü ki, deformasyona uğramış GaInAsN kuantum kuyu lazerlerinden InP üzerine büyütülenler GaAs üzerine büyütülenlerden daha iyi band hizalanmasına sahiptirler ve her iki tutucu da daha derin bir iletim kuyusu sağlar. Bununla birlikte, bariyer malzemesine, kuyununkine uygulananın tersi yönünde deformasyon uygulanırsa yüksek sıcaklıklarda yüksek verime yol açan derin elektron kuyusu elde edilmiş olur. Ayrıca, hesaplamalarımız gösteriyor ki, yüksek indium yoğunluğuna sahip deformasyona uğramış GaInAsN/InP kuantum kuyu lazer sistemleri GaInAsN/GaAs lazerlerinin ideal band hizalanması özelliği ile yarışabilecek durumdadır.

Nitrojen(N) ve antimonite(Sb) katkısının, GaAs ve InP ile (111) ya da (001) yönünde büyütülmüş deformasyona uğramış GaInAsNSb kuantum kuyu lazerlerinin kritik kalınlıkları üzerindeki rolünü incelemek için hesaplar yapıldı. Bu hesaplar gösterdi ki, deformasyona uğramış GaInAs kuyularında kritik kalınlığın sınırları InP üzerine yapılan büyütme ile aşılabılır. Indium gibi, Sb katkısı da kritik kalınlığı düşürmektedir. Fakat, kuyu malzemesi olarak InGaAs yerine GaAsSb'in kullanılmasının, kritik kalınlık açısından yararlı olduğu görülmüştür. GaAsSb'in kritik kalınlığı InGaAs'a göre oldukça büyüktür. Bu çalışmada, InP üzerine büyütülen GaInAsN'nin kritik kalınlığı iyileştirdiği saptanmıştır. GaInAsNSb kritik kalınlık açısından sınırlı bir malzeme olmakla beraber, InP üzerine büyütüldüğünde kritik kalınlıkta artış gözlemlenmiştir. Yeni bir analitik metod kullanılarak, nitrojen katkısının GaAsN alaşımı içinde bulunan sığ donörlerin bağlanma enerjisi ve etkin Bohr yarıçapı ile perdeleme parametresi ve taşıyıcı yoğunluğu üzerindeki etkisi incelenmiştir. Nitrojen ve bağlanma enerjisi arasında güçlü bir ilişki vardır. Ayrıca perdeleme parametresinin yükselmesi bağlanma enerjisinin düşmesine sebep olmaktadır. Yarıiletken kuantum kuyu lazerlerinin dizaynı için temel faktörlerden bir tanesi de optiksel mod hapsolmasıdır(ışığın hapsedilmesi). GaAs ve InP üzerine büyütülmüş GaInAsN lazer malzemelerinin kırılma indisi ve buna bağlı optiksel hapsolma faktörleri incelenmiştir. Hesaplama sonuçları göstermiştir ki, 1,3 μm III-V lazer sistemleri optiksel hapsolma faktörü bakımından III-N-V lere göre daha iyidir. Bununla birlikte, hesaplarımız optiksel hapsolmanın deformasyon telafili bariyerler sayesinde iyileştirilebileceğini göstermiştir.

Anahtar kelimeler: GaInAs(Sb), azot, optiksel hapsolma, elektron hapsolması, kritik kalınlık, band genişliği, bağlanma enerjisi.

I dedicate this work to my wife ElifNur and my family.

ACKNOWLEDGEMENTS

I am greatly indebted to my supervisor Prof. Dr. Beşire Gönül for her patiently and kindly guiding me throughout my work towards thesis.

I also extend my gratitude to Prof.Dr. Bülent Gönül who gave me an opportunity to study on quantum mechanics and yield valuable papers.

I wish to thank Prof. Dr. Jamal Berakdar who provided me to study for a semester in his group in Germany and guided me about valuable subjects.

I also want to thank TUBITAK who financially supported me during my PhD program.

TABLE OF CONTENTS

CHAPTER

1	INTRODUCTION	1
1.1	Historical Background	2
1.2	Thesis Outline	4
2	THE PHYSICS BEHIND INCORPORATION OF NITROGEN INTO GAINAS	6
2.1	Introduction	6
2.2	Nitrogen isoelectronic impurities in GaInAs	7
2.3	Nitrogen induced band formation in GaInAsN	9
2.4	Band anti crossing model(BAC)	11
2.5	Conclusions	13
3	COMPARISON AND ANALYSIS OF THE BAND ALIGNMENT OF STRAINED AND STRAIN-COMPENSATED GAINASN QWS ON GAAS AND INP SUBSTRATES	16
3.1	Introduction	16
3.2	The Models	18
3.2.1	Band anti-crossing model	18
3.2.2	Model Solid Theory	19
3.3	Comparison of the band alignment of strained and strain- compensated GaInAsN QWs on GaAs and InP substrates	21
3.3.1	GaInAsN/GaAs/GaAs	21
3.3.2	GaInAsN/GaAsP/GaAs	23
3.3.3	InGaAs/InP/InP	24
3.3.4	GaInAsN/InP/InP	26
3.3.5	GaInAsN/InAsP/InP	27
3.4	Analysis of the band alignment of highly strained indium-rich GaInAsN QWs on InP substrates	28
3.4.1	InGaAs/InP/InP	28
3.4.2	GaInAsN/InP/InP	30
3.4.3	GaInAsN/InAlAs/InP	30
3.4.4	GaInAsN/AlGaInAs/InP	31
3.4.5	InGaAs/InAlAs/InP	31
3.5	Conclusions	32
4	CRITICAL LAYER THICKNESS OF GAIN(N)AS(SB) QWS ON GAAS AND INP SUBSTRATES FOR (001) AND (111) ORIENTATIONS	36
4.1	Introduction	36

4.2	Theoretical models	39
4.2.1	Force balance model of Matthews and Blakslee for h_c	39
4.2.2	Interpolation method for the quinary alloy	40
4.3	InGaAs QW on GaAs and InP substrates for (001) and (111) orientation	41
4.4	GaAsSb QW on GaAs and InP substrates for (001) and (111) orientation	45
4.5	$\text{Ga}_{1-x}\text{In}_x\text{As}_{1-y}\text{N}_y\text{Sb}_z$ QW on GaAs and InP substrates for (001) and (111) orientation	47
4.6	Conclusions	51
5	THE ANALYTICAL SOLUTION OF SCREENED COULOMB POTENTIAL AND BINDING ENERGIES OF DONOR IN GAASN	53
5.1	Introduction	53
5.2	Theory	54
5.3	Calculation of binding energy of donors in GaAsN by using the analytical method	56
5.4	Conclusions	61
6	A THEORETICAL INVESTIGATION OF OPTICAL MODE CONFINEMENT IN GAINASN QWS ON GAAS AND INP	63
6.1	Introduction	63
6.2	Theory	64
6.2.1	Adachi's model for refractive index	64
6.2.2	Five-layer symmetric slab theory	64
6.3	Calculation of refractive index and optical confinement factor in InGaAsN by using the analytical method	68
6.4	Conclusions	72
7	CONCLUSIONS AND FUTURE WORK	75
	REFERENCES	79
	CURRICULUM VITAE	89
	PUBLICATIONS	90

LIST OF TABLES

Table

3.1	Some material parameters which have been used in calculations of band alignment.	19
4.1	The stiffness and lattice constants of binary compounds.	40
4.2	The parameters which are used in calculations according to the directions.	41
6.1	The required parameters related to the refractive index of the materials.	65
6.2	The refractive index values of three different layers for the systems of $\text{Ga}_{0.33}\text{In}_{0.67}\text{P}_{0.28}\text{As}_{0.72}$ / $\text{Ga}_{0.1}\text{In}_{0.9}\text{P}_{0.78}\text{As}_{0.22}$ / InP, $\text{Al}_{0.175}\text{Ga}_{0.095}\text{In}_{0.73}\text{As}$ / $\text{Al}_{0.27}\text{Ga}_{0.21}\text{In}_{0.52}\text{As}$ / InP and $\text{Ga}_{0.7}\text{In}_{0.3}\text{N}_{0.022}\text{As}_{0.978}$ QWs between GaAs barriers and $\text{Al}_{0.1}\text{Ga}_{0.9}\text{As}$ cladding layers.	72

LIST OF FIGURES

Figure

2.1	The representation of the change of CB, VB and N impurity energy levels in momentum space by applied hydrostatic pressure.	9
2.2	The variation of band gap of GaInAsN according the band anti-crossing model.	14
2.3	Temperature and nitrogen dependence of band gap of GaInAsN for In content of 0%(yellow) and 20%(green).	14
2.4	The variation of E_+ and E_- versus N and In concentration.	15
3.1	The nitrogen N concentration (in well) dependence of the conduction and valence band offset ratios, Q_c and Q_v , (inset figure) and the corresponding conduction and valence band offsets, ΔE_c and ΔE_v , of the uncompensated compressively strained $\text{Ga}_{0.70}\text{In}_{0.30}\text{N}_y\text{As}_{1-y}$ quantum wells with GaAs barriers on GaAs substrates.	22
3.2	The variation of conduction (upper curve) and valence (lower curve) band offsets, ΔE_c and ΔE_v , with nitrogen concentration which results compressive strain (in well) for $\text{Ga}_{0.70}\text{In}_{0.30}\text{N}_y\text{As}_{1-y}$ quantum wells and with phosphorus concentration which results tensile strain (in barrier) for compensated $\text{Ga}_{0.70}\text{In}_{0.30}\text{N}_y\text{As}_{1-y}$ / GaAsP quantum wells on GaAs substrates.	23
3.3	The indium concentration (in well) dependence of the conduction and valence band offset ratios, Q_c and Q_v , (inset figure) and the corresponding the conduction and valence band offsets, ΔE_c and ΔE_v , of the tensilely strained uncompensated $\text{In}_x\text{Ga}_{1-x}\text{As}$ / InP QW laser system on InP substrates. RHS of the y-axis shows the energy difference between the transition energies of $c_1 - lh_1$ and $c_1 - hh_1$ from the respective band edges.	25
3.4	The variation of the conduction and valence band offsets, ΔE_c and ΔE_v , with indium concentration and tensile strain (in well) for uncompensated $\text{Ga}_{1-x}\text{In}_x\text{N}_{0.02}\text{As}_{0.98}$ /InP QWs on InP substrates. RHS of the y-axis shows the energy difference between the transition energies of $c_1 - lh_1$ and $c_1 - hh_1$ from the respective band edges.	26
3.5	The calculated variation of the conduction and valence band offsets, ΔE_c and ΔE_v , with arsenide concentration and compressive strain (in barrier) for compensated $\text{Ga}_{0.90}\text{In}_{0.10}\text{N}_{0.03}\text{As}_{0.97}$ / $\text{In}_x\text{As}_{1-x}\text{P}$ / InP laser system.	27

3.6	The indium concentration dependence of the conduction and valence band offset ratios, Q_c and Q_v , (inset figure) and the corresponding conduction and valence band offsets, ΔE_c and ΔE_v , of the strained $\text{Ga}_{1-x}\text{In}_x\text{As}$ quantum wells with InP barriers on InP substrates.	29
3.7	The variation of conduction and valence band offsets, ΔE_c and ΔE_v , with nitrogen and indium concentration for compressively strained for $\text{Ga}_{1-x}\text{In}_x\text{N}_y\text{As}_{1-y}$ quantum wells with InP barrier and InP substrate	33
3.8	The nitrogen concentration dependence of conduction and valence band offset ratios, Q_c and Q_v , (inset figure) and the corresponding the conduction and valence band offsets, ΔE_c and ΔE_v , of the compressively strained $\text{Ga}_{0.22}\text{In}_{0.78}\text{N}_y\text{As}_{1-y}$ well with $\text{In}_{0.52}\text{Al}_{0.48}\text{As}$ barriers QW laser system on InP substrates.	33
3.9	The calculated results of the nitrogen concentration dependence of conduction and valence band offset ratios, Q_c and Q_v , (inset figure) and the corresponding the conduction and valence band offsets, ΔE_c and ΔE_v , of the compressively strained $\text{Ga}_{0.22}\text{In}_{0.78}\text{N}_y\text{As}_{1-y}$ well with $\text{Al}_{0.15}\text{Ga}_{0.32}\text{In}_{0.53}\text{As}$ barriers QW laser system on InP substrates.	34
3.10	The indium concentration dependence of conduction and valence band offset ratios, Q_c and Q_v , (inset figure) and the corresponding the conduction and valence band offsets, ΔE_c and ΔE_v , of the nitrogen free compressively strained $\text{Ga}_{1-x}\text{In}_x\text{As}$ well with $\text{In}_{0.52}\text{Al}_{0.48}\text{As}$ barrier QW laser system on InP substrates.	34
3.11	The comparison of the substrate dependence of strain as a function of nitrogen and indium concentration in $\text{Ga}_{1-x}\text{In}_x\text{N}_y\text{As}_{1-y}$ QW.	35
4.1	The calculated variation of the critical thickness of $\text{In}_x\text{Ga}_{1-x}\text{As}$ QW versus In concentration on GaAs substrates for (001) and (111) growth orientations. Dashed- and solid line represents the variation for (001) and (111) growth orientations, correspondingly. The inset figure shows the magnitude of strain versus In concentration on GaAs substrate. Closed and open dots represents the experimental values.	42
4.2	The calculated variation of the critical thickness of $\text{In}_x\text{Ga}_{1-x}\text{As}$ QW versus In concentration on InP substrates for (001) and (111) growth orientations. Dashed- and solid line represents the variation for (001) and (111) growth orientations, correspondingly. The inset figure shows the magnitude of strain versus In concentration on GaAs substrate. Closed and open dots represents the experimental values.	43
4.3	The calculated variation of the critical thickness of $\text{GaAs}_{1-x}\text{Sb}_x$ QW versus In concentration on GaAs substrates for (001) and (111) growth orientations. Dashed- and solid line represents the variation for (001) and (111) growth orientations, correspondingly. Closed squares represents the experimental values for (001) orientation.	46

4.4	The calculated variation of the critical thickness of $\text{GaAs}_{1-x}\text{Sb}_x$ QW versus In concentration on InP substrates for (001) and (111) growth orientations. Dashed- and solid line represents the variation for (001) and (111) growth orientations, correspondingly. Closed squares represents the experimental values for (001) orientation.	46
4.5	The calculated variation of the critical thickness of $\text{GaAs}_{1-x}\text{N}_x$ QW versus In concentration on GaAs substrates for (001) and (111) growth orientations. Dashed- and solid line represents the variation for (001) and (111) growth orientations, correspondingly. Closed dots represents the experimental values for (001) orientation.	48
4.6	The calculated variation of the critical thickness of $\text{Ga}_{1-x}\text{In}_x\text{N}_y\text{As}_{1-y-z}\text{Sb}_z$ QW versus In concentration on GaAs substrates for (001) and (111) growth orientations. Dashed- and solid line represents the variation for (001) and (111) growth orientations, correspondingly. Closed dots represents the experimental values.	49
4.7	The calculated variation of the critical thickness of $\text{Ga}_{1-x}\text{In}_x\text{N}_y\text{As}_{1-y-z}\text{Sb}_z$ QW versus In concentration on InP substrates for (001) and (111) growth orientations. Dashed- and solid line represents the variation for (001) and (111) growth orientations, correspondingly. Closed dots represents the experimental values.	50
5.1	Minimum band gap(solid line) calculated by Eq. 3.1 and static dielectric constant(dashed line) obtained by Eq. 5.15 as a function of the N fraction for $\text{GaAs}_{1-y}\text{N}_y$	58
5.2	Electron effective mass(solid line) at Γ valley and effective bohr radius(dotted line) as a function of N concentration.	59
5.3	The variation of screening parameter α (dashed lines) and intrinsic carrier concentration(solid line) with increasing nitrogen concentration. α is also dependent on donor concentration.	60
5.4	The binding energy variation(solid line) for the ground state as a function of the nitrogen concentration. The change of effective Bohr radius(dashed line) and screening parameter can be seen in this figure.	61
6.1	The illustration of the five layer slab waveguide.	66
6.2	Calculated refractive index values for GaAs, InGaAs and GaInNAs with increasing N concentration.	68
6.3	GaInNAs on GaAs substrate as a function of N concentration and wavelength of photon. The top x -axis shows the energy of photon and right y -axis shows the strained band gap of the GaInNAs on GaAs substrate for N concentrations stated on the left y -axis.	70
6.4	Contour maps of refractive index of GaInNAs well as a function of In and N concentration.	71
6.5	The variation of the optical confinement factor Γ versus the thickness of the active region for the laser structures of InGaAsP, Al-GaInAs, and GaInNAs with an emission wavelength of $1.3 \mu\text{m}$	74

6.6	The calculated variation of Γ of N-based uncompensated (blue-line) laser system with that of the compensated laser systems with GaAsN (red-line) and GaAsP (black-line) barrier.	74
-----	--	----

LIST OF SYMBOLS

e : electron charge

\hbar : Planck's constant

k_B : Boltzman's constant

T : Temperature

E_g : Band gap(eV)

Δ_0 : Spin-orbit splitting(eV)

C_{11} : Elastic Stiffness constant(GPa)

C_{12} : Elastic Stiffness constant(GPa)

C_{44} : Elastic Stiffness constant(GPa)

b : Deformation potential(eV)

a : Lattice constant(\AA)

a_c : Hydrostatic deformation potential for conduction band(eV)

a_v : Hydrostatic deformation potential for valence band(eV)

$\mathbf{E}_{v,av}$: Average valence band level(eV)

CHAPTER 1

INTRODUCTION

Semiconductors are very important for device applications of electronics and optoelectronics in technology. Initial work about semiconductors was based on Si, Ge and GaAs of which fundamental properties are now well known. After the possibility of alloying, different semiconductor alloys could be produced which have new fundamental and electronic properties. For example, GaAs and AlAs lattice matched binary semiconductors can be alloyed and one can produce AlGaAs which has different characteristics from GaAs and AlAs. Anymore, lattice mismatched alloys have been growth via modern growth techniques.

Ga(In)AsN which is an example of lattice mismatched alloys has unusual properties and advantageous in device applications. GaInAsN can be grown on GaAs, InP and last years Si and GaP. This material is proposed to be used in quantum well laser systems, infrared detectors, high-efficiency multijunction solar cells and high speed transistors. Furthermore, it has very important physics because N atoms affect the band structure anomalously, split the conduction band in two parts and a few percent of nitrogen concentration in InGaAs causes a huge reduction in band gap.

Kondow et al. have proposed application of GaInAsN to optoelectronic devices [1]. GaInAsN can be used as a light-emitting material with a band gap energy suitable for long-wavelength laser diodes(1.3 – 1.55 μm and longer wavelengths) and can be grown pseudomorphically on a GaAs substrate. By combining GaInAsN with any wide band gap materials that can be grown on a GaAs substrate, it is possible to achieve a Type-I band lineup and ideal band offset. This allows to fabricate very deep quantum wells which bring many advantages in terms of laser performance, including high operating speeds and excellent temperature stability of threshold current and lasing wavelength. GaInAsN is also promising as a material for use in long-wavelength vertical-cavity surface-emitting lasers (VCSELs), because a GaInAsN active layer can be grown on a highly reflective GaAs/AlAs distributed bragg reflector (DBR) mirror over a

GaAs substrate in a single stage of epitaxial growth [2, 3].

The field of intersubband transitions (ISBTs) which is basic of quantum well infrared photodetectors(QWIP) is important in electron accumulation layers in GaAs based QWs. GaInAsN QWs have been proposed to use as QWIPs to reach wavelengths below 4 μm [4], current limit in GaAs based materials. The first observations of ISBTs were made recently in GaInAsN/GaAs QWs [5], of which the ideal band offset, specially large conduction band offset makes it good candidate for QWIPs. Recently, intersubband transitions(ISBTs) at very short wavelengths(1.24 μm) were reported in highly confined GaInAsN QWs [6, 7].

Because of its low-band gap characteristics, GaInAsN can be used as solar cells to efficiently collect the low-photon-energy portion of the solar spectrum. However there are some problems to use GaInAsN as a solar cell material. Although the collection of minority carriers is central to the function of solar cells [2], N into GaInAs dramatically reduces the mobility and minority-carrier lifetime. Nevertheless, new works are currently performed to overcome the problems of short minority carrier life times and low-diffusion lengths which lower the efficiency in conventional GaInAsN solar cells [8]. The incorporation of GaInAsN in the base of heterojunction bipolar transistors is a scientifically interesting and commercially important addition to the material and band gap engineering capabilities for III-V compound devices [9]. There are also new works on using of GaInAsN in high speed transistors and its transport properties [10].

1.1 Historical Background

In the mid-1960s, the studies on nitrogen impurities in the semiconductors showed that substitution of small amount of nitrogen($10^{16} - 10^{19} \text{ cm}^{-3}$) into GaP produces bound states in the forbidden band gap of this material and it was reported that *isolated N atoms* and *NN pair states* can bound exciton. In the late-1960s, it was found that the *isolated N state lies above the conduction band* in GaAsP and InGaP for some values of In or As concentration. Later, it was shown that the *pressure dependence of N level* is much smaller than that of the band gap. During the extensive studies were performed on optical properties of *GaAsP:N*, the observation of the N state in GaAs remained elusive. In the early 1980s, N state was forced into the band gap of GaAs by the application of hydrostatic pressure and therefore photoluminescence was observed. The incorporation of much higher N content into GaAs was reported, *large band gap bowing* was observed in $\text{GaAs}_{1-x}\text{N}_x$ with $0 < x < 0.015$ in 1992 by Weyers et al. and in 1994 by Kondow et al. for the first time. In 1996, Sato et al. succeeded in growing *GaInAsN with excellent crystallinity* despite the previous failure of several groups

to do this. A dislocation-free *III-V-N layer was grown on a Si* substrate for the first time by molecular beam epitaxy (MBE) by Yonezu et al. in 1998. The *GaInAsN alloy also was grown on InP* substrates in order to extend the emission wavelength range as compared with conventional GaInAsP alloy by Gokhale et al. in 1999. Sopenan et al. first reported the fabrication of *GaInAsN quantum dots* by self-organization using gas-source molecular beam epitaxy (GSMBE) in 2000. The *role of hydrogen* on dilute nitrides was investigated firstly in 2002. It was reported that, the incorporation of *hydrogen passivates the N-related electronic states* and increases the band gap. The studies have been performed on *electron spin dynamics in dilute nitride* compounds since 2005. An experimental and theoretical study on the absorption coefficient of *GaInAsN quantum wires* was also published in 2006 by Feltrin et al. and may lead to novel detector devices.

In order to explain unusual behaviour of GaInAsN, a large number of studies has been performed and some models have been proposed. *Band anticrossing model* is proposed by Shan et al. in 1999 which describes the strong band gap bowing observed at low N composition in Ga(In)AsN in terms of an interaction between the Ga(In)As host matrix conduction band edge and a higher lying band of localized N states. O'reilly et al. applied the *k · p method* to GaAsN in 1999. Whereas in previous studies 8-band $\mathbf{k} \cdot \mathbf{p}$ has been used to calculate the band structure of GaAs, O'reilly et al. proposed modified *10-band k · p Hamiltonian* for GaInAsN in which the additional 2 bands indicate localized N state. In 2001, Kent et al. developed *an atomistic model* based upon large-scale atomistic supercell calculations and the empirical pseudopotential method which is able to explain some experimentally observed phenomena in GaInAsN. In this study, the model is compared with band anticrossing model. Lindsay and O'Reilly developed an accurate *sp³s* tight-binding Hamiltonian* to describe the electronic structure of GaInAsN in 2002. They compared the results with observed experimental data and pseudopotential calculations.

Device application of N incorporated semiconductors began in 1960s. In the years between 1968 and 1972, *green light emitting diodes* (LEDs) based on *GaP:N*, LEDs based on *GaAsP:N* (peak emission energies in 1.8 – 2.2 eV range) and *optically-pumped laser action* (stimulated emission) in *GaAsP:N* were reported. First operational laser diodes based on III-V-N semiconductor alloys were reported in 1994. Laser operation of a GaInAsN *vertical-cavity surface-emitting laser* (VCSEL) diode emitting at 1.2 μm (at room temperature and pulsed) was achieved for the first time in 1997 by Hitachi group. Geisz and Friedman addressed the application of III-N-V semiconductor alloys to *high-efficiency multijunction solar cells* in 1998. The incorporation of GaInAsN in the base of *heterojunction bipolar transistors* was proposed in 1999. In 2000,

1.3 μm -range, room-temperature, continuous wave operation was realized and first demonstration of 10–Gb/sec, 10–km communication was performed by a group. In 2001, GaInAsN VCSELs went on the market. While the first observations of intersubband transitions in GaInAsN/GaAs QWs were made by Duboz et al. in 2002, the first fabrication and characterization of *quantum well infrared photodetectors* based on *GaAsN* and *GaInAsN* was reported in 2003 and 2007, respectively.

1.2 Thesis Outline

In this thesis, we aim to investigate some optical and electronic properties of GaInAsN for QW lasers applications. These properties have been not carried out by previous studies up to our knowledge.

In chapter 2, we discuss the origin of the unusual physical properties of GaInAsN. We present the issue of isoelectric impurities in semiconductors and the difference of nitrogen from other conventional isoelectronic impurities. We discuss the effect of nitrogen bound states on conduction band of GaInAs and introduce band anticrossing model.

We examine the relative band alignment of the band edges of $\text{Ga}_{1-x}\text{In}_x\text{As}_{1-y}\text{N}_y$ between the quantum well and the barrier in chapter 3. We present band alignment calculations for GaAs and InP substrates with strained and strain compensated barriers. These calculations reveal the advantageous of N incorporation into InGaAs systems and show how nitrogen improves electron confinement. This chapter consists of two parts; first part is dealing with GaInAsN with low In concentration to produce 1.3 and 1.55 μm , second part is concentrated on GaInAsN with high In concentration to produce 2.3 μm . Band anti crossing model(BAC) which explains the conduction band splitting due to N addition into InGaAs is used to calculate band gap and model solid theory is used to obtain the corresponding band alignments.

In chapter 4, we calculate critical thickness(h_c) values for Ga(In)As(N)(Sb) QW due to the strain compensating effect of N atoms. Additionally, the effect of antimonite(Sb) and indium(In) on critical thickness of quantum well material is investigated. The effect of growth directions of (111) and (100) is shown for different alloy combinations of Ga, In, N, As and Sb. Furthermore, we investigate substrate dependence of h_c of (Ga)InAs(N)(Sb) wells grown on InP and GaAs substrates. In this chapter we use interpolation method to calculate the parameters of ternary, quaternary and quinary heterostructures. Critical thickness calculations are performed by means of using force balance model of Matthews and Blakslee.

The effect of nitrogen on binding energy of shallow donors in GaAsN alloys is examined in chapter 5. We derive an analytical solution of screening coulomb potential in this study. Binding energy of shallow donors is calculated by using this analytical solution. Strong nitrogen concentration dependence of intrinsic carrier density, screening parameter and effective Bohr radius are investigated. We explain the meaning of screening parameter for GaAsN as the inverse of screening parameter being equal to another well known parameter, Debye length.

Chapter 6 introduces a theoretical investigation of optical confinement factor of GaInAsN based quantum wells. We examine how the refractive index of GaInAsN material is affected by nitrogen and indium concentration and the wavelength of applied photon. A comparative study of optical confinement factor of GaInAsN wells is undertaken by means of considering the refractive index differences between the well and that of barrier and cladding layer. Refractive index calculations are performed by using Adachi's model and optical confinement factor is calculated by five-layer slab model.

Chapter 7 gather together the major conclusions from the work described in this thesis. Future work is also provided in this chapter.

CHAPTER 2

THE PHYSICS BEHIND INCORPORATION OF NITROGEN INTO GAINAS

2.1 Introduction

Alloying semiconductors with large size-mismatched atoms induces unusual electronic properties that can be exploited in a range of otherwise unavailable applications, such as long wavelength lasers and high performance solar cells [11]. In III-V semiconductors, the replacement of a few percent of the group V element by small, highly electronegative and isoelectronic nitrogen atoms results in a dramatic reduction of fundamental band gap of approximately 100 meV per atomic per cent of nitrogen. This enables the band gap of the resulting dilute III-V nitride alloys to be tuned to particular energies for optoelectronic applications by changing the nitrogen content. Since only small amounts of nitrogen are required to produce large changes in the band gap, the material, enabling high quality alloys to be grown epitaxially and incorporated into the existing optoelectronics infrastructure.

During the past decade, dilute nitrides, particularly the quaternary material system of GaInAsN have attracted a great deal of attention, both because of unusual physical properties and potential applications in a variety of optoelectronic devices. In this chapter we discuss the origin of the unusual physical properties of GaInAsN. We present the issue of isoelectric impurities in semiconductors and the difference of nitrogen from other conventional isoelectronic impurities. We discuss the effect of nitrogen bound states on conduction band of GaInAs and introduce band anticrossing model.

2.2 Nitrogen isoelectronic impurities in GaInAs

In order to understand the effect of nitrogen on GaInAs band structure, we have to interest in isoelectronic impurities in semiconductors. Isoelectronic (isovalent) impurity atoms have the same outer electron configuration as the atoms of host crystal which they replace. Examples are germanium in silicon and arsenic in gallium phosphide. Whereas an isovalent impurity always creates a perturbation to the host band structure, this perturbation is usually small, hybridizes with the host states and remains unnoticeable. However, if the isovalent impurity and the atom it replaces have very distinct properties, the isovalent impurity can create a significant perturbation to the electronic charge distribution. In 1969, Dean et al. found that bismuth in GaP can bind a hole with 39.7 meV ionization energy. It was observed that an exciton can be bound to nitrogen in GaP with total binding energy 21 meV [12], to bismuth in GaP with binding energy 107 meV [13] and to oxygen in ZnTe with binding energy 404 meV [14]. These experiments have shown that isovalent impurities can create bound states and can be attractive to electrons and holes. An electron (hole) which is trapped by an isoelectronic impurity can subsequently bind a carrier of opposite charge via coulombic interaction, therefore an isoelectronic impurity can bind an exciton. Experimentally found that an isoelectronic impurity may bind

- a hole only if its electronegativity is smaller than that of the host atom which it replaces(N and O), [15]
- an electron only if its electronegativity is larger than that of the host atom which it replaces(Te and Bi), [15]
- an exciton(N, O, Bi) [16].

Nitrogen atoms also behave as isoelectronic impurities in GaInAs with concentration of $10^{16} - 10^{18} \text{ cm}^{-3}$. The N atoms can cause a strong perturbation to the host band structure, create a localized impurity levels and bind excitons. There are two main reasons of this strong perturbation; large difference in atomic size and electronegativity between nitrogen and arsenide atoms. Because a nitrogen atom lacks p orbitals in its core states, it is smaller and much more attractive to electrons than arsenic. Furthermore, the Ga-P and Ga-N bond lengths difference leads to lattice relaxation and important local redistribution of the charge density. The potential created by nitrogen atoms is not coulombic and has short range interaction.

Nitrogen impurities act as deep centers with localized potentials. Because the wavefunctions of these centers are localized in real space, they are comprised of wavefunctions originating from many bands in a wide region of k -space and the impurity levels are not sensitive to the positions of the conduction and valence band edges. Thus they are not expected to shift significantly in energy with a change in composition or pressure. The presence of an impurity atom alters the bonding-antibonding energy of the host crystal, introducing an impurity-related deep trap state. Deep trap states with A_1 symmetry tend to lie in a range of energies relative to the vacuum level that happens to be near the conduction band edges of most semiconductors, while those with T_2 symmetry are located near the valence band edges. Assessment of the relative energy levels of these deep states can be carried out within the Koster–Slater model using a tight-binding basis. This generalized theory is intended to identify the broad chemical trends in the localized levels of the impurities and is therefore effective in predicting the approximate behavior of an impurity within a host crystal. The calculations consider the interaction of the host semiconductor with a localized potential introduced by the impurity and can be determined by solving the subsequent Schrödinger equation. When the defect potential is restricted to nearest neighbor distances, the problem is simplified to a difference in s -orbital energies of the impurity and host for A_1 symmetries and p -orbital energies for T_2 symmetries. The nature of the impurity within the host will ultimately determine the symmetry of the deep center and consequently its location within the bandstructure of the host semiconductor. Highly electronegative isoelectronic impurities, such as N in III–V compounds, act as weak acceptors and localize electrons in A_1 states near the conduction band edge of the host. For example, the Koster–Slater theory predicts that the N defect level is resonant with the conduction band in GaAs. These calculations correspond quite well with experimental observations. Oxygen in II–VI compounds behaves in a similar manner and is a bound A_1 state in ZnTe. Likewise, C is expected to lie within the conduction band of both Si and Ge. Metallic impurities, on the other hand, act as weak donors and localize holes in a T_2 state near the valence band of the host semiconductor. For example, the As defect level lies just above the valence band edge of GaN. Antimony and Bi have a lower ionization energy than As as well, and their defect levels are also predicted to lie near or within the valence bands of other III–V compounds. These approximate trends serve as a guide to the behavior of dilute nitrides and other moderately and highly mismatched alloys.

N impurity level can not be observed directly because it is resonant with conduction band. Nevertheless, being its pressure dependence smaller than that of band gap of Ga(In)As, impurity level can be placed below CB minimum

via hydrostatic pressure. As can be seen in fig. 2.1, when a critical value of hydrostatic pressure is applied to the crystal, nitrogen impurity level is below the CB minimum. Therefore, value of this level can be determined by exciton decay. In fig. 2.1, the nitrogen energy level is resonant with CB without applied

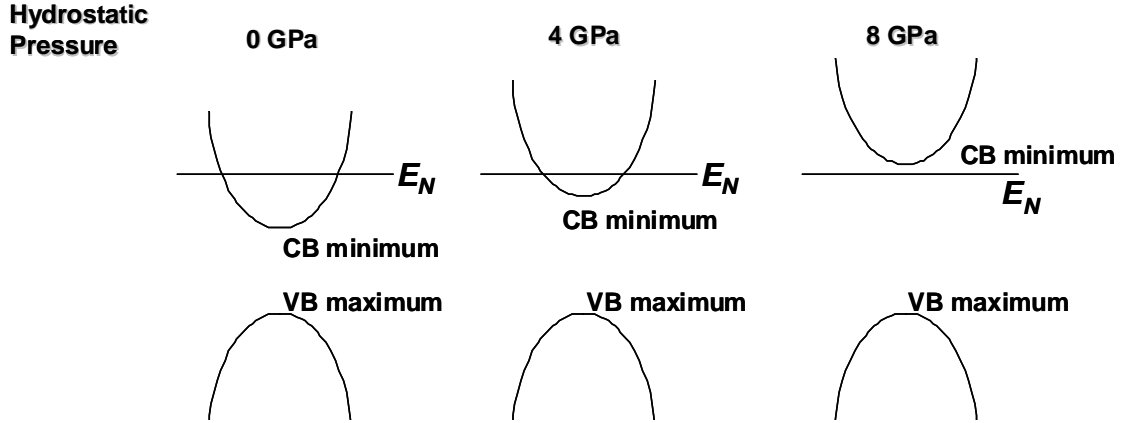


Figure 2.1: The representation of the change of CB, VB and N impurity energy levels in momentum space by applied hydrostatic pressure.

pressure. With increasing of hydrostatic pressure, CB minimum is increasing and impurity level is in the band gap at 8 GPa. As a result of extrapolation, the value of nitrogen impurity level can be found as 1.65 eV above the valence band maxima and 150 meV above the conduction band minima of GaAs [17]. The nitrogen impurity level in GaInAs is same within that of GaAs.

Binding mechanism of nitrogen isoelectronic impurities is explained in the paper of Zhang and Ge [18] explicitly. The binding of an exciton to the nitrogen centers is explained as a consequence of the difference in electronegativity χ between nitrogen and arsenide. Because of $\chi_N \succ \chi_{As}$, nitrogen tends to bind electron; then via the Coulomb interaction, an exciton is bound to nitrogen. Although the nitrogen bound state is very close to the band gap, in the sense of being able to capture an electron, it is considered as a deep acceptor [18].

When nitrogen atoms are incorporated into the GaInAs with concentration of above 10^{18} cm^{-3} , nitrogen induced band formation exists in GaInAsN and new features appears in the semiconductor. In next section we present how nitrogen induces a band with increasing of nitrogen concentration.

2.3 Nitrogen induced band formation in GaInAsN

Kent and his coworkers [19] review all steps during nitrogen induced band formation phenomena in their study about pseudopotential theory of dilute III-V nitrides. While they discuss the experimental observations which reveal the unusual behaviour of nitrogen incorporated III-V's, they compare the properties of conventional isoelectronic impurities/alloys with those of nitrogen isoelectronic impurities/alloys. When nitrogen concentration in GaInAs is lower than 0.01%, the followings are observed;

- localized and single-impurity levels appear above the band gap. In conventional isovalent alloys as GaInAs:P the perturbation potential of phosphorous isovalent atoms is too weak to create a bound state. In GaInAs:N, bound state appears as a sharp resonance above the conduction band minimum.
- because shallow impurity levels(Si in GaInAs) are constructed from the wavefunction of the single nearest host crystal state, applied pressure causes to change the energy of impurity levels at the same rate as the energetically nearest host crystal state. However, the wavefunction of nitrogen impurity levels is constructed from many bands of the host crystal, these levels in GaInAs:N have small pressure dependence.
- while usual isovalent pairs leads to broad resonances within conduction band and valence band, N-N pairs leads to discrete levels inside the band gap. This leads to sharp photoluminescence lines.
- In nitrogen incorporated InGaAs, the emission lines are redshifted with respect to absorption; in N-free InGaAs alloys absorption and emission occur at the same energy.

These properties of nitrogen incorporated GaInAs disappear with increasing of nitrogen concentration. Furthermore, addition of nitrogen causes new features in GaInAsN. When nitrogen concentration is higher than 0.01%

- It is observed that increase of nitrogen composition has no effect on N pair levels. The sharp emission lines due to pair levels remain at same energy. This behaviour is characteristics of deep transition metal impurities, but not hydrogenic impurities (like Si in GaInAs). This behaviour is called as composition-pinning of the impurity pair energy levels and shows that the impurities don't interact with each other.

At the higher nitrogen concentration, the different regions of GaInAs crystal affected by N clusters start to overlap. Thus, the transition from nitrogen acting as an isoelectronic impurity to forming nitrogen-induced bands take place at that concentration. Klar et al. [20] claim that this transformation is at 0.2% for GaAsN. Alloy properties of Ga(In)AsN can be described with concentration ranges as described below [19],

- Band-gap shows huge and composition-dependent optical bowing and significantly decreases with increasing N content.
- Electron mass is anomalously heavy but decreases with nitrogen concentration,
- Reduction in band-gap with increased temperature slows down with nitrogen addition [19],
- New energy state E_+ takes place.

2.4 Band anti crossing model(BAC)

In order to obtain band structure of the semiconductors, there are empirical(like $\mathbf{k} \cdot \mathbf{p}$), semiempirical(like tight-binding, pseudopotential) and ab-initio methods(like density functional theory). The success of a band structure calculation technique is dependent on agreement of its results with experimental observations. Ab initio and empirical techniques are generally very successful to analyze band structure of the simple or alloy semiconductors and bulk or low dimensional systems. Until now, to obtain the band structure properties of dilute nitride systems, microscopic models like tight-binding, empirical supercell pseudopotential and $\mathbf{k} \cdot \mathbf{p}$ models have been used. Even if these models explain some properties of dilute nitride alloys, they are not able to give a complete explanation of the conduction band of dilute nitrides. The BAC model, despite its simplicity when compared to fully microscopic models, successfully describes the macroscopic behavior of the material.

As will be treated in section 3.2, BAC model provides a good explanation of the huge bowing in the band gap of GaInAsN. This model describes the composition dependence of band gap energy of GaInAsN and has been successfully used to describe the dependences of the upper and lower subband energies on nitrogen concentration. The model manages to explain the basic properties of the material and to provide analytical expressions, such as conduction band edge dispersion relations and electron effective mass. The model is based on the interaction of the lowest conduction band with the highly localized N-induced

energy level E_N . An anti-crossing interaction of the localized N states with the extended state of GaInAs leads to a characteristic splitting of the conduction band into two non-parabolic subbands. The variation of band gap of GaInAsN is calculated by BAC.

The band anticrossing is proposed as a macroscopic model to simply describe the interaction between a localized nitrogen impurity level and conduction band. Wu et al. derived BAC model from many-impurity Anderson model. We can also derive this model from simple perturbation theory. Let us denote the conduction band and nitrogen states by Φ_{CB} and Φ_N . Perturbing potential due to the nitrogen is ΔV . In this case we can write the Hamiltonian as

$$H \Phi_n = E \Phi_n \quad (2.1)$$

where

$$H = H_0 + \langle \Phi_n | \Delta V | \Phi_n \rangle + \sum_{m \neq n} \frac{|\langle \Phi_m | \Delta V | \Phi_n \rangle|^2}{E_m - E_n} \quad (2.2)$$

In first order correction because $\langle \Phi_{CB} | \Delta V | \Phi_{CB} \rangle = V_{CC}$ and $\langle \Phi_{NN} | \Delta V | \Phi_{NN} \rangle = V_{NN}$ indicate the N-N or CB-CB interactions, they can be assumed as zero. In second order correction $\langle \Phi_{CB} | \Delta V | \Phi_N \rangle = \langle \Phi_N | \Delta V | \Phi_{CB} \rangle = V_{NC}$ is the repulsion term which gives the band anticrossing and has a value. Substituting the eq. 2.2 into eq. 2.1, we get the determinant

$$\begin{vmatrix} E_N - E & V_{NC} \\ V_{NC} & E_{CB} - E \end{vmatrix} = 0 \quad (2.3)$$

which results in the energies

$$E_{\pm} = \frac{1}{2}(E_N + E_{CB} \pm \sqrt{(E_N - E_{CB})^2 + 4V_{NC}^2}) \quad (2.4)$$

The BAC is very successful to calculate the band gap of GaInAsN semiconductor. In fig. 2.2, the variation of band gap versus In and N content is calculated by means of using this model. As can be seen from fig. 2.2, increase of indium concentration leads to slight reduction in band gap energy. In nitrogen-free case, the value of band gap changes from the band gap of GaAs(1.424 eV) to that of InAs(0.417 eV) as expected from usual alloys. However, in fig. 2.2 we see that a little increase of nitrogen causes rapid reduction in band gap. This behaviour is most important unusual characteristics of nitrogen incorporated alloys, because the band gap doesn't change linearly between those of GaN(3.299 eV)/InN(0.78 eV) and GaAs(1.424 eV)/InAs(0.417 eV).

There is a relationship between nitrogen, temperature and band gap. According to the experimental study of Onabe et al. [21], the band gap of GaAsN is reduced as temperature is increased and this reduction slows down dramatically

with small addition of nitrogen. In fig. 2.3, this behaviour can be seen for the In concentrations of 0% and 20%.

Experiments [22] show that GaInAsN has three additional optical transitions compared with GaInAs above the N concentration of 0.2%. The source of these transitions are a new energy level E_+ which is a result of nitrogen incorporation in crystal. Fig. 2.4 shows the behaviour of E_+ and E_- in GaInAsN semiconductor alloy. This figure illustrates the most important result of BAC model which claims the splitting of conduction band due to nitrogen isoelectronic impurities.

2.5 Conclusions

In summary, this chapter presents an overview of the physics behind the unusual properties and band anticrossing model to explain electronic structure of dilute nitrides and GaInAsN. We have seen that nitrogen atoms have strong perturbation effect on the host semiconductor "GaInAs" because of their very different electronegativity than that of As atoms. Furthermore, the difference between the bond lengths of Ga-As(In-As) and Ga-N(In-N) causes a lattice relaxation and charge redistribution in the semiconductor. The differences between observed experimental properties of usual and nitride alloys also has been mentioned in this chapter. The derivation of band anticrossing model by means of perturbation theory has been introduced in the last section of this chapter. After the model has been described shortly, the figures obtained from the band anticrossing model has been shown.

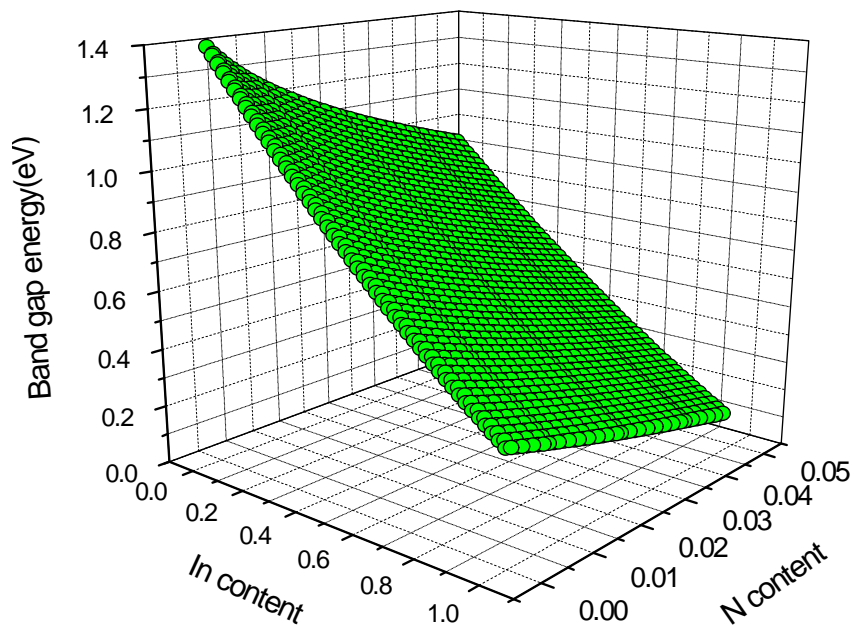


Figure 2.2: The variation of band gap of GaInAsN according the band anticrossing model.

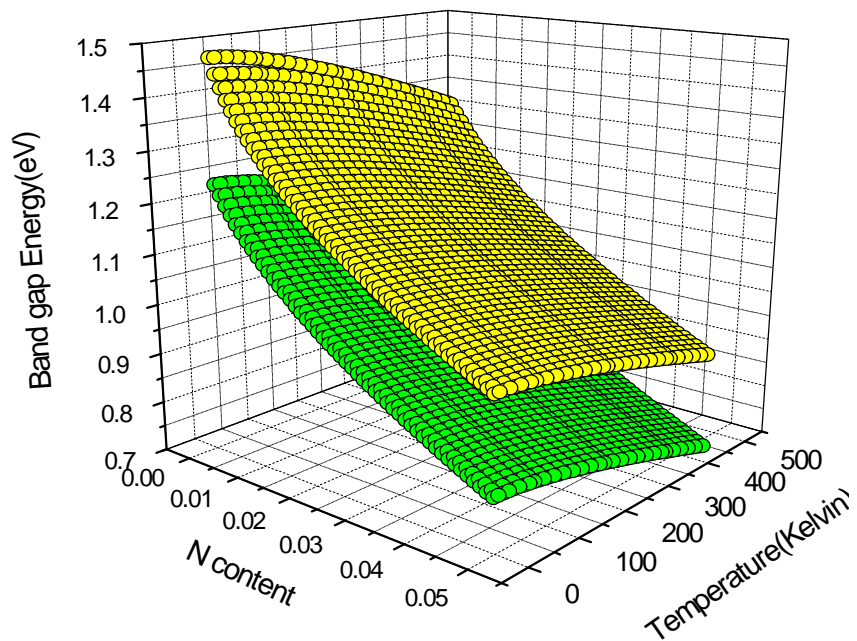


Figure 2.3: Temperature and nitrogen dependence of band gap of GaInAsN for In content of 0%(yellow) and 20%(green).

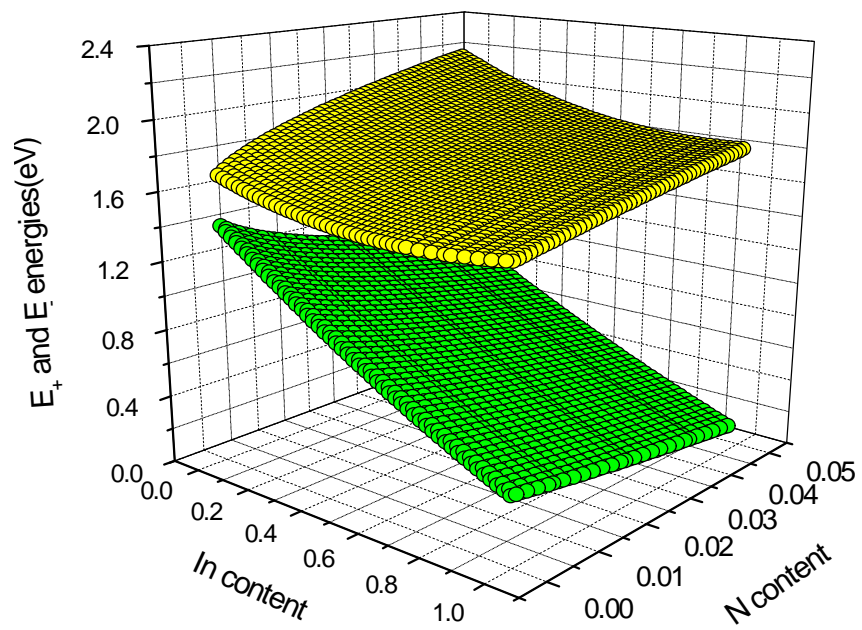


Figure 2.4: The variation of E_+ and E_- versus N and In concentration.

CHAPTER 3

COMPARISON AND ANALYSIS OF THE BAND ALIGNMENT OF STRAINED AND STRAIN-COMPENSATED GaInAsN QWS ON GaAs AND InP SUBSTRATES

3.1 Introduction

Recently, there has been much interest in dilute nitride compound semiconductors of $\text{Ga}_{1-x}\text{In}_x\text{As}_{1-y}\text{N}_y$ since the incorporation of nitrogen in $\text{Ga}_{1-x}\text{In}_x\text{As}$ has a profound influence on the electronic properties of these materials and allows widely extended band structure engineering. Numerous experimental and theoretical work have been published about the $\text{Ga}_{1-x}\text{In}_x\text{As}_{1-y}\text{N}_y$ on GaAs substrates [23, 24, 25, 26]. For laser applications this material system has several important advantages as compared to the most commonly used GaInAsP/InP systems. First of all, a better high temperature performance of the laser structures is achieved due to a larger conduction band offset and, thus, improved electron confinement and decreased electron spill out at room temperature and above, thereby minimizing the threshold current in these lasers. Secondly, the increase of the electron effective mass with the addition of nitrogen provides a close match between the effective mass values for electrons and holes, beneficial for laser applications. Moreover, GaInAsN gives the flexibility of tailoring in the bandgap and an increase in the lattice parameter. Hence GaInAsN gives the potential to produce material lattice matched or mismatched to GaAs with a wide range of bandgap energies (from 1.5 eV to less than 0.8 eV) [27].

GaInAsN alloy also can be grown without any strain on common substrate InP. The addition of nitrogen to lattice-matched or compressively strained GaInAs on InP results in a sizeable reduction of the band gap energy of the resulting InP-based GaInAsN layer, accompanied by a reduction in the lattice constant as it is similar to dilute GaInAsN on GaAs. Some reports [28, 29, 30] demonstrated that strained and lattice-matched $\text{Ga}_{1-x}\text{In}_x\text{As}_{1-y}\text{N}_y$ alloys on InP can also extend the wavelength of photonic device operation beyond that accessible to the $\text{Ga}_{1-x}\text{In}_x\text{As}_{1-y}\text{N}_y/\text{InP}$ system. Increasing In content in $\text{Ga}_{1-x}\text{In}_x\text{As}$ on InP beyond 53% results in a decrease of the band gap energy which, however, is partially offset by increasing compressive strain. Adding N to $\text{Ga}_{1-x}\text{In}_x\text{As}$ reduces the band gap energy even further. Moreover, the incorporation of N compensates for compressive strain in the case of $x > 0.53$ and introduces tensile strain in the case of $x \leq 0.53$, resulting an additional reduction of band gap energy for both cases. There are limited works so far on the growth of strained $\text{Ga}_{1-x}\text{In}_x\text{As}_{1-y}\text{N}_y$ on InP substrates [30, 31, 32, 33, 34, 35, 36] and there is no work about the band alignment of the $\text{Ga}_{1-x}\text{In}_x\text{As}_{1-y}\text{N}_y$ alloys on InP substrates up to our knowledge. Furthermore, only a few studies have been published so far on high indium concentration (beyond 53%) $\text{Ga}_{1-x}\text{In}_x\text{As}_{1-y}\text{N}_y$ on InP [30, 31, 32, 33, 34]. Gokhale et. al [30] demonstrated that strained and lattice-matched GaInAsN alloys on InP can extend the wavelength of photonic device operation beyond that accessible to the GaInAsP/InP system.

Although, the incorporation of nitrogen into GaInAsN allows emission wavelengths as long as $1.55 \mu\text{m}$ to be reached [37], the optical material quality deteriorate significantly with increasing N mole fractions [38], resulting in a much higher threshold current density of GaInAsN/GaAs lasers compared with that of GaInAs/GaAs lasers. In order to improve the performance of GaInAsN/GaAs quantum well lasers, the nitrogen composition of GaInAsN well should be reduced, although, this leads to an increased strain in the quantum wells. By introducing a strain-compensated barrier to this system it is possible to grow highly strained GaInAsN wells free of misfit dislocations. In strain-compensated QWs opposite strains are introduced in the well and barrier regions. These opposite strains balance each other and the average strain in the structure is reduced. In addition, for some laser configurations, such as short cavity lasers or distributed Bragg reflector lasers, a large number of QWs may be required for optimal performance [38]. As the number of strained QWs is increased, the total strain in the structure accumulates and the total strained layer thickness approaches a critical thickness at which lattice misfit dislocations start to form [39]. In strain-compensated QWs, the well width and the total number of wells can thus be increased, leading to an enhanced optical confinement. By means of introducing

strains of opposite signs in the well and barrier layers to simultaneously vary the offsets of the heavy- and light-hole states, it is also possible to reduce the mixing between heavy- and light-hole states by means of spatially separating them to different layers [40]. Experimental results [41, 42] showed that the strain-compensated QW lasers are desirable for optical applications with low threshold current and high efficiency. In addition, strain compensation gives access to a wider range of material composition, and thus improved possibilities to select band-edge offsets tailored to specific needs [43]. Therefore, there has been an interest in strain-compensated quantum well structures.

3.2 The Models

3.2.1 Band anti-crossing model

It has been reported that band anticrossing (BAC) model [44] can describe the composition dependence of band gap energy of GaInAsN on GaAs substrates. The recently proposed model has particular importance since, despite its simplicity, it manages to explain the basic properties of the material and to provide analytical expressions, such as conduction band edge dispersion relations and electron effective mass. The BAC has been successfully used to describe the dependences of the upper and lower subband energies on nitrogen concentration. The model is based on the interaction of the lowest conduction band with the highly localized N-induced energy level E_N , located 1.64 eV above the valence band edge of GaAs.

It has been shown that an anti-crossing interaction of the localized N states with the extended state of GaAs or GaInAs leads to a characteristic splitting of the conduction band into two non-parabolic subbands [45]. The low energy edges of the subbands are given by

$$E_{\pm} = (E_N + E_M \pm [(E_N - E_M)^2 + 4V_{MN}^2]^{1/2})/2 \quad (3.1)$$

where E_M and E_N are the energies of the extended state and of the N level relative to the top of the valence band (VB), respectively. V_{MN} ($= C_{MN}\sqrt{y}eV$) [46], where y is the N composition) is the matrix element of the term describing the interaction between localized N states and the extended states. The predicted splitting of the conduction band into subbands has been confirmed experimentally [45, 44]. The nitrogen level dependence on the nitrogen composition is $E_N = 1.52 - 3.9y$ [17]. The conduction band energy E_M of the matrix semiconductor is taken to vary in the presence of nitrogen as $E_M = E_0 - 1.55y$ where E_0 is the energy in the absence of nitrogen [17]. We have used the band anticrossing

Material	GaAs	GaN	InAs	InP	InN	AlAs
a_e (Å)	5.6533	4.5	6.0584	5.8697	4.98	5.66
E_g (eV)	1.424	3.299	0.417	1.4236	0.78	3.09
Δ_0 (eV)	0.34	0.017	0.39	0.108	0.005	0.28
a_c (eV)	-7.17	-6.71	-5.08	-6.0	-2.65	-5.6
a_v (eV)	-1.16	-0.69	-1.0	-0.6	-0.7	-2.4
C_{11} (Gpa)	1221.0	293.0	832.9	1011.0	187.0	1250.0
C_{12} (Gpa)	566.0	159.0	452.6	561.0	125.0	534.0
b (eV)	-2.0	-2.0	-1.8	-2.0	-1.2	-2.3
$\mathbf{E}_{v,av}$	-6.92	-	-6.67	-7.04	-	-7.49

Table 3.1: Some material parameters which have been used in calculations of band alignment.

model with an interaction parameter of $C_{MN} = 2.3eV$ [34] for indium rich highly strained GaInAsN quantum wells on InP substrates. The interaction parameter is an average value for high indium containing samples taken from Serries et al [33].

For the band structures of laser systems, the material parameters except for the band gap energies are linearly interpolated from those of the binary materials [47] and these are tabulated in 3.1. The bulk band energy of $Ga_{1-x}In_xAs_{1-y}N_y$ is calculated by means of equation 3.1.

3.2.2 Model Solid Theory

The relative band alignment of the band edges between quantum well and barrier is the total band discontinuity distributed over the conduction and valence bands, ΔE_c and ΔE_v , respectively. The band discontinuity depends on the semiconductors and the amount of mismatch strain at the interface. It has been commonly accepted that the nitrogen incorporation mainly affects the conduction band states of the GaInAsN alloys leading to an increase in the conduction band offset Q_c , and a small discontinuity in the valence band edge [48]. According to Van de Walle's model solid theory [49] the band offset ratio for conduction and valence band, $Q_{c,v}$, is determined by discontinuity fractions of $\Delta E_{c,v}/\Delta E_g$. The energy of the potential barrier, ΔE_g is determined from the difference between the bulk bandgap energy of the barrier layers and the strained bandgap energy of the active layer. The effects of strain in the plane of the epitaxial growth is calculated as

$$\varepsilon = \frac{a_s - a_e}{a_e} \quad (3.2)$$

where a_s is the lattice constant of substrate and a_e is the lattice constant of quaternary epitaxial layer. The conduction band position can be calculated by simply adding the strained bandgap energy to the valence band position. The unstrained valence band-edge of the active region material is set as the reference energy of zero. The valence band position is given by

$$E_v(x, y) = \begin{cases} E_{v,av}(x, y) + \frac{\Delta_0(x, y)}{3} + \delta E_{hh}(x, y), & \text{for hh (compressive strain)} \\ E_{v,av}(x, y) + \frac{\Delta_0(x, y)}{3} + \delta E_{lh}(x, y), & \text{for lh (tensile strain)} \end{cases} \quad (3.3)$$

where $E_{v,av}(x, y)$ is the average valence subband energy and Δ_0 is the spin-orbit split-off band energy. These values are obtained by linear interpolation method where the binary values are listed in 3.1. The conduction band is shifted by the energy $\delta E_c(x, y)$

$$\delta E_c(x, y) = 2a_c \left(1 - \frac{C_{12}}{C_{11}}\right) \varepsilon \quad (3.4)$$

the valence bands are shifted by energy, $\delta E_{hh}(x, y)$ and $\delta E_{lh}(x, y)$

$$\begin{aligned} \delta E_{hh}(x, y) &= -P_s - Q_s \\ \delta E_{lh}(x, y) &= -P_s + Q_s \end{aligned} \quad (3.5)$$

where

$$\begin{aligned} P_s &= -2a_v \left(1 - \frac{C_{12}}{C_{11}}\right) \varepsilon \\ Q_s &= -b \left(1 + \frac{2C_{12}}{C_{11}}\right) \varepsilon \end{aligned} \quad (3.6)$$

where a_c and a_v are the conduction- and valence-band hydrostatic deformation potentials, b is the valence band shear deformation potential and C_{11} and C_{12} are elastic stiffness constants. The strained band gaps can then be expressed as

$$\begin{aligned} E_{c-hh}(x, y) &= E_g(x, y) + \delta E_c(x, y) - \delta E_{hh}(x, y) \\ E_{c-lh}(x, y) &= E_g(x, y) + \delta E_c(x, y) - \delta E_{lh}(x, y) \end{aligned} \quad (3.7)$$

The conduction band position is

$$E_c(x, y) = \begin{cases} E_v(x, y) + E_{c-hh}(x, y), & \text{for hh (compressive strain)} \\ E_v(x, y) + \delta E_{c-lh}(x, y), & \text{for lh (tensile strain)} \end{cases} \quad (3.8)$$

The conduction band offset is given by

$$\frac{\Delta E_c}{\Delta E_g} = 1 - \frac{E_v^w - E_v^b}{E_g^b - E_g^w} \quad (3.9)$$

where E_v^w and E_v^b are the valence band positions in the well and barrier materials, respectively, and E_g^w and E_g^b are the strain adjusted bandgaps (E_{c-hh} , for compressive strain and E_{c-lh} , for tensile strain) for the well and barrier materials.

3.3 Comparison of the band alignment of strained and strain- compensated GaInAsN QWs on GaAs and InP substrates

In this work we concentrate on the relative band alignment of the band edges of $\text{Ga}_{1-x}\text{In}_x\text{As}_{1-y}\text{N}_y/\text{InP}$ between the quantum well and the barrier which is very important for modelling semiconductor quantum well structures. We will present the results in the case of tensile strained $\text{Ga}_{1-x}\text{In}_x\text{As}_{1-y}\text{N}_y$ quantum wells with In concentrations of $x \leq 0.53$ which provides the possibility of reaching TM mode emission at $1.55 \mu\text{m}$ and above in telecommunication band which is difficult to reach with standard InGaAsP strained QW structures [36]. The GaInAsN/InP system combined with confinement layers, such as InAsP, could lead to the fabrication of tensile strained QW lasers as well as the development of optical isolators requiring TM polarization [28, 29].

Furthermore, this work investigates how the unique features of GaInAsN/GaAs and GaInAsN/InP quantum wells offer the best band alignment by means of using model solid theory. We also investigate the effect of the strain compensation on the band-alignments for the GaInAsN on GaAs and InP substrates. These calculations provide the first clear comparison of the strain-compensated band-alignment of the GaInAsN on two common substrates as a laser system and will enable us to predict the effect of the strain-compensation on band-offset energies for quantum well laser structures. For the band structures of laser systems, the material parameters except for the band gap energies are linearly interpolated from those of binary materials [47, 50].

3.3.1 GaInAsN/GaAs/GaAs

We first present the band alignment of $\text{Ga}_{1-x}\text{In}_x\text{As}_{1-y}\text{N}_y$ on GaAs substrates, which we consider to be a reference necessary for the understanding of the following results derived for low In containing $\text{Ga}_{1-x}\text{In}_x\text{As}_{1-y}\text{N}_y$ on InP substrates. Figure 3.1 presents the calculated band offset ratios (Q_c and Q_v) and band offsets (ΔE_c and ΔE_v) for uncompensated compressively strained $\text{Ga}_{0.70}\text{In}_{0.30}\text{N}_y\text{As}_{1-y}$ quantum wells with GaAs barriers on GaAs substrates. The addition of N to GaInAs causes substantial changes in the band alignments; adding N to GaInAs

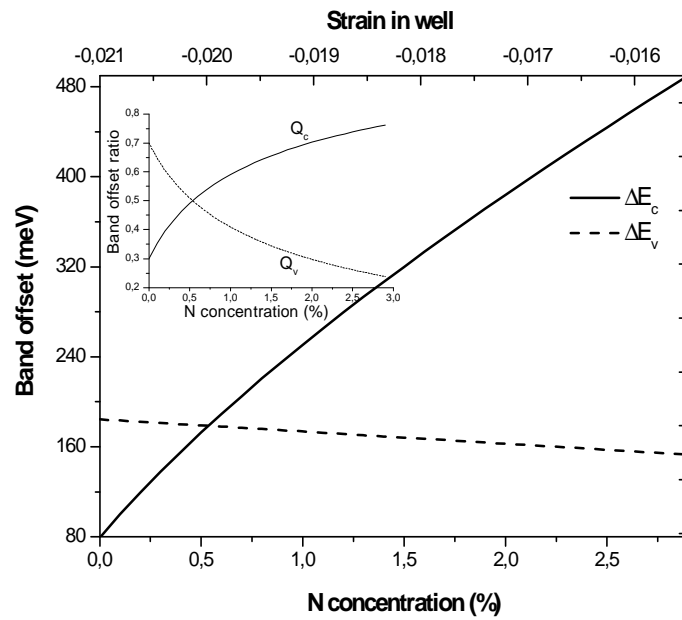


Figure 3.1: The nitrogen N concentration (in well) dependence of the conduction and valence band offset ratios, Q_c and Q_v , (inset figure) and the corresponding conduction and valence band offsets, ΔE_c and ΔE_v , of the uncompensated compressively strained $\text{Ga}_{0.70}\text{In}_{0.30}\text{N}_y\text{As}_{1-y}$ quantum wells with GaAs barriers on GaAs substrates.

increases the conduction band offset ratio Q_c and decreases the valence band offset ratio Q_v . At first a rapid and then a gradual change in band offset ratios have been calculated.

The corresponding band offsets are also shown in figure 3.1 which illustrates the fact that the addition of nitrogen into GaInAs leads the N-containing system having a band alignment of that of the ideal case (deep conduction- and shallow valence-wells) certainly. On the other hand, the addition of nitrogen deteriorates laser parameters, so one should keep the N composition as low and low N leads high strains. So strain compensation can be offered as a solution in this novel material system and this can be achieved by means of using GaAsP barriers instead of GaAs barriers.

3.3.2 GaInAsN/GaAsP/GaAs

Figure 3.2 illustrates the effect of compensation of the compressive strain in the well by means of applying tensile strain in the barrier. The well is

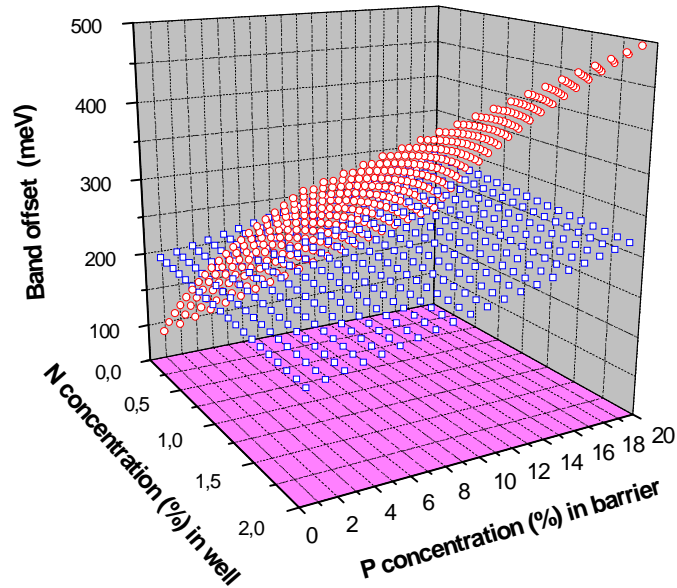


Figure 3.2: The variation of conduction (upper curve) and valence (lower curve) band offsets, ΔE_c and ΔE_v , with nitrogen concentration which results compressive strain (in well) for $\text{Ga}_{0.70}\text{In}_{0.30}\text{N}_y\text{As}_{1-y}$ quantum wells and with phosphorus concentration which results tensile strain (in barrier) for compensated $\text{Ga}_{0.70}\text{In}_{0.30}\text{N}_y\text{As}_{1-y} / \text{GaAsP}$ quantum wells on GaAs substrates.

$\text{Ga}_{0.70}\text{In}_{0.30}\text{N}_y\text{As}_{1-y}$ and the barrier is $\text{GaAs}_{1-x}\text{P}_x$ and compressive strain in the well / tensile strain in the barrier is varied by means of increasing nitrogen N concentration in well / phosphorus P concentration in barrier, correspondingly,

see figure 3.2. The uncompensated system corresponds to zero P concentration in the barrier. Upper curve represent the variation of the conduction band offset ΔE_c and lower curve represent the valence band offset ΔE_v with nitrogen concentration in well and phosphorus concentration in barrier, correspondingly, for $\text{Ga}_{0.70}\text{In}_{0.30}\text{N}_y\text{As}_{1-y}$ quantum well. First, it should be noticed from the variations of figure 3.2 that ΔE_v (lower curve) decreases and ΔE_c (upper curve) increases with increasing N concentration.

It should also to be noted from figure 3.2 that strain compensation by means of using GaAsP barriers instead of GaAs barriers improves the band alignment since ΔE_c further increases with an increase of P concentration in barrier. As an overall, by means of strain compensation, i.e. the increase of P concentration in barrier, it is possible to get deeper wells, leading to much better confinement both in conduction and valence band. Therefore, strain compensation improves the band alignment and brings great advantageous to this laser system of $\text{Ga}_{1-x}\text{In}_x\text{As}_{1-y}\text{N}_y$ on GaAs substrates.

3.3.3 InGaAs/InP/InP

We now want to compare the band alignment of $\text{Ga}_{1-x}\text{In}_x\text{As}_{1-y}\text{N}_y$ QWs on GaAs substrates with that of the InP substrates. It is well known that the $\text{Ga}_{1-x}\text{In}_x\text{As}$ can be grown lattice matched to InP for $x = 0.535$. Lowering the indium content or introducing N into the $\text{Ga}_{1-x}\text{In}_x\text{As}$ induces a tensile strain. A sufficiently high tensile strain will lead the light-hole, lh , band being above that of the heavy-hole, hh , band. So fundamental transition will be due to $c1 - lh1$ giving rise a TM-mode polarization emission. There are some reports [51, 52, 53, 54] which emphasize the potential advantages of tensile strained QW lasers in terms of threshold current density, radiative characteristics, gain and loss mechanisms. Therefore, it is interesting to investigate the band alignment of $\text{Ga}_{1-x}\text{In}_x\text{As}_{1-y}\text{N}_y$ quantum wells under tensile strain grown on an InP substrate for $1.5 - 1.6 \mu\text{m}$ emission wavelength.

We present the band alignment of conventionally tensile strained $\text{Ga}_{1-x}\text{In}_x\text{As}$ wells with unstrained InP barriers, as shown in figure 3.3, according to the model solid theory. As can be seen from figure 3.3, the valence band offset ratio Q_v is greater than that of the conduction band offset ratio Q_c which is not desirable for high temperature operation. It is seen from figure 3.3 that lowering In concentration of tensile strained $\text{Ga}_{1-x}\text{In}_x\text{As}$ alloy decreases both conduction and valence band offset at the expense of increasing the tensile strain in the well. In addition, the valence band offset ΔE_v is greater than the conduction band offset ΔE_c .

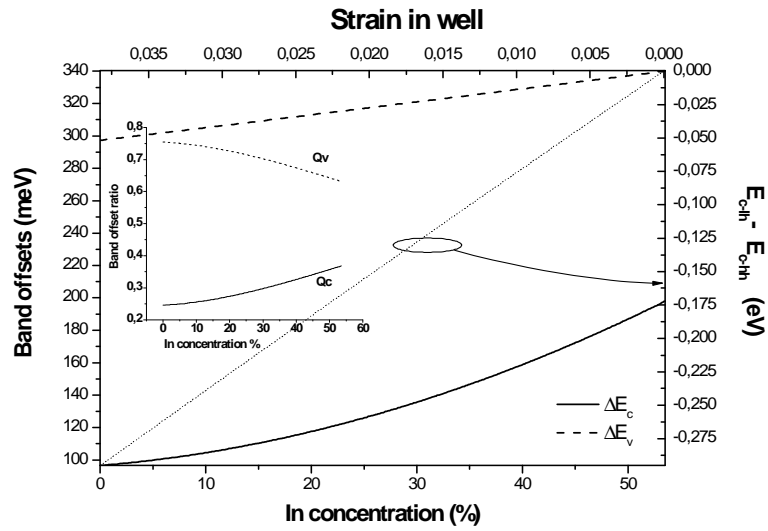


Figure 3.3: The indium concentration (in well) dependence of the conduction and valence band offset ratios, Q_c and Q_v , (inset figure) and the corresponding the conduction and valence band offsets, ΔE_c and ΔE_v , of the tensile strained uncompensated $\text{In}_x\text{Ga}_{1-x}\text{As} / \text{InP}$ QW laser system on InP substrates. RHS of the y-axis shows the energy difference between the transition energies of $c_1 - lh_1$ and $c_1 - hh_1$ from the respective band edges.

The right-hand-side of the y -axis of figure 3.3 shows the energy difference between the transition energies of $c_1 - lh_1$ and $c_1 - hh_1$ from the respective band edges. The negative energy difference shows that the polarization transition is TM since light-hole band lies above the heavy-hole band.

3.3.4 GaInAsN/InP/InP

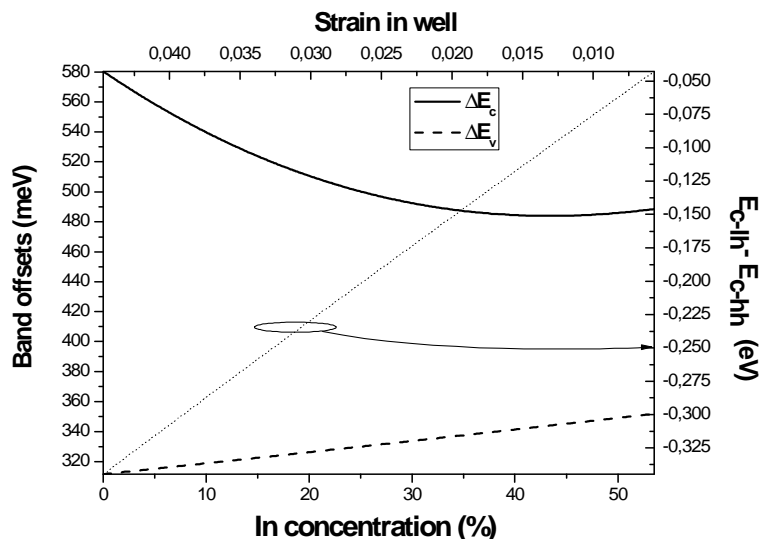


Figure 3.4: The variation of the conduction and valence band offsets, ΔE_c and ΔE_v , with indium concentration and tensile strain (in well) for uncompensated $\text{Ga}_{1-x}\text{In}_x\text{N}_{0.02}\text{As}_{0.98}$ /InP QWs on InP substrates. RHS of the y -axis shows the energy difference between the transition energies of $c_1 - lh_1$ and $c_1 - hh_1$ from the respective band edges.

The introduction of N to the well of $\text{Ga}_{1-x}\text{In}_x\text{As}$ improves the band alignment on InP substrate significantly ; ΔE_c becomes greater than ΔE_v as shown in figure 3.4. The nitrogen concentration is held fixed at 2.5%. It is clear from figure 3.4 that increases rapidly and ΔE_v decreases with decreasing In concentration, i.e. by means of increasing tensile strain in the QW.

The comparison of figure 3.4 with that of figures 3.1-3.3 reveals the fact that tensile strained $\text{Ga}_{1-x}\text{In}_x\text{As}_{1-y}\text{N}_y$ quantum wells on InP substrates have a deeper conduction well than that of the compressively strained $\text{Ga}_{1-x}\text{In}_x\text{As}_{1-y}\text{N}_y$ quantum wells on GaAs substrates.

3.3.5 GaInAsN/InAsP/InP

In order to have much deeper conduction wells than that of the valence band one should keep the In concentration as low as possible, and this leads to the problem of the critical thickness due to the high tensile strain in the well. Therefore we consider a strain compensated laser device of GaInAsN/InAsP/InP;

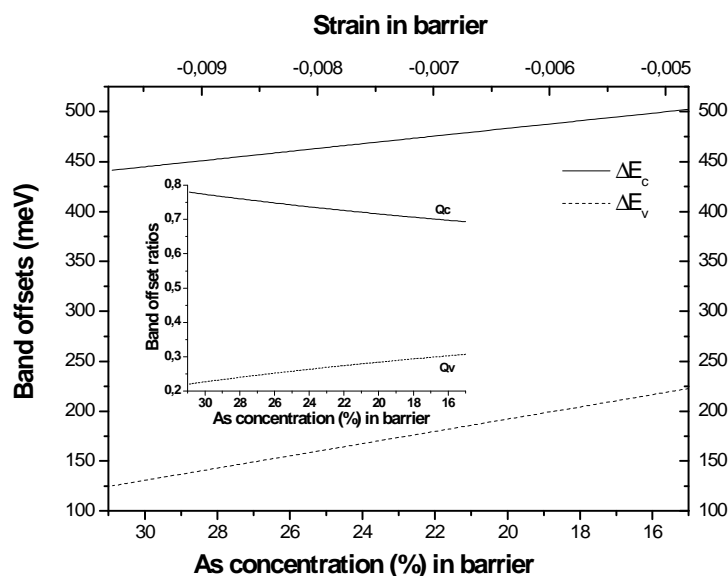


Figure 3.5: The calculated variation of the conduction and valence band offsets, ΔE_c and ΔE_v , with arsenide concentration and compressive strain (in barrier) for compensated $\text{Ga}_{0.90}\text{In}_{0.10}\text{N}_{0.03}\text{As}_{0.97} / \text{In}_x\text{As}_{1-x}\text{P} / \text{InP}$ laser system.

the well composition is held fixed with a 10% In and 3% N and the arsenide concentration of the barrier of InAsP is varied. This results a compressive strain in the barrier to compensate the tensile strain in the well. Figure 3.5 illustrates the effect of the strain compensation on the band alignment for this laser system; the valence band offset ratio Q_c is being greater than that of the conduction band offset ratio Q_v for the stated range of As concentration and both ΔE_c and ΔE_v increases with increasing As concentration. It is seen from figure 3.5 that compensation decreases the Q_c and increases the Q_v value. Therefore the compensation can be thought as to bring disadvantageous to this laser system. Fortunately, this is not the case. Although Q_c and Q_v show opposite trend with compensation, both conduction- and valence-band offsets increases with compensation, as shown in figure 3.5.

This strange behaviour of the increase of Q_v with decreasing Q_c can be explained as follows; the variation of the conduction band offset is a result of

the combined effect of the variation of Q_c and ΔE_g since $\Delta E_c = Q_c \Delta E_g$ and ΔE_g is the difference of the strained bandgap of the barrier and well. The rapid increase in with As concentration eliminates the effect of the decrease in Q_c with increasing As concentration and as an overall results an increase in ΔE_c with increasing As concentration. So compensation again can be considered a solution to balance the tensile strain in the well of GaInAsN alloy on InP substrates as in the case GaAs substrates.

3.4 Analysis of the band alignment of highly strained indium-rich GaInAsN QWs on InP substrates

We concentrate on the band alignment of indium rich highly compressively strained GaInAsN quantum wells on InP substrates which allows an emission wavelength of $2.3 \mu m$ by means of using the model solid theory. Our chosen structures will be those of the structures proposed by Köhler et. al [34] who demonstrated that long wavelength emission beyond $2 \mu m$ can be achieved by means of $\text{Ga}_{0.22}\text{In}_{0.78}\text{N}_{0.01}\text{As}_{0.99}$ well with lattice-matched $\text{In}_{0.52}\text{Al}_{0.48}\text{As}$ barriers and $\text{Ga}_{0.22}\text{In}_{0.78}\text{N}_{0.01}\text{As}_{0.99}$ well with lattice-matched $\text{Al}_{0.15}\text{Ga}_{0.32}\text{In}_{0.53}\text{As}$ barrier quantum well laser structures.

3.4.1 InGaAs/InP/InP

We first present the band alignment of nitrogen free $\text{Ga}_{1-x}\text{In}_x\text{As}$ QW on InP substrate in order to provide a comparison of the band alignment of indium rich highly compressively strained $\text{Ga}_{1-x}\text{In}_x\text{As}_{1-y}\text{N}_y$ QWs on InP substrates by means of model solid theory. Figure 3.6 presents the band alignment of $\text{Ga}_{1-x}\text{In}_x\text{As}$ with InP barrier. As can be seen from Figure 3.6, the valence band offset ratio Q_v is greater than that of the conduction band offset ratio Q_c for the whole range of the indium concentration which is not desirable for high temperature operation. It is seen from figure 3.6 that increasing indium concentration of unstrained and strained $\text{Ga}_{1-x}\text{In}_x\text{As}$ alloy increases the conduction- and decreases the valence-band offset ratio. The $\text{Ga}_{1-x}\text{In}_x\text{As}$ alloy on InP substrate is compressively strained in the case of $x > 0.53$ and tensile strained in the case of $x < 0.53$.

The rate of change band offset ratio is different for tension and compression. It is also seen from figure 3.6 that valence band offset ΔE_v is being greater than that of the conduction band offset ΔE_c for the whole range of indium

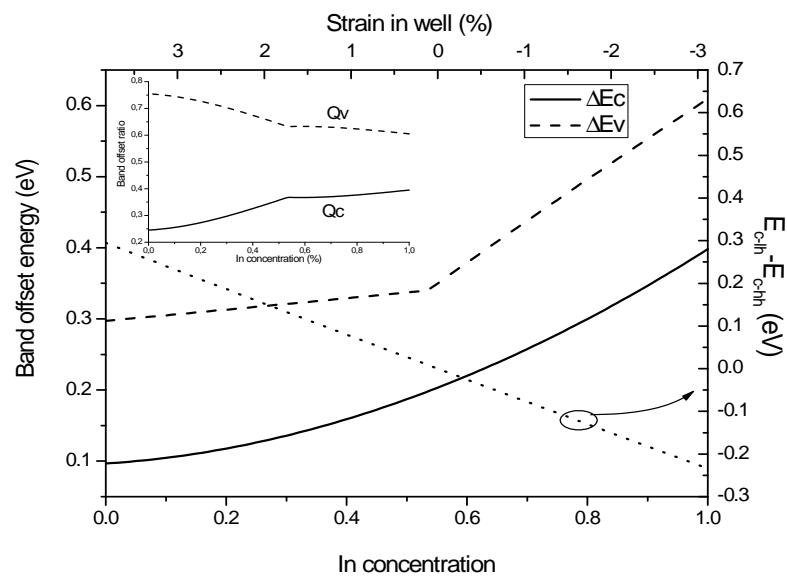


Figure 3.6: The indium concentration dependence of the conduction and valence band offset ratios, Q_c and Q_v , (inset figure) and the corresponding conduction and valence band offsets, ΔE_c and ΔE_v , of the strained $\text{Ga}_{1-x}\text{In}_x\text{As}$ quantum wells with InP barriers on InP substrates.

concentrations. Similar calculations have been obtained using lattice-matched GaInAsP and InGaAlAs barriers. It should be noticed from figure 3.6 that the wells get deeper in the case of the compressive strain ($x > 0.53$) than that of the tensile strain ($x < 0.53$). In addition, although Q_v and Q_c show opposite trend, see figure 3.6, with an increase in indium concentration both conduction- and valence-band offsets increase with indium concentration. This strange behaviour of the increase of ΔE_v with decreasing Q_v can be explained as follows; the variation of the valence band offset ΔE_v is a result of the combined effect of the variation of the valence band offset ratio Q_v and the difference of strained band gap of the well and barrier ΔE_g according to $\Delta E_v = Q_v \Delta E_g$. The rapid increase in with indium concentration eliminates the effect of the decrease in Q_v with increasing indium concentration and results an increase in ΔE_v with increasing indium concentration as an overall. The right-hand-side of the y -axis of figure 3.6 shows the energy difference between the transition energies of $c1 - lh1$ and $c1 - hh1$ from the respective band edges. The negative energy difference shows that the polarization transition is TM since light-hole (lh) band lies above the heavy-hole (hh) band for tensile strain whereas the positive energy difference shows that the polarization transition is TE since heavy -hole band lies above the light -hole band for compressive strain.

3.4.2 GaInAsN/InP/InP

We want to illustrate at this point how the introduction of N to the well of $\text{Ga}_{1-x}\text{In}_x\text{As}$ containing more than 53% indium improves significantly the band alignment on InP substrate with InP barriers holding the N concentration being greater than 1.5%. As shown in figure 3.7, ΔE_c increases quickly whereas ΔE_v increases slightly with N concentration and ΔE_c becomes greater than ΔE_v when $N > 1.5\%$.

It is also seen from figure 3.7 that both wells get deeper with increasing indium concentration. Therefore, in order to achieve long wavelength emission of $2.3 \mu\text{m}$ and more by means of growing GaInAsN on InP with an indium concentration being greater than 0.535, one should keep the $N > 1.5\%$ from the band alignment point of view to have high temperature characteristics.

3.4.3 GaInAsN/InAlAs/InP

Köhler et. al [6] demonstrated the growth of $\text{Ga}_{0.22}\text{In}_{0.78}\text{N}_{0.01}\text{As}_{0.99}$ wells with two different lattice-matched barriers of $\text{In}_{0.52}\text{Al}_{0.48}\text{As}$ and $\text{Al}_{0.15}\text{Ga}_{0.32}\text{In}_{0.53}\text{As}$ for long wavelength emission up to $2.3 \mu\text{m}$. Figure 3.8 shows our calculated results of the band alignment of $\text{Ga}_{0.22}\text{In}_{0.78}\text{N}_y\text{As}_{1-y}$ well with $\text{In}_{0.52}\text{Al}_{0.48}\text{As}$ bar-

riers. As can be seen from figure 3.8, ΔE_c is slightly greater than ΔE_v for the low values of nitrogen. ΔE_c increases rapidly and ΔE_v decreases slowly with an increase of nitrogen and the difference gets bigger for larger nitrogen concentrations.

3.4.4 GaInAsN/AlGaInAs/InP

Figure 3.9 shows the band alignment of the same QW with a lattice-match quaternary barrier of $\text{Al}_{0.15}\text{Ga}_{0.32}\text{In}_{0.53}\text{As}$. It can be seen from figure 3.9 that ΔE_c becomes smaller than ΔE_v in the case of the quaternary barrier for low nitrogen concentrations. This brings a disadvantage for the confinement of electrons and results poor temperature characteristics. Therefore, the ternary barrier should be preferred compared to the quaternary barrier. On the other hand, conduction band offset gets deeper with increasing N concentration in both laser structures of ternary and quaternary barriers.

We would like to point out at this point that, figure 3.8 illustrates how the band alignment of the growth of GaInAsN QW containing more than 53% indium with lattice matched $\text{In}_{0.52}\text{Al}_{0.48}\text{As}$ barriers on InP substrates compete with the unique band alignment of GaInAsN quantum wells on GaAs substrates. Therefore, $\text{Ga}_{0.22}\text{In}_{0.78}\text{N}_{0.01}\text{As}_{0.99}$ well with $\text{In}_{0.52}\text{Al}_{0.48}\text{As}$ barrier on InP substrates can be offered as a laser system having the ideal band alignment.

3.4.5 InGaAs/InAlAs/InP

We now show how the incorporation of nitrogen into GaInAs with lattice-matched $\text{In}_{0.52}\text{Al}_{0.48}\text{As}$ barrier brings the system having an ideal band alignment although nitrogen free counterpart doesn't have an ideal band alignment. For nitrogen free $\text{Ga}_{1-x}\text{In}_x\text{As}$ QW with $\text{In}_{0.52}\text{Al}_{0.48}\text{As}$ barrier both conduction- and valence-wells have similar depths as shown in figure 3.10. The introduction of nitrogen into $\text{Ga}_{1-x}\text{In}_x\text{As}$ reduces the energy band gap significantly causing the system having a band alignment of that of the ideal case.

Figure 3.11 compares the substrate dependence of strain as a function of nitrogen and indium concentration in $\text{Ga}_{1-x}\text{In}_x\text{As}_{1-y}\text{N}_y$ QW on GaAs and InP substrates. Compressive strain decreases with increasing nitrogen concentration whereas it increases with increasing indium concentration for both substrates of GaAs and InP.

This figure reveals the fact that the growth of indium rich $\text{Ga}_{1-x}\text{In}_x\text{As}_{1-y}\text{N}_y$ QW can only be possible on InP substrates since high indium results very high values of the compressive strain in the case of GaAs substrates. This leads to

the problem of the critical thickness due to the high compressive strain in the well.

3.5 Conclusions

The design of GaInAsN based devices requires a deep knowledge of the alloy's electronic properties and a development of accurate models. Band alignment of the QWs is one of the important properties while modelling the QW structures since this property determines the high temperature performance of the laser structures. Therefore, first part of this work presents theoretical calculations to compare the band alignments of the N-free and N-included laser devices on GaAs and InP substrates emitting in the neighborhood of 1.3 μm and 1.6 μm . Our calculations indicate that the band alignment of the N-based conventionally strained QW laser systems on InP is better than that of the GaAs substrate and both substrates provide deeper conduction wells. Therefore, tensile strained $\text{Ga}_{1-x}\text{In}_x\text{As}_{1-y}\text{N}_y$ quantum wells with In concentrations of $x \leq 0.53$ on InP substrates can be used safely from the band alignment point of view when TM polarization is required. The introduction of opposite strain to the barrier in N-based lasers on both GaAs and InP substrates not only result deep electron wells but also cause the electron wells being much deeper than that of the hole wells which is essential to have good high temperature characteristics. Therefore, these calculations enlighten the intrinsic superiority of N-based lasers and offer conventionally strained the strain-compensated N-based laser system on GaAs and InP substrates as ideal candidates for high temperature operation.

It has been stated [30, 31, 32, 33, 34] that long wavelength emission of 2.3 μm can be achieved by means of growing GaInAsN on InP keeping the indium concentration being greater than 0.535 which results compressive strain in conjunction with typical 1 – 2 % N to compensate the excess strain plus additionally lowering the band gap energy. In second part of this work we examine the band alignment of these long wavelength laser systems of which no work has been reported up to our knowledge. Our calculations indicate that the band alignment of N-based conventionally strained QW laser systems on InP with high indium concentration (beyond 53%) compete with the ideal band alignment of GaInAsN / GaAs lasers. Therefore, compressively strained $\text{Ga}_{1-x}\text{In}_x\text{As}_{1-y}\text{N}_y$ quantum wells with indium concentrations of $x > 0.53$ on InP substrates can be used safely from the band alignment point of view when long wavelength emission of 2.3 μm is required.

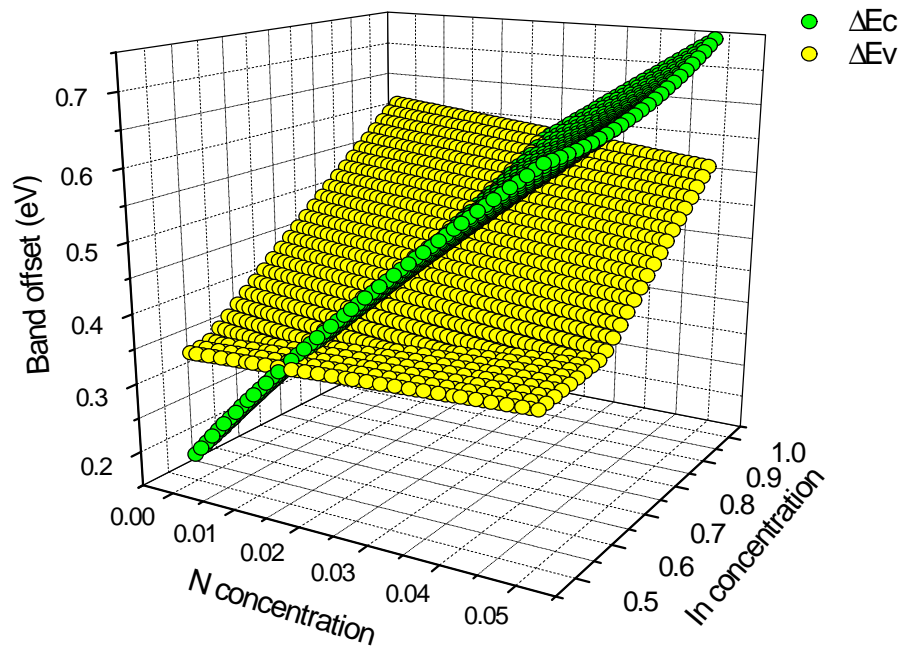


Figure 3.7: The variation of conduction and valence band offsets, ΔE_c and ΔE_v , with nitrogen and indium concentration for compressively strained $\text{Ga}_{1-x}\text{In}_x\text{N}_y\text{As}_{1-y}$ quantum wells with InP barrier and InP substrate

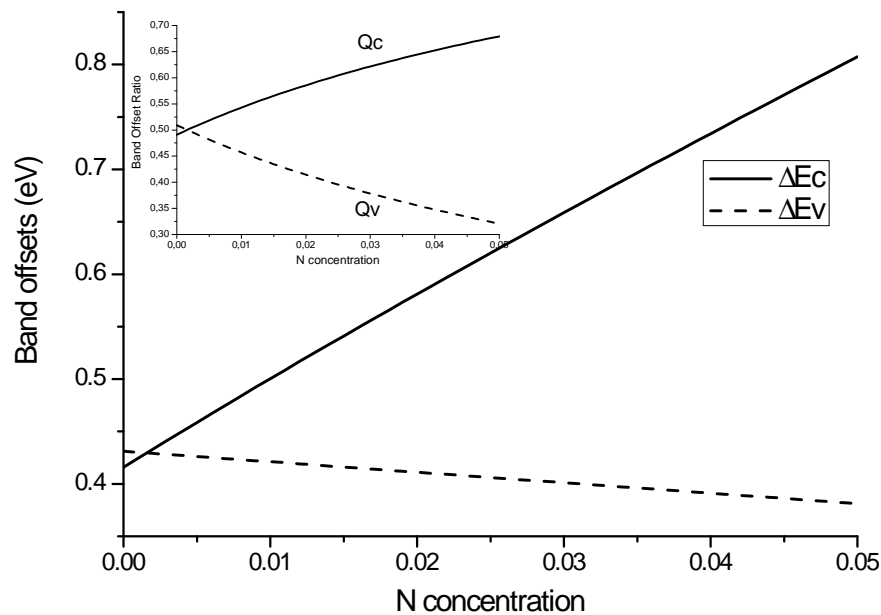


Figure 3.8: The nitrogen concentration dependence of conduction and valence band offset ratios, Q_c and Q_v , (inset figure) and the corresponding conduction and valence band offsets, ΔE_c and ΔE_v , of the compressively strained $\text{Ga}_{0.22}\text{In}_{0.78}\text{N}_y\text{As}_{1-y}$ well with $\text{In}_{0.52}\text{Al}_{0.48}\text{As}$ barriers QW laser system on InP substrates.

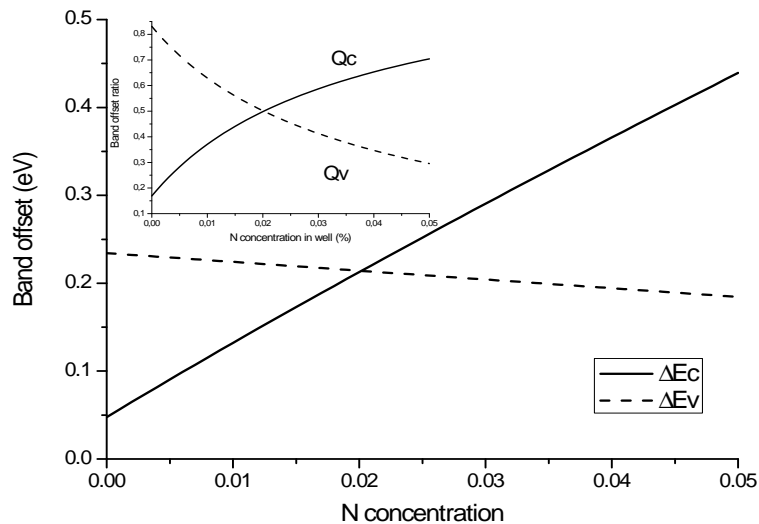


Figure 3.9: The calculated results of the nitrogen concentration dependence of conduction and valence band offset ratios, Q_c and Q_v , (inset figure) and the corresponding the conduction and valence band offsets, ΔE_c and ΔE_v , of the compressively strained $\text{Ga}_{0.22}\text{In}_{0.78}\text{N}_y\text{As}_{1-y}$ well with $\text{Al}_{0.15}\text{Ga}_{0.32}\text{In}_{0.53}\text{As}$ barriers QW laser system on InP substrates.

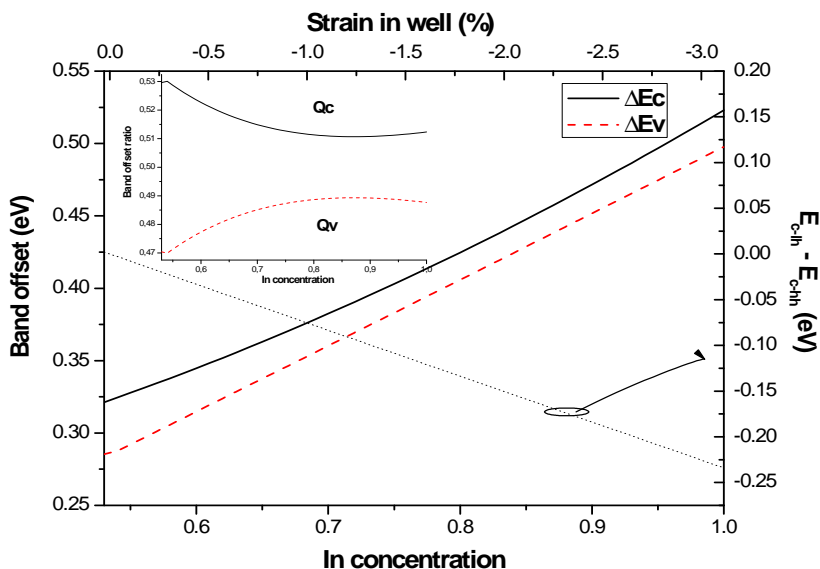


Figure 3.10: The indium concentration dependence of conduction and valence band offset ratios, Q_c and Q_v , (inset figure) and the corresponding the conduction and valence band offsets, ΔE_c and ΔE_v , of the nitrogen free compressively strained $\text{Ga}_{1-x}\text{In}_x\text{As}$ well with $\text{In}_{0.52}\text{Al}_{0.48}\text{As}$ barrier QW laser system on InP substrates.

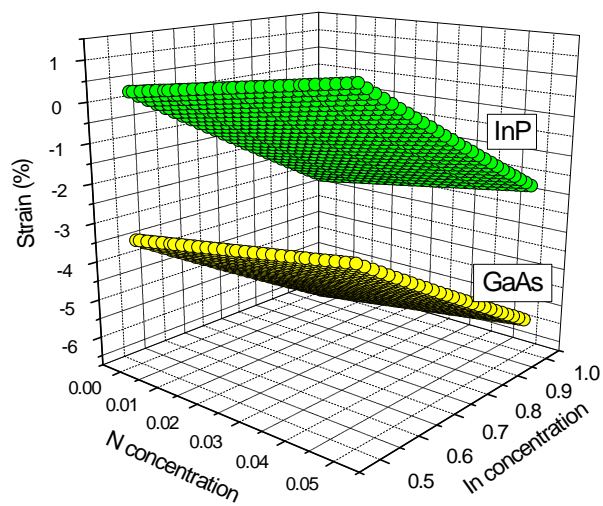


Figure 3.11: The comparison of the substrate dependence of strain as a function of nitrogen and indium concentration in $\text{Ga}_{1-x}\text{In}_x\text{N}_y\text{As}_{1-y}$ QW.

CHAPTER 4

CRITICAL LAYER THICKNESS OF GAIN(N)AS(SB) QWS ON GAAS AND INP SUBSTRATES FOR (001) AND (111) ORIENTATIONS

4.1 Introduction

The rapid growth of optical communication networks in the last decade has created a significant demand for low-cost, high-performance semiconductor laser sources for the 1.3 μm and 1.55 μm wavelength regimes. Currently, only the 1.3 μm InGaAsP/InP vertical-cavity surface-emitting diode lasers (VCSELs) seem to close to a commercial availability [55] for the wavelength (1.3 μm and 1.5 μm) optical fibre communication. However, the manufacturing of InGaAsP/InP VCSELs is too expensive and troublesome to become lasing carrier sources in the mass optical-fibre communication. On the other hand, GaAs-based devices are regarded as extremely reliable; their technology is well known and relatively simple. Therefore, much research has been devoted to creating long-wavelength VCSELs on GaAs substrates to leverage the mature AlAs oxidation techniques [56] as well as the large refractive index contrast of GaAs/AlGaAs distributed Bragg reflectors. The GaInAsN material system has generated the most interest as an active material for long-wavelength VCSELs on GaAs substrates primarily because of the large band gap bowing which results from adding relatively small amounts, 1% of nitrogen N [57]. Many researchers have demonstrated 1.3 μm VCSELs using GaInAsN as the active material [58]. However, there are still essential problems to reach 1.55 μm emission with these devices. To achieve such a long wavelength emission with GaInAsN/GaAs QWs, the indium concentration should exceed 38% with the high N concentration of about 5%. Because of different crystal structures of GaInN and InGaAs, small sizes of N atoms compared

with arsenide As ones and the high electronegativity [59], such a high N concentration leads to creation of many nonradiative centres in the active layer which essentially makes reaching lasing threshold difficult. On the other hand, some In segregation, disordering a layer growth and optical degradation of a semiconductor crystal, would follow it. This problem can be overcome in new quinary QW system of GaInAsNSb/GaNAs [59]. It has been recently shown by several groups that the addition of antimonite Sb to the GaInAsN system extends the QW emission wavelength up to $1.55 \mu m$. The photoluminescence properties of $1.5 \mu m$ range GaInAsNSb/GaNAs QWs are quite comparable to the $1.3 \mu m$ QWs, revealing the positive effect of Sb on improving the optical quality of the QWs. Incorporating Sb to form a quinary GaInAsNSb alloy enables an essential improvement in the quality of semiconductor layers for over $1.5 \mu m$ emission because Sb (*i*) acts as a surfactant, improving the surface kinetics thus maintaining two-dimensional growth under high surface stress, (*ii*) incorporates into the lattice of GaInAsN, shrinking the band gap, and (*iii*) enhances the differential gain of a laser. All these effects indicate that a quinary QW might be suitable for $1.4 - 1.5 \mu m$ lasers. In addition, it has been shown that the surfactant effect of Sb in the GaInAsN system [60] enables the growth of GaInAsN quantum wells QWs beyond the calculated critical thickness [61]. The surfactant properties of Sb have also enabled the growth of coherently strained QWs with higher In compositions, 40% which are necessary for reaching the $1.55 \mu m$ wavelength range [62].

Most attention to date has been focused on $Ga_{1-x}In_xAs_{1-y}N_y$ quantum wells (QWs) on GaAs substrates. Recently, some reports [29, 30] demonstrated that strained and lattice-matched $Ga_{1-x}In_xAs_{1-y}N_y$ alloys on InP can also extend the wavelength of photonic device operation beyond that accessible to the $Ga_{1-x}In_xAs_{1-y}N_y / GaAs$ and $InGaAsP / InP$ system [30]. Increasing In concentration in $In_xGa_{1-x}As$ on InP beyond 53% results in a decrease of the band gap energy which, however, is partially offset by increasing compressive strain. Adding N to $In_xGa_{1-x}As$ reduces the band gap energy even further. Moreover, the incorporation of N compensates for compressive strain in the case of $x > 0.53$ and introduces tensile strain in the case of $x \leq 0.53$, resulting an additional reduction of band gap energy for both cases. It has been stated that tensile strained $Ga_{1-x}In_xAs_{1-y}N_y$ quantum wells with In concentrations of $x \leq 0.53$ provides the possibility of reaching TM mode emission at $1.55 \mu m$ and above in telecommunication band which is difficult to reach with standard InGaAsP strained QW structures [36]. GaInAsN/InP system combined with confinement layers, such as InAsP, could lead to the fabrication of tensile strained QW lasers as well as the development of optical isolators requiring TM polarization [28, 29].

In addition, GaInAsN on InP have been proposed as an optical source for spectroscopy instead of the InGaAsP material system [32].

It is known that the molecular beam epitaxy growth of strained zincblende materials on $\{111\}$ orientation shows some interesting properties. In particular, strained QWs grown in these orientations are piezoelectric [63] such that their optical transitions are red-shifted relatively to the (001) ones. The $\{111\}$ strained layers also show larger critical thicknesses for strain relaxation compared to (001) oriented ones [64]. These two properties make it possible achievement of strained QWs emitting at longer wavelength than for (001). Blanc et al [65] has shown that the growth orientation has a great influence on the structural and optical characteristics of N diluted alloys, and the use of alternative growth orientations could help to get a better insight into the peculiar properties of these materials, which open a new challenge to GaAs optoelectronics.

The use of mismatched epitaxial layers allows much greater freedom in designing heterostructure devices with desired characteristics. In a strained QW system a deformation potential due to the built-in strain modifies the band gap energy. To obtain high optical quality structures, pseudomorphic growth is necessary. However, pseudomorphic growth is possible only for a layer thickness less than the so called critical layer thickness h_c . If the lattice mismatch between the epilayers and substrate is small and the layer is thin, the mismatch is accommodated by strain in layer. In the case, when the mismatch or the layer thickness is increasing, the formation of misfit dislocation at substrate-layer interface is energetically favourable. However, lattice relaxation via misfit dislocation degrades the quality of the material in terms of reduced carrier lifetime, reduced radiative efficiency, and reduced carrier mobility. Thus, the critical layer thickness h_c of the strained layer is one of the most important material parameters that we have to consider when we utilize the built-in strain in lattice mismatch systems. Little work has been done in terms of strain relaxation in dilute nitride QWs [66], although one might expect that N would increase the critical thickness of InGaNAs. The addition of impurities has often been found to reduce the rate of plastic deformation in crystalline material. Nitrogen is found to reduce the rates of deformation of float-zone Si wafers by diffusing to dislocation cores and pinning dislocations [67]. Strain relaxation in tensile strained GaAsN/GaAs and GaPN/GaP epilayers (N < 2%) have higher critical thicknesses compared to similar mismatched systems including GaP/Si [68], a result also attributed to dislocation pinning at N atoms and to hardening of lattice due to Ga-N bonds. Both surface reconstruction and surface strain relief depend on the substrate crystalline orientation and it has been claimed that surface reconstruction and strain play an important role in the incorporation of N [69]. On the other hand, N

incorporation has been found to be highly dependent on the substrate orientation [70].

Although lots of efforts have been concentrated on the effects of N on the electronic properties, little work has been done on the effects of N-induced critical layer thickness and no work on the effects of Sb-induced critical layer thickness up to our knowledge. It would be then of a great interest to present a comprehensive investigation of critical layer thickness h_c taking into account the orientation and substrate dependence of the new quinary laser system of GaInAsNSb QW starting from the ternary InGaAs with an emission wavelength of 1.1 μm .

4.2 Theoretical models

4.2.1 Force balance model of Matthews and Blakslee for h_c

In lattice-matched heterostructure systems, the number and the thickness of quantum wells in the structure is not a design constraint. In a strained layer, lattice-mismatched system, however, the elastic accommodation of the strain energy associated with the mismatch, without the formation of misfit dislocations, must be considered [71, 72]. A strained overlayer is thermodynamically stable for thicknesses $h < h_c$, while for $h > h_c$ it is energetically preferable to relieve the strain via the formation of dislocations. The critical layer thickness h_c can be defined in terms of elastic constants of the materials. Predicted and experimentally determined h_c 's are strongly dependent on the models, experimental methods, and growth conditions [73, 74, 75, 76, 77, 78, 79]. The subject has been extensively investigated through the works [80, 81, 82, 73] and shown that the reports are in agreement with Matthews and Blakeslee equilibrium theory [80, 81]. Therefore, we use the simple and reasonable force balance model of Matthews and Blakeslee [73] which is derived from the study of Van der Merve [74] to determine the h_c of single strained quantum well throughout our investigation. Matthews and Blakeslee calculate the critical thickness for layers in a superlattice having as equal elastic constants:

$$Bbh_c\varepsilon_0 \cos \theta = Db(1 - \sigma \cos^2 \alpha) \left[\ln \left(\frac{h_c}{b} + 1 \right) \right] \quad (4.1)$$

where B and D are constants concerned with elasticity defined below, b is the amplitude of the Burgers vector which is defined as $b = \frac{a}{\sqrt{2}}$ for (001) and (111) orientations. σ is Poisson's ratio, $\sigma = C_{12}/(C_{11} + C_{12})$ and ε_0 is the misfit

	$a_0 (A^0)$	$C_{11} (GPa)$	$C_{12} (GPa)$	$C_{44} (GPa)$
GaAs	5.6533	1221.0	566.0	600.0
InAs	6.0584	832.9	452.6	395.0
GaSb	6.09059	884.2	402.6	432.2
InSb	6.4794	684.7	373.5	311.1
GaN	4.5	293.0	159.0	155.0
InN	4.98	187.0	125.0	86.0

Table 4.1: The stiffness and lattice constants of binary compounds.

strain which is defined simply as $\varepsilon_0 = \left| \frac{\Delta a}{a} \right|$ and a is the lattice constant of the strained layer. θ is the angle between the slip direction and that direction in the interface which is perpendicular to the line of intersection of the slip plane and the interface, while α is the angle between the dislocation line and the Burgers vector. The value of $\cos \theta$ is $\frac{1}{2}$ and $\frac{1}{2\sqrt{3}}$ for (001) and (111) orientations, respectively. The expressions for the coefficients σ , B , G and D for (001) and (111) orientations are listed in table 4.1. Table 4.2 presents the binary material parameters for the related binaries.

4.2.2 Interpolation method for the quinary alloy

To calculate the lattice constant, elastic stiffness constants and the related parameters we use the linear interpolation of the experimentally determined values of the binary alloy. A bowing parameter C is usually included in the interpolation of the band parameter P for ternary alloys to account for the deviation from the linear interpolation between two binary alloys A and B :

$$P(A_{1-x}B_x) = (1-x)P(A) + xP(B) - x(1-x)C \quad (4.2)$$

For most $III-V$ alloys e.g., the alloy bandgap is typically smaller than the linear interpolation result and so C is positive. A non-zero bowing parameter, C_p , may be included to account for non-linearity in a parameter, P , in a similar fashion to the band gap bowing parameter. For quaternary alloys of the form $D_xE_{1-x}F_yG_{1-y}$ (two column III elements, D and E, and two column V elements, F and G), a weighted average of the four ternary alloys: DEF, DEG, DFG, EFG is used and additional bowing is neglected:

$$P_{DEFG} = \frac{x(1-x)(1-y)P_{DEG} + xy(1-x)P_{DEF}}{x(1-x) + y(1-y)} + \frac{y(1-y)(1-x)P_{DFG} + xy(1-y)P_{EFG}}{x(1-x) + y(1-y)} \quad (4.3)$$

Provided that either x or y is strictly between zero and one, i.e. a true quaternary and not a ternary. For the quinary $D_{1-x}E_xF_yG_{1-y-z}H_z$ with a third column V

	(001)	(111)
σ	$\frac{C_{12}}{(C_{11}+C_{12})}$	$\frac{(C_{11}+2C_{12}-2C_{44})}{2(C_{11}+2C_{12}+C_{44})}$
B	$\frac{(C_{11}+2C_{12})(C_{11}-C_{12})}{C_{11}}$	$\frac{6(C_{11}+C_{12})C_{44}}{(C_{11}+2C_{12}+C_{44})}$
G	$\frac{(C_{11}-C_{12})}{2}$	C_{44}
D	$\frac{G_0 G_S b}{2\pi(G_0+G_S)(1-\sigma)}$	$\frac{G_0 G_S b}{2\pi(G_0+G_S)(1-\sigma)}$

Table 4.2: The parameters which are used in calculations according to the directions.

element, H, the average can be expressed in terms of the nine ternary alloys [82] and additional bowing is neglected:

$$P_{DEFGH} = \frac{\sum c_{ijk} P_{ijk}}{\sum c_{ijk}} \quad (4.4)$$

where

$$\begin{aligned} \sum c_{ijk} P_{ijk} = & xy(1-x)P_{DEF} + x(1-x)(1-y-z)P_{DEG} \\ & +xz(1-x)P_{DEH} + xy(1-y-z)P_{EFG} \\ & +xyzP_{EFH} + xz(1-y-z)P_{EGH} \\ & +y(1-y-z)(1-x)P_{DFG} + yz(1-x)P_{DFH} \\ & +z(1-y-z)(1-x)P_{DGH} \end{aligned} \quad (4.5)$$

$$\begin{aligned} \sum c_{ijk} = & xy(1-x) + x(1-x)(1-y-z) \\ & +xz(1-x) + xy(1-y-z) \\ & +xyz + xz(1-y-z) \\ & +y(1-y-z)(1-x) + yz(1-x) \\ & +z(1-y-z)(1-x) \end{aligned} \quad (4.6)$$

where are the fractional composition components, e.g. $c_{ijk} = xy(1-y-z)$ for EFG and the ternary parameter P_{EFG} is calculated for the same F:G ratio as was present in the quinary. Again, it is necessary that at least one of x , y or z is strictly between zero and one so that the denominator is nonzero.

4.3 InGaAs QW on GaAs and InP substrates for (001) and (111) orientation

The emission wavelength of InGaAs/GaAs QW lasers was limited to 1.1 μm for a long time. Due to the constraints of high strain and limited critical thickness, the optical quality of InGaAs/GaAs QWs degrades rapidly when the indium concentration is higher than 0.35. To get high quality and un-relaxed InGaAs/GaAs QWs with high indium concentration, great care must be taken

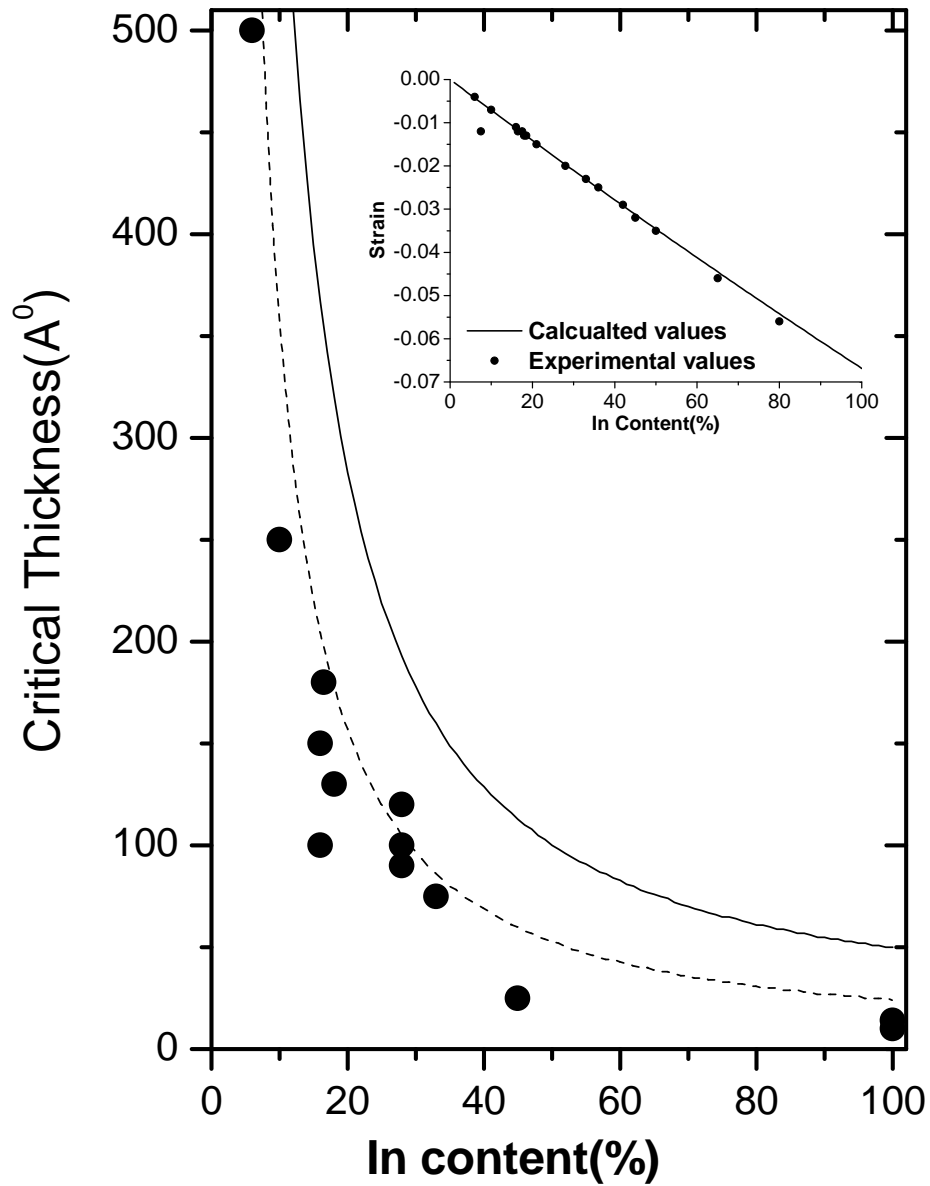


Figure 4.1: The calculated variation of the critical thickness of $\text{In}_x\text{Ga}_{1-x}\text{As}$ QW versus In concentration on GaAs substrates for (001) and (111) growth orientations. Dashed- and solid line represents the variation for (001) and (111) growth orientations, correspondingly. The inset figure shows the magnitude of strain versus In concentration on GaAs substrate. Closed and open dots represents the experimental values.

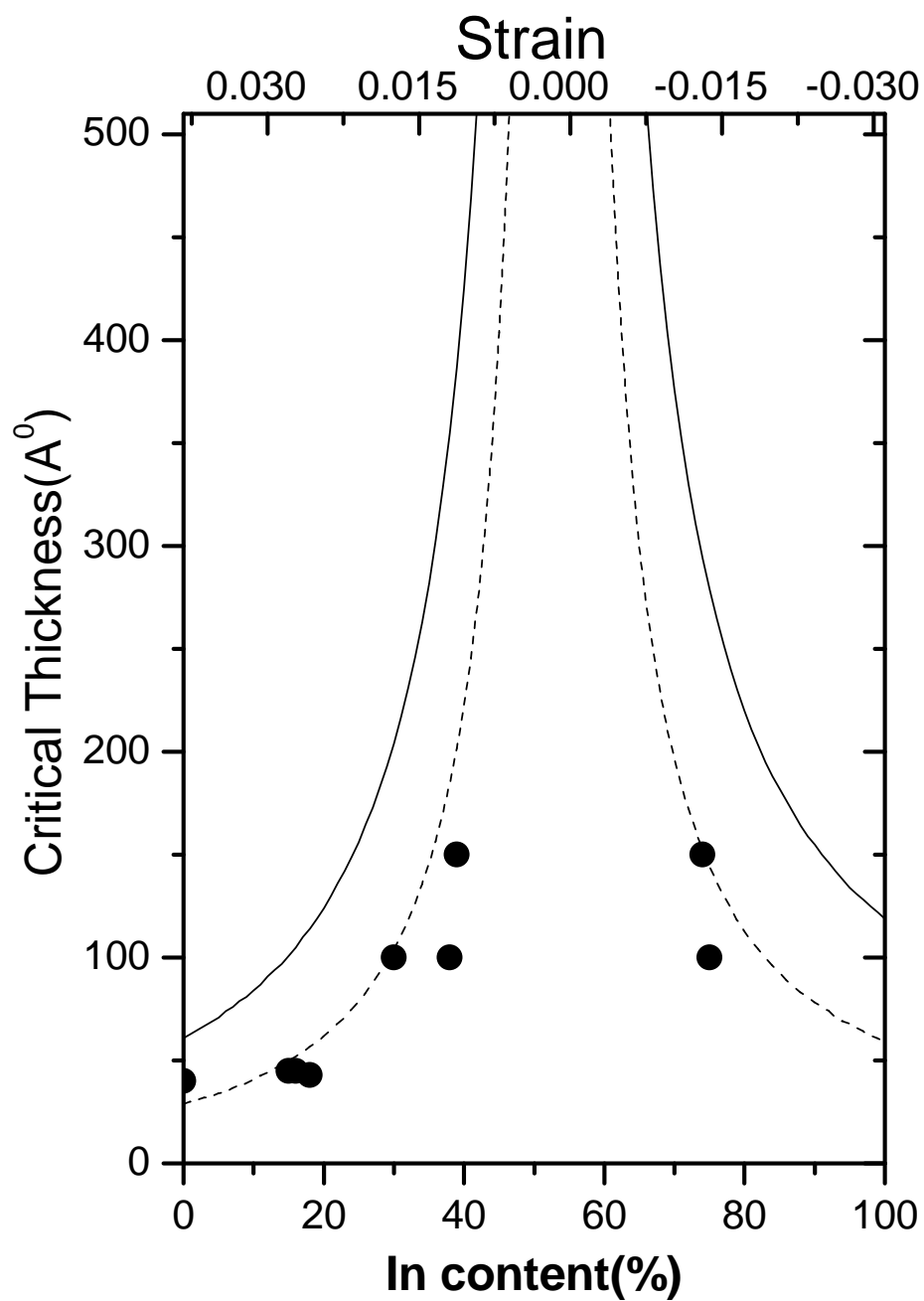


Figure 4.2: The calculated variation of the critical thickness of $\text{In}_x\text{Ga}_{1-x}\text{As}$ QW versus In concentration on InP substrates for (001) and (111) growth orientations. Dashed- and solid line represents the variation for (001) and (111) growth orientations, correspondingly. The inset figure shows the magnitude of strain versus In concentration on GaAs substrate. Closed and open dots represents the experimental values.

with respect to the control of the growth condition. Jiang et al [83] has shown that by optimizing the growth conditions, especially by using Sb as a surfactant at low temperature it has been successful to grow highly strained InGaAs/GaAs QWs and extend the emission wavelength to nearly $1.25 \mu\text{m}$ with a high luminescence efficiency at RT. The highly strained InGaAs/GaAs QW laser whose operating wavelength reaches a little beyond $1.2 \mu\text{m}$ is still a promising candidate for laser applications due to the relatively simple and mature techniques [84, 85, 86]. Moreover, the proper growth control of highly strained InGaAs QW growth is also an important step for the optimization of GaInAsN QW lasers.

It is well known that $\text{In}_x\text{Ga}_{1-x}\text{As}$ can be grown to lattice-matched to InP for $x = 0.535$. Lowering the In concentration of the alloy induces a tensile strain. A sufficiently high tensile strain will lead to a $e_1 - lh_1$ fundamental transition, giving rise to TM-mode polarization emission. The potential advantages of tensile-strained QW lasers (in terms of threshold current density and loss mechanisms) were predicted more than ten years ago [52, 53]. Therefore, in this section we present the orientation and substrate dependence of the critical thickness h_c of $\text{In}_x\text{Ga}_{1-x}\text{As}$ QW by means of Matthews and Blakeslee force balance model.

It is known that the h_c of $\text{In}_x\text{Ga}_{1-x}\text{As}$ QW decreases rapidly with increasing In concentration due to the increase in compressive strain on GaAs substrate for both (001) and (111) orientation, see Figure 4.1. The experimental results [87, 88] for (001) orientation is presented in figure 4.1 and 4.2. h_c is enhanced on (111) orientation as shown in figure 4.1 and is seen that the calculated results are in good agreement with experiment. h_c is in the order of 80 \AA on (001)- and 150 \AA on (111)-orientation for an indium concentration of 0.35. The calculated critical thickness on (111) is about two times larger than that on (001) over the entire indium concentration. This difference is mainly caused by the different θ value between (001) and (111) directions; i.e., $\cos \theta = 1/2$ for (001) and $\cos \theta = 1/2\sqrt{3}$ for (111). This means that the force acting to form the misfit dislocation is $\sqrt{3}$ times smaller for (111), thus resulting in wider critical thickness h_c . The enhancement of the critical layer thickness allows an increase of the In concentration in (111) strained $\text{In}_x\text{Ga}_{1-x}\text{As}$ quantum well lasers, which could in principle lead to emission at longer wavelengths on (111) substrates than that of (001) substrates.

Figure 4.2 presents the calculated h_c of $\text{In}_x\text{Ga}_{1-x}\text{As}$ QW on InP substrate. The corresponding strain values are also provided (top x-axis) in figure 4.2. $\text{In}_x\text{Ga}_{1-x}\text{As}$ is lattice-matched to InP for an indium concentration of 53%. $\text{In}_x\text{Ga}_{1-x}\text{As}$ on InP introduces compressive strain in the case of $x > 0.53$ and tensile strain in the case of $x \leq 0.53$. As can be seen from figure 4.2, h_c decreases

with increasing tensile and compressive strain; rapid reductions are calculated for the compressive strain side due to the larger magnitude of strain. The agreement with experimental results are also obtained on an InP substrate. The close investigation of figure 4.2 reveals the fact that indium-rich $\text{In}_x\text{Ga}_{1-x}\text{As}$ QW can be grown on InP substrate. This leads to reach the longer emission wavelength than that of the $\text{In}_x\text{Ga}_{1-x}\text{As}$ QW grown on GaAs substrate. It is also clear that the constraint of critical thickness and high strain is eliminated when InGaAs QW is grown on InP substrate. We have found that the effect of the elastic constants on the critical thickness is negligible and the concentration dependence of h_c is mainly governed by the lattice mismatches.

4.4 GaAsSb QW on GaAs and InP substrates for (001) and (111) orientation

The prospect of realizing active layers for $1.3 \mu\text{m}$ lasers on GaAs substrate are of special technological interest for making vertical cavity surface-emitting laser (VCSEL) devices [89]. For this purpose, the strained GaAsSb is a potential candidate as demonstrated by Anan et al [90]. GaAsSb QWs grown on GaAs substrates, with an antimonite fraction of approximately 30% emit at wavelengths near $1.3 \mu\text{m}$. However, the critical layer thickness of GaAsSb is limited [91] due to its large lattice mismatch with GaAs substrates and the higher concentration of Sb in GaAsSb/ GaAs QW is normally hard to be available for high quality device structures.

It has been stated by Tian et al [92] that the calculated critical thickness of GaAsSb layer on GaAs substrate by force balance model is in good agreement with experimental reports.

We therefore provide in this section the comparison of the critical layer thickness with the incorporation of antimonite Sb into GaAs on GaAs and InP substrates by means of force balance model. Figures 4.3 and 4.4 shows the calculated critical thickness of $\text{GaAs}_x\text{Sb}_{1-x}$ as a function of Sb concentration on GaAs and InP substrates for both (001) and (111) orientations. The experimental results [91, 93] are also provided. The critical thickness decrease accordingly with increasing compressive strain on GaAs substrate. It also decreases with increasing compressive and tensile strain on InP substrate. The comparison of figures 4.1 and 4.2 with that of the figures 4.3 and 4.4 shows that the critical thicknesses of $\text{In}_x\text{Ga}_{1-x}\text{As}$ QW and $\text{GaAs}_x\text{Sb}_{1-x}$ QW are quite similar. This is due to the fact that the magnitudes of strains in both ternaries are almost equivalent for layers grown on GaAs and InP substrates. However, the ternary

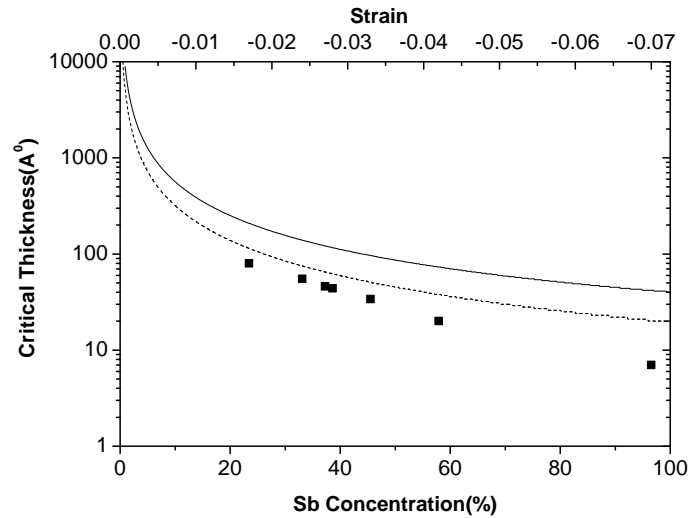


Figure 4.3: The calculated variation of the critical thickness of $\text{GaAs}_{1-x}\text{Sb}_x$ QW versus In concentration on GaAs substrates for (001) and (111) growth orientations. Dashed- and solid line represents the variation for (001) and (111) growth orientations, correspondingly. Closed squares represents the experimental values for (001) orientation.

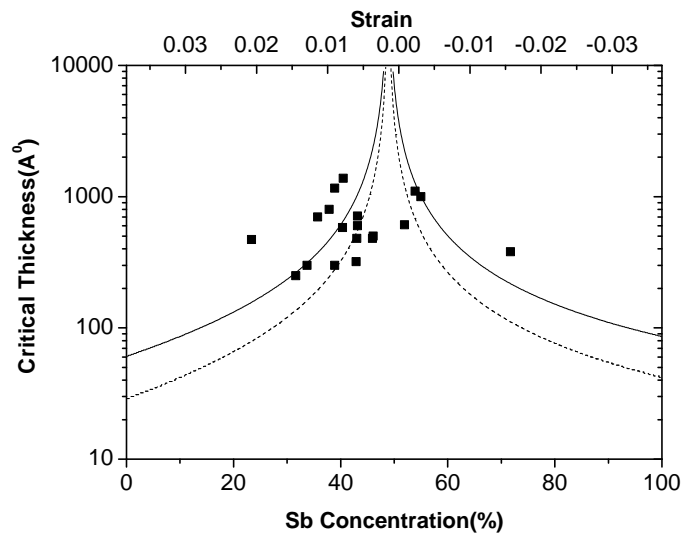


Figure 4.4: The calculated variation of the critical thickness of $\text{GaAs}_{1-x}\text{Sb}_x$ QW versus In concentration on InP substrates for (001) and (111) growth orientations. Dashed- and solid line represents the variation for (001) and (111) growth orientations, correspondingly. Closed squares represents the experimental values for (001) orientation.

GaAs_xSb_{1-x} has a higher bowing coefficient than that of In_xGa_{1-x}As. As a consequence, for $0 < x < 0.5$, GaAs_xSb_{1-x} has a lower bandgap than In_xGa_{1-x}As [94]. Keeping in mind that the magnitudes of strains in both ternaries are almost equivalent for layers grown on GaAs and InP substrates, longer wavelength can be achieved with GaAs_xSb_{1-x} than that of the In_xGa_{1-x}As QW for the same magnitude of strain. This brings an advantage for the h_c since a fixed emission wavelength can be obtained for lower concentration of Sb in GaAs_xSb_{1-x}QW with respect to that of the In in In_xGa_{1-x}As. Therefore, the constraint of critical thickness is improved for GaAsSb QWs compared to that of the InGaAs QWs allowing to use the wider QWs for GaAsSb structure safely.

4.5 Ga_{1-x}In_xAs_{1-y}N_ySb_z QW on GaAs and InP substrates for (001) and (111) orientation

In this section we will concentrate on the h_c of Ga_{1-x}In_xAs_{1-y}N_y on GaAs and InP substrates which is very important for modelling semiconductor quantum well structures. We first want to show the validity of Matthews and Blakeslee model to obtain h_c when N is incorporated to GaAs. Fig. 4.5 presents the comparison of calculated h_c with that of the experimental results [95]. The force balance model can be said to be in agreement with the experimental results in the case of incorporation of N into GaAs. We then present in figure 4.6 and 4.7 the calculated variation of GaInAsN QW grown on GaAs and InP substrate as a function of indium concentration for various nitrogen concentrations on (001) orientation (upper group of curves). First of all, the substrate dependence is similar to previous diagrams i.e. h_c decreases with increasing In concentration when GaInAsN QW is grown on GaAs substrate (fig. 4.6) and h_c decreases with increasing tensile and compressive strain when GaInAsN QW is grown on InP substrate (fig. 4.7). Secondly, our calculations clearly illustrate that h_c of GaInAsN QW on GaAs substrate increases slightly with increasing N concentration due to the strain compensating effect of N. Finally, the N dependence of h_c of GaInAsN QW on InP substrate shows different behaviour for low indium ($\tilde{x} < 0.53$) which results tensile-strain and high indium ($\tilde{x} \geq 0.53$) which results compressive-strain; h_c as a function of In concentration decreases with increasing N concentration on the low In side whereas it increases with increasing N concentration on the high In side. The critical thickness h_c on InP substrate is much larger than that of the critical thickness on GaAs substrate for high In concentration. It is clear from this figure that the growth of indium rich

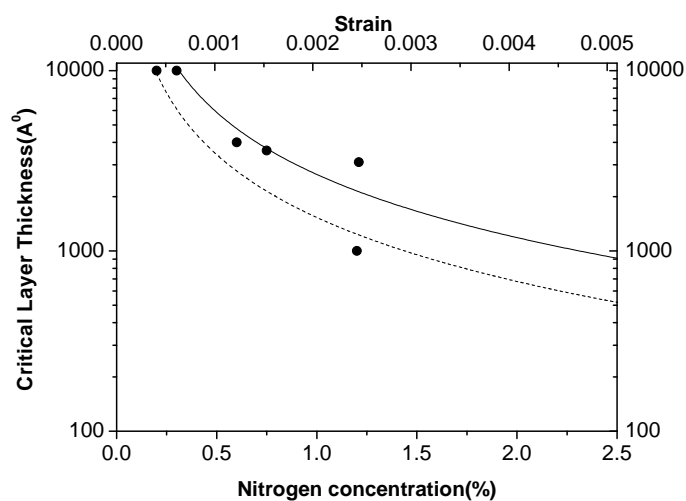


Figure 4.5: The calculated variation of the critical thickness of $\text{GaAs}_{1-x}\text{N}_x$ QW versus In concentration on GaAs substrates for (001) and (111) growth orientations. Dashed- and solid line represents the variation for (001) and (111) growth orientations, correspondingly. Closed dots represents the experimental values for (001) orientation.

$\text{Ga}_{1-x}\text{In}_x\text{As}_{1-y}\text{N}_y$ QW can only be possible on InP substrates due to the large critical thickness allowing to reach longer wavelengths than that of the GaAs substrate.

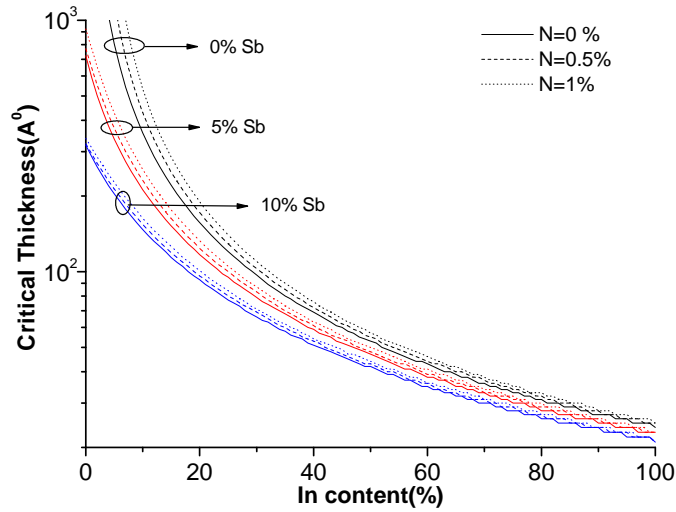


Figure 4.6: The calculated variation of the critical thickness of $\text{Ga}_{1-x}\text{In}_x\text{N}_y\text{As}_{1-y-z}\text{Sb}_z$ QW versus In concentration on GaAs substrates for (001) and (111) growth orientations. Dashed- and solid line represents the variation for (001) and (111) growth orientations, correspondingly. Closed dots represents the experimental values.

We also present in fig.'s 4.6 and 4.7 an investigation of the effect of the antimonite on critical thickness of GaInAsN alloys with widely varying compositions of antimonite, indium and nitrogen. Fig 4.6 and 4.7 presents a detailed study of the interactions between these atoms to help an understanding of the role of antimonite in h_c in dilute nitride materials. The combined effect of In, Sb and N can be summarized when the compressively strained GaInAsNSb QW is grown on GaAs substrate as;

- (1) In concentrations cause faster reductions in h_c .
- (2) Sb concentrations also lowers h_c but these reductions are much slower compared to that of the In concentration.
- (3) N concentrations cause an increase in h_c when the compressively strained GaInAsNSb QW grown on GaAs substrate.

When the GaInAsNSb QW is grown on InP substrate;

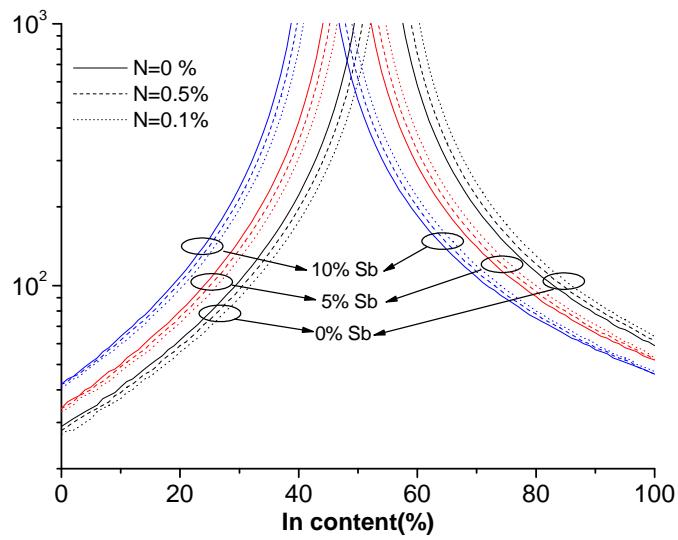


Figure 4.7: The calculated variation of the critical thickness of $\text{Ga}_{1-x}\text{In}_x\text{N}_y\text{As}_{1-y-z}\text{Sb}_z$ QW versus In concentration on InP substrates for (001) and (111) growth orientations. Dashed- and solid line represents the variation for (001) and (111) growth orientations, correspondingly. Closed dots represents the experimental values.

- (1) In concentrations cause faster reductions in h_c for both increasing tensile and compressive strain.
- (2) Sb concentrations cause a decrease in h_c on compressive side, however cause an increase in h_c on tensile side.
- (3) N concentrations cause an increase in h_c on compressive side and a decrease in h_c on tensile side. Although the effect of Sb and N are reserved on tensile and compressive side, it is clear from 4.7 critical thickness values are greatly improved except for low- and too high indium concentrations in GaInAsNSb on InP substrates.

4.6 Conclusions

Long wavelength semiconductor lasers in the range of $1.3 \mu m - 1.55 \mu m$ are very important sources for optical fiber communication. Due to the highly nonlinear effects of N on band gap of the InGaAs grown on GaAs substrate, N is incorporated in InGaAs to decrease the band gap and make GaInAsN a suitable material for long wavelength semiconductor laser diodes at $1.3 \mu m - 1.55 \mu m$. Before the development of GaInAsN, it was impossible to obtain these wavelengths from a coherently grown material on GaAs due to the very high strain in the active region.

Since GaInAsN system has been proposed as a material for $1.3 \mu m$ emitting lasers on GaAs substrate, it has been realized that the optical quality of the material deteriorates due to a restriction in the optimal growth parameters when the nitrogen concentration is above 2.5%. The degradation results in a higher threshold current density for lasers. Recently, GaInAsNSb has been found to be a potentially superior material to GaInAsN for long wavelength laser applications. It has been explored that the addition of Sb to the GaInAsN system improves the crystal quality. In addition, the introduction of Sb atoms to the GaInAsN compound is an approach to shift the laser emission wavelength of GaInAsN system to $1.55 \mu m$. This makes it possible to obtain low bandgap energy at a relatively low nitrogen concentration.

Enormous progress has been achieved in GaInAsN semiconductor alloy on GaAs substrate for both its fundamental properties and its potential applications for $1.3 \mu m - 1.55 \mu m$ lasers. In contrast to this large amount of work reported on dilute $Ga_{1-x}In_xAs_{1-y}N_y$ on GaAs, only a few studies have been published so far on the growth of strained $Ga_{1-x}In_xAs_{1-y}N_y$ on InP substrates and there is no work about the comparison of the h_c of the $Ga_{1-x}In_xAs_{1-y}N_y$ alloys on GaAs and InP substrates up to our knowledge. In this work, we have investigated

the role of N and Sb on the critical thickness of strained GaInAsNSb QWs on GaAs and InP substrate for (001) and (111) orientations. We have shown the expected variation of which the critical thickness h_c decreases with increasing In concentration when the InGaAs layer is grown on GaAs substrate. We have illustrated that the limitation of h_c is eliminated when the compressive InGaAs wells are grown on InP substrate. At the second part of our calculations we have examined the effect of the addition of Sb atoms to GaAs. Our calculated results were in agreement with experimental results. It has been seen from the results that the effect of addition of Sb atoms is similar to that of the In atoms of both causing a reduction in h_c . However, the use GaAs_xSb_{1-x} QW instead of In_xGa_{1-x}As brings an advantage from the point of view of h_c . Since a fixed emission wavelength can be obtained for lower concentration of Sb in GaAs_xSb_{1-x} QW than that of the In concentration in In_xGa_{1-x}As, much larger critical layer thicknesses can be obtained for GaAs_xSb_{1-x} QWs.

At the third part of our calculations we have calculated improved h_c values for GaInAsN QW due to the strain compensating effect of N atoms. It has been noticed from our calculations that the variation of h_c with increasing N concentration is different when GaInAsN wells are grown on InP substrate. We have shown that the growth of indium rich GaInAsN QW is possible on InP substrates due to the improved critical layer thickness. The problems that has been met in GaInAsN QW due to the high In and N concentrations can be eliminated by means of introduction of Sb atoms into GaInAsN. The calculated results indicate that GaInAsNSb has still the constraint of critical layer thickness. On the other hand, the use of quinary GaInAsNSb on InP substrate brings improvements in critical thickness, enables incorporation of the desired indium concentration and allows tuning of the required wavelength. Therefore, this wide wavelength range coverage makes GaInAsNSb QWs on GaAs and InP substrates as a great active layer candidate for long wavelength lasers.

CHAPTER 5

THE ANALYTICAL SOLUTION OF SCREENED COULOMB POTENTIAL AND BINDING ENERGIES OF DONOR IN GAASN

5.1 Introduction

There is a lot of work on the impurities in semiconductors because they have a very special role in controlling the conductivity of semiconductors. When an impurity is added into the lattice, mobility and its transport properties change. With doping, one can observe impurity states and these states have bearing on the electronic and optical properties of semiconductor heterostructures. In particular, the hydrogenic shallow donor state of electron bound by Coulombic electrostatic force of excess charge of impurity is used to construct semiconductor diodes, transistors and numerous types of semiconductor electronic and optoelectronic devices, including lasers [96]. The dielectric constant of the crystal and screening effect by free carriers are the important factors which determine the coulombic force.

In this study, we investigate the effect of screening and dielectric constant on electrostatic force of a shallow donor impurity and its binding energy in GaAsN heterostructure. Screening occurs due to the free carriers in semiconductor. The electrostatic interaction is shielded by the carriers which exist between ionized shallow donor and its bound electron. We aim to present the relationship of screening factor, temperature, nitrogen and free carrier density for GaAsN alloys in this study. We try to reveal the effect of the dielectric constant on the interaction between shallow donor and its bound electron.

In GaAsN, Si is a typical donor and sits on the Ga site [97]. Si being a group *IV* element gives an electron into the crystal as a shallow donor. Binding

energy of this electron will be calculated by solving screened coulomb potential. When we consider GaAsN as a bulk semiconductor, electron effective mass will be proportional to the inverse of second derivative of conduction band dispersion relationship for a parabolic band. The non-parabolic dispersion and strong N dependency of conduction band of GaAsN causes unusual behaviour of electron effective mass and binding energy of shallow donor. This unusual behaviour of electron effective mass and the variation of mass-dependent binding energy will also be presented in this study.

We assume that the interaction between the electron and ionized donor is described by the screened coulomb potential which is given by

$$V(r) = -\frac{e^2}{4\pi\epsilon r} \exp(-\alpha r) \quad (5.1)$$

where α is the screening parameter which is due to free charge carriers in the semiconductor and e is the carrier charge while ϵ is the dielectric constant. Because the corresponding Schrödinger equation for this potential does not admit exact analytic solutions for non-zero angular momentum, various numerical and approximate methods [98, 99, 100, 101, 102, 103, 104, 105] have been developed in the past. More recently, a new methodology [106, 107] has been introduced. The results of our calculations in the frame of [106, 107] show that binding energy is strongly dependent on temperature, free carrier density and Nitrogen concentration of III-V-N alloy.

We first present this novel formalism used in our calculations to obtain bound states of the related screened coulomb interaction. Then we discuss in detail the corresponding screening parameter α in the present work and the related Bohr radius as a function of nitrogen concentration and present the calculated binding energy versus increasing nitrogen for the ground state. Finally, we outline the results.

5.2 Theory

In the model presented by authors [106, 107] the Schrödinger equation is safely decomposed in two parts. In other words, the potential in eq. 5.1 is splitted in two pieces

$$V_{total}(r) = V_{exact}(r) + V_{pert}(r) \quad (5.2)$$

where V_{exact} represents an exactly solvable part that corresponds to the Coulomb potential and V_{pert} denotes a perturbation term. Then, one can treat the Coulomb potential easily using the supersymmetric quantum theory [108] defining a proper

superpotential such that

$$W_n = -\frac{\hbar}{\sqrt{2m}} \frac{n + \ell + 1}{r} + \sqrt{\frac{m}{2}} \frac{e^2}{4\pi\epsilon(n + \ell + 1)\hbar} \quad (5.3)$$

leading to

$$V_{exact}(r) = V_{coulomb}(r) = W_n^2 - \frac{\hbar}{\sqrt{2m}} W_n' = -\frac{e^2}{4\pi\epsilon r} + \frac{me^4}{2\hbar^2(4\pi\epsilon)^2(n + \ell + 1)^2} + \frac{\hbar^2}{2m} \frac{\ell(\ell + 1)}{r^2}, \quad n = 0, 1, 2, \dots \quad (5.4a)$$

therefore, the related wavefunction appears as

$$\begin{aligned} \chi_n(r) = & \left(\frac{2me^2}{4\pi\epsilon(n + \ell + 1)\hbar^2} \right)^{\ell+1} \left(\frac{1}{n + \ell + 1} \right) \\ & \times \frac{r^{\ell+1}}{\sqrt{\frac{4\pi\epsilon\hbar}{me^2n!}}(n + 2\ell + 1)!} \exp\left(-\frac{me^2}{4\pi\epsilon(n + \ell + 1)\hbar^2} r \right) \\ & L_n^{2\ell+1} \left(\frac{2me^2}{4\pi\epsilon(n + \ell + 1)\hbar^2} r \right) \end{aligned} \quad (5.5)$$

in which L_n^ℓ is an associate Laguarre polynomial. For the calculation of the corrections to the leading orders of energy and wavefunction for the perturbed piece of the potential in the light of [106, 107], one needs to use that in the first order

$$\Delta\varepsilon_{n1} = \int_{-\infty}^{\infty} \chi_n^2 \left(-\frac{e^2\alpha^2}{2(4\pi\epsilon)} r \right) dr \quad (5.6)$$

$$\Delta W_{n1}(r) = \frac{\sqrt{2m}}{\hbar} \frac{1}{\chi_n^2} \int \chi_n^2(r) \left(\Delta\varepsilon_{n1} + \frac{e^2\alpha^2}{2(4\pi\epsilon)} r \right) dr \quad (5.7)$$

and in the second order

$$\Delta\varepsilon_{n2} = \int_{-\infty}^{\infty} \chi_n^2 \left(\frac{e^2\alpha^3}{6(4\pi\epsilon)} r^2 - \Delta W_{n1}^2(r) \right) dr \quad (5.8)$$

$$\Delta W_{n2}(r) = \frac{\sqrt{2m}}{\hbar} \frac{1}{\chi_n^2} \int \chi_n^2(r) \left(\Delta\varepsilon_{n2} + \Delta W_{n1}^2(r) - \frac{e^2\alpha^3}{6(4\pi\epsilon)} r^2 \right) dr \quad (5.9)$$

where ΔW terms are related to the corrections for the superpotential term (eq. 5.3) which are strongly required for the corrections to the zeroth order energy term. It is stressed that the unperturbed zeroth order energy corresponding to the Coulomb potential is the one appears as the second term in right hand side of eq. 5.4. Hence, the approximate analytical expression for the low-level ($n = 0$)

energy of the full potential of interest is given by

$$\begin{aligned}
E_{n=0} = & -\frac{me^4}{2\hbar^2(4\pi\varepsilon)^2(\ell+1)^2} \\
& + \frac{e^2}{(4\pi\varepsilon)}\alpha - \frac{\hbar^2}{4m}\alpha^2(\ell+1)(2\ell+3) \\
& + \frac{(4\pi\varepsilon)\hbar^4}{12e^2m^2}\alpha^3(\ell+1)^2(\ell+2)(2\ell+3) \\
& - \frac{\hbar^6(4\pi\varepsilon)^2}{16e^4m^3}\alpha^4(\ell+1)^4(\ell+2)(2\ell+3) \quad (5.10)
\end{aligned}$$

for different suborbitals ($\ell \geq 0$). We observed in our earlier work [106] that the above novel discussion is capable of producing physically acceptable successful results which were found in very good agreement with the accurate numerical integration results.

5.3 Calculation of binding energy of donors in GaAsN by using the analytical method

There are measurements and theoretical works for shallow donor states of Si-doped n-type GaAs semiconductors. For example, in the study of Sze [109], measured value of the binding energy of shallow donor in Si-doped GaAs is given as 0.006 eV. In order to calculate this value, the most known way is to consider the unionized donor as an electron-proton pair in hydrogen atom. Therefore, it can be described by semiclassical model by Bohr [110]. The ground state binding energy of the neutral donor-electron pair for bulk is given by coulomb energy

$$E_D = -\frac{m_e^*}{2\hbar^2(\ell+1)^2} \frac{e^4}{(4\pi\varepsilon)^2} \quad (5.11)$$

similar to the Coulomb energy in eq. 5.10. From de Broglie wavelength $\lambda = h/p$, we can write Bohr radius as following

$$a_B^{n,\ell} = \frac{\lambda}{2\pi} = \frac{h}{2\pi\sqrt{2m_e^*E_D}} = \frac{4\pi\varepsilon\hbar^2(\ell+1)}{m_e^*e^2} \quad (5.12)$$

For GaAs, if the Γ valley electron effective mass is taken as $m_e^* = 0.067 m_e$ and the relative dielectric constant $\varepsilon = 13.2 \varepsilon_0$ [111], the energy and the Bohr radius for $\ell = 0$ can be found as

$$E_{D(GaAs)} = -5.23 \text{ meV} \quad (5.13a)$$

$$a_{B(GaAs)} = 104 \text{ \AA} \quad (5.13b)$$

Up to our knowledge, measurement for the binding energy of shallow donor in bulk GaAsN doesn't exist in literature and the study of Wu et. al. [111] is the available single theoretical work on this subject. Wu et. al. has used the variational technique to obtain binding energy of shallow donor with screening effect. However, in that study the meaning of screening parameter has not been emphasized and binding energy has been found only for a specific value. We aim to clarify the meaning of screening parameter α , find out the influence of it on potential and calculate the binding energy of shallow donor for GaAsN by using screened coulomb potential. Therefore, we take into account the contribution of free electron screening in the system using eq. 5.10 by which binding energy of shallow donor can be obtained.

Effective mass of conduction electron is found by using the relation between k -dependent non-parabolic conduction band energy of GaAsN and electron mass which is

$$m_{k=0}^* = \frac{\hbar^2}{\partial^2 E_-(k, y) / \partial k^2} \quad (5.14)$$

where conduction band dispersion relationship $E_-(k, y)$ is given by eq. 3.1. The static dielectric constant ε is dependent on variation of band gap and lattice constant. We can write an equation for static dielectric constant ε which is adoption of empirical equation proposed by Chadi and Cohen [112]

$$\varepsilon(y) = \left[13.2 + \beta \left(\frac{1}{a_{lat}^{3/2}(y) E_g(y)} - \frac{1}{a_{lat}^{3/2}(0) E_g(0)} \right) \right] \varepsilon_0 \quad (5.15)$$

where lattice constant of GaAsN can be found by using interpolation method

$$a_{lat}(y) = y * a_{lat-GaN} + (1 - y) * a_{lat-GaAs} \quad (5.16)$$

and $E_g(y)$ is $E_-(k, y)$ at $k = 0$. β is an empirical value which equals to $159.0 \text{ eV}\text{\AA}^{3/2}$. As can be understood from the eqs. 5.14, 5.15 and 5.16, binding energy of GaAsN is affected by band gap, mass and lattice constant.

The calculated variation of E_g for GaAsN according to eq. 3.1 gives a rapid decrease band gap energy as can be seen in fig. 5.1. The addition of 1% N into GaAs leads to a change of 0.1 eV in the band gap. This result which is obtained by BAC model is agreed with the experiments. The change of static dielectric constant as a function of nitrogen concentration for GaAsN is also shown in fig. 5.1. The static dielectric function increase ε almost linearly with increasing N concentration in contrast to the rapid variation of the energy band gap with N concentration. The reason of this behaviour is the inverse relationship of static dielectric constant with band gap (eq. 5.15).

The effective Bohr radius is calculated by using eq. 5.12 and effective mass is obtained from the relationship $m^* = \hbar^2 / (\partial^2 E_-(k, y) / \partial k^2)$. Fig. 5.2

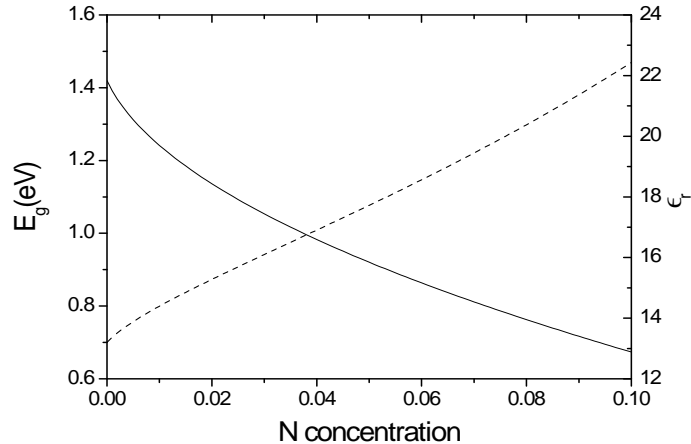


Figure 5.1: Minimum band gap(solid line) calculated by Eq. 3.1 and static dielectric constant(dashed line) obtained by Eq. 5.15 as a function of the N fraction for $\text{GaAs}_{1-y}\text{N}_y$.

presents the expected increase of effective mass with N concentration. Effective mass increases rapidly up to $\sim 1\%$ of N, after this value the increase is slow. As can be seen from eq. 5.12 effective Bohr radius is dependent on effective mass and static dielectric constant. For N concentration $< \sim 1\%$, the effective mass is a dominant factor causing a rapid fall of effective Bohr radius; whereas for N concentration $> \sim 1\%$ static dielectric constant is the dominant factor causing an increase of effective Bohr radius. These results are valid in the case of $\alpha = 0$.

The background mobile electron density increases with increase of the doping levels. This background density causes screening of the bare coulomb potential ($1/r$) which is produced by the impurity itself. The screening parameter α for GaAsN can be found by solving Poisson's equation as described below. The concentration of impurities, holes and electrons induce a charge distribution. This charge distribution can be expressed by Poisson's equation as

$$\nabla^2 V = -\frac{q}{\epsilon} (p - n + N_D) \quad (5.17)$$

where local hole density p is $n_i e^{-q(V+\phi_b)/kT}$, local electron density n is $n_i e^{q(V+\phi_b)/kT}$, impurity concentration N_D is $n_0 - p_0 = n_i e^{q\phi_b/kT} - n_i e^{-q\phi_b/kT}$. The Poisson's equation exists around an ionic charge q . The potential V is described by screened coulomb potential which is given by eq. 5.1. We get an analytical equation of screening parameter for GaAsN followed by Young et al. [113]. Putting known parameters into Poisson's equation, we get

$$\nabla^2 V = -\frac{q}{\epsilon} \left(\begin{array}{l} n_i e^{-q(V+\phi_b)/kT} - n_i e^{q(V+\phi_b)/kT} \\ + n_i e^{q\phi_b/kT} - n_i e^{-q\phi_b/kT} \end{array} \right) \quad (5.18)$$

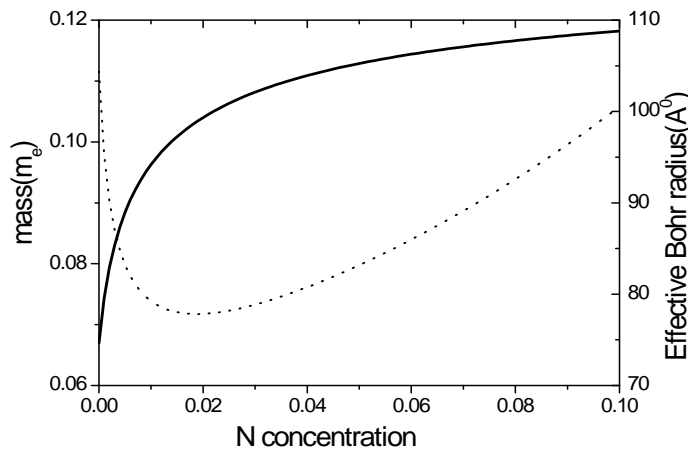


Figure 5.2: Electron effective mass(solid line) at Γ valley and effective bohr radius(dotted line) as a function of N concentration.

where k , T , q , n_i , ϕ_b are Boltzman constant, temperature, electronic charge, intrinsic electron concentration at temperature T and Fermi-level shift, respectively. For $V \ll kT$ Poisson's equation becomes

$$\nabla^2 V = -\frac{q}{\varepsilon} \begin{pmatrix} -\frac{qV}{kT} n_i e^{-q\phi_b/kT} + \frac{qV}{kT} n_i e^{q\phi_b/kT} \\ + n_i e^{-q\phi_b/kT} - n_i e^{q\phi_b/kT} \\ + n_i e^{q\phi_b/kT} - n_i e^{-q\phi_b/kT} \end{pmatrix} \quad (5.19)$$

$$\nabla^2 V = \frac{q}{\varepsilon} (n_i e^{-q\phi_b/kT} + n_i e^{q\phi_b/kT}) \frac{qV}{kT} \quad (5.20)$$

$$\nabla^2 V = \frac{2n_i q^2}{\varepsilon kT} V \cosh \frac{q\phi_b}{kT} \quad (5.21)$$

Substituting the eq. 5.1 into eq. 5.21, we get

$$\alpha(T, n_i, \phi_b) = \sqrt{\frac{2n_i q^2 \cosh \frac{q\phi_b}{kT}}{\varepsilon kT}} = \sqrt{\frac{q^2 (N_D^2 + 4n_i^2)^{1/2}}{\varepsilon kT}} \quad (5.22)$$

where intrinsic carrier concentration n_i can be obtained using the empirical equation[114]

$$n_i(y, T) = (N_c(y) N_v(y))^{1/2} \exp\left(-\frac{E_g(y)}{kT}\right) \text{ cm}^{-3} \quad (5.23a)$$

$$\text{where } N_c(y) = 2 \left(\frac{2\pi m_c kT}{\hbar^2}\right)^{3/2} \quad \text{and} \quad (5.23b)$$

$$N_v(y) = 2 \left(\frac{2\pi m_v kT}{\hbar^2}\right)^{3/2} \quad (5.23c)$$

m_c is the effective electron mass in conduction band, m_v is effective hole mass in valence band. From interpolation method the effective hole mass can be written as

$$m_v = 0.62 + 0.2354y \quad (5.24)$$

According to the eqs. 5.22 and 5.23, α , n_i and N_c strongly depend on temperature and nitrogen concentration. Figure 5.3 shows the close relationship between N

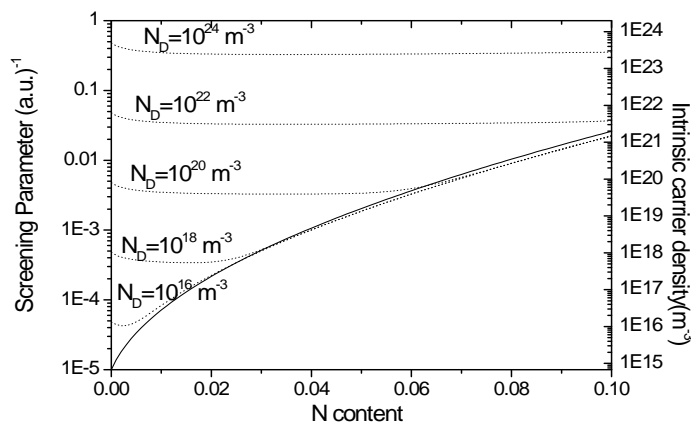


Figure 5.3: The variation of screening parameter α (dashed lines) and intrinsic carrier concentration(solid line) with increasing nitrogen concentration. α is also dependent on donor concentration.

concentration, the amount of donor impurities, the intrinsic carrier concentration and the strength of screening parameter. The rise of nitrogen concentration causes an increasing of intrinsic carrier concentration (see solid line). Dotted lines show the donor concentration dependence of screening parameter α which is described in atomic unit. Nitrogen and donor concentrations result an increase in screening. An interesting point in figure 5.3; the solid line which shows N-intrinsic carrier relationship and the junction of the dotted lines which shows the donor-screening relationship are overlapped.

Wu et. al. [111] has taken the screening parameter as 1 a.u.^{-1} during the calculations of the binding energies by using variational technique. However, the screening parameter can not be chosen arbitrarily due to its dependence of temperature and N concentration. In this case, the screening parameter should be taken as the values which are allowed by eq. 5.22. Therefore, the survey of screening parameter α has provided more sophisticated comprehension of the relationship between nitrogen and binding energy. Fig. 5.4 illustrates how the binding energy varies with N concentration and the screening parameter α . After a small increase of binding energy up to $N < 0.5\%$, the energy is decreasing with

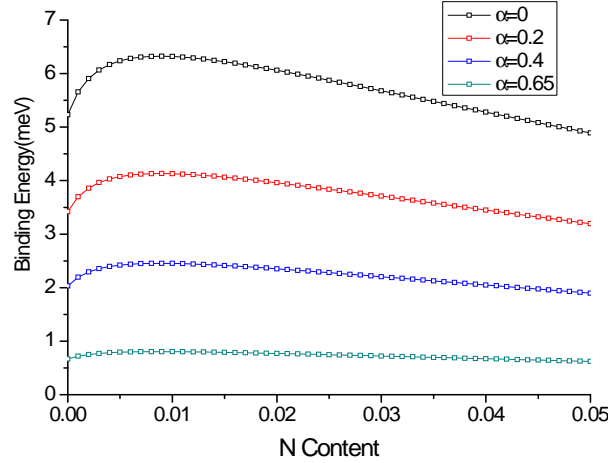


Figure 5.4: The binding energy variation (solid line) for the ground state as a function of the nitrogen concentration. The change of effective Bohr radius (dashed line) and screening parameter can be seen in this figure.

N concentration. As mentioned before, the reason of this behavior is mass- and dielectric constant-dependence of the binding energy. The initial dominance of effective mass causing an increase of binding energy, for $N > 0.5\%$, static dielectric constant becomes dominant causing a decrease of binding energy. This result is in agreement with the study of [111]. An increase of screening parameter causes a decrease of binding energy. This behaviour is also in agreement with the result of [111]. Furthermore according to the empirical expression of [115] which is given by

$$E_D = E_{D0} \left(1 - \left(\frac{N_D}{N_{crit}} \right)^{1/3} \right) \quad (5.25)$$

where E_{D0} is binding energy without screening. According to this equation binding energy vanishes if donor concentration N_D is equal to critical value N_{crit} which is different for materials. Eq. 5.25 supports reliability of our results because the binding energy is going to zero with increasing of donor concentration in our calculations.

5.4 Conclusions

We have investigated the effect of nitrogen on intrinsic carrier density, screening parameter, effective Bohr radius and binding energy of shallow donors in GaAsN alloys. We explain the meaning of screening parameter for GaAsN as the inverse of screening parameter being equal to another well known parameter,

Debye length.

In literature, the problems which are related to coulomb and screening coulomb interaction for bulk and low dimensional semiconductors are generally solved by using variational variable technique. However, this technique is tedious and the results can be found by solving integrations by aid of computer and the results are not reliable and stable. Under consideration of these reasons, we have used more effective, reliable and simple equation(eq. 5.10) of Gonul et. al. [107] which has been proposed to solve Yukawa-type potentials. In the present study this efficient model is used to investigate the relation between the binding energy of hydrogenic shallow donor in bulk GaAsN alloys for different screening parameter and N concentration observed that the screening parameter appearing in our work causes a strong variation of the both, binding energy and N concentration. The analytical method of [107] can also be applied to solve the problem for low-dimensional systems and excitons as well. Along this line, the works are in progress.

CHAPTER 6

A THEORETICAL INVESTIGATION OF OPTICAL MODE CONFINEMENT IN GAINASN QWS ON GAAS AND INP

6.1 Introduction

Both carrier and optical mode confinements are the basic ingredients while designing the semiconductor quantum well lasers. The former strongly depends on the band offsets of the heterostructures and the latter is mainly associated with the difference in the refractive index between the wave guiding core and the cladding layers. It is known that the refractive index strongly depends on the direct band gap of the semiconductor materials and the band gap of the III-N-V semiconductor layer can be engineered by means of adding nitrogen into InGaAs. We investigate, in this work, the refractive indices of the heterostructures and the corresponding optical confinement factors of the proposed III-N-V laser material systems on GaAs and InP substrates.

Experimental studies have shown that GaInAsN alloy has also some interesting optical parameters such as refractive index which increases with an increase of N concentration for strained GaInAsN layers [116, 117, 118]. This enables GaInAsN to be used as an active layer in vertical-cavity surface-emitting laser structure [118]. The band gap of the GaInAsN semiconductor layer can be engineered by means of adding N into InGaAs; an increase in N concentration of bulk GaInAsN causes energy gap reduction and this result in increase in refractive index values. Therefore, the tendency for the refractive index to increase with decreasing band gap energy is the same as that observed in conventional III-V semiconductors. This may lead to better optical confinement in GaInAsN semiconductors which has already the superior property of better electron con-

finement. Better carrier and optical confinement greatly reduces the threshold current density and permits continuous operation at room temperature [119]. We have previously shown that conventionally- and strain-compensated N-based lasers have better band alignment than that of the III-V semiconductor laser systems and therefore N-based lasers can be offered as ideal candidates for high temperature operation. In order to be a complementary study from the confinement point of view, we present in this work the calculations of refractive index and optical confinement factor of III-V and III-N-V semiconductor systems and provide the comparison of the confinement in conventional semiconductors with that of dilute nitride semiconductors. There has been no extensive theoretical work about refractive index and optical confinement factor of GaInAsN up to our knowledge.

6.2 Theory

6.2.1 Adachi's model for refractive index

A more physics-based model of dielectric function for photon energies close to and above the band gap is Adachi's model. This model can be simplified for the transparency region $\hbar\omega < E_g$ by considering only the first band gaps($E_g, E_g + \Delta_0$)

$$n_r^2(\omega) = A f(x_1) + 0.5 \left(\frac{E_g}{E_g + \Delta_0} \right)^{1.5} f(x_2) + B \quad (6.1)$$

where A and B are the empirical parameters which are given in table.

$$f(x_1) = \frac{1}{x_1^2} (2 - \sqrt{1 + x_1} - \sqrt{1 - x_1}) \quad (6.2)$$

where $x_1 = \frac{\hbar\omega}{E_g}$ and

$$f(x_2) = \frac{1}{x_2^2} (2 - \sqrt{1 + x_2} - \sqrt{1 - x_2}) \quad (6.3)$$

where $x_2 = \frac{\hbar\omega}{E_g + \Delta_0}$. A and B parameters of quaternary compound semiconductors are calculated by interpolation method.

6.2.2 Five-layer symmetric slab theory

The obtained laser light should be confined in heterostructure as electron. For this aim different type waveguides have been produced. One of these waveguides is five-layer slab waveguide so we made our calculations according this type waveguide. The structure of this waveguide is shown in 6.1.

Parameter	A	B	E_g (eV)	Δ_0 (eV)
GaAs	6.3	9.4	1.42	0.34
InP	8.4	6.6	1.35	0.11
AlAs	25.3	-0.8	2.95	0.28
InAs	5.14	10.15	0.36	0.38
GaP	22.25	0.9	2.74	0.08
AIP	24.1	-2.0	3.58	0.07
GaN	9.31	3.03	3.299	0.0
InN	53.37	-9.19	1.89	0.0

Table 6.1: The required parameters related to the refractive index of the materials.

(1) Electric field distribution for core region (well region):

$$\xi_{y1}(x, z, t) = A \cos(h_1 x) e^{i(\omega t - \beta z)}; 0 \leq |x| \leq a \quad (6.4)$$

(2) Electric field distribution for barrier region :

$$\xi_{y2}(x, z, t) = B \cos(h_2 x) e^{i(\omega t - \beta z)}; a \leq |x| \leq b \quad (6.5)$$

(3) Electric field distribution for cladding layer region :

$$\xi_{y3}(x, z, t) = C e^{-h_3 x} e^{i(\omega t - \beta z)}; b \leq |x| \leq c \quad (6.6)$$

The field distributions for even-order modes are written:

$$kn_2 \geq \beta \geq kn_3 \quad (6.7)$$

For now, we don't consider exponential complex part; If we apply the boundary conditions to electric fields, we can see that; At $x = a$; $\xi_{y1}(a) = \xi_{y2}(a)$ and so $A \cos(h_1 a) = B \cos(h_2 a)$

$$B = \frac{A \cos(h_1 a)}{\cos(h_2 a)} \implies \xi_{y2}(x) = \frac{A \cos(h_1 a)}{\cos(h_2 a)} \cos(h_2 x) \quad (6.8)$$

At $x = b$; $\xi_{y2}(b) = \xi_{y3}(b)$ and so

$$\frac{A \cos(h_1 a)}{\cos(h_2 a)} \cos(h_2 b) = C e^{-h_3 b} \quad (6.9)$$

$$C = \frac{A \cos(h_1 a) e^{h_3 b}}{\cos(h_2 a)} \cos(h_2 b) \implies \xi_{y3}(x) = \frac{A \cos(h_1 a)}{\cos(h_2 a)} \cos(h_2 b) e^{h_3(b-x)} \quad (6.10)$$

At $x = a$; $\frac{\partial \xi_{y1}(x)}{\partial x} = \frac{\partial \xi_{y2}(x)}{\partial x}$ and so

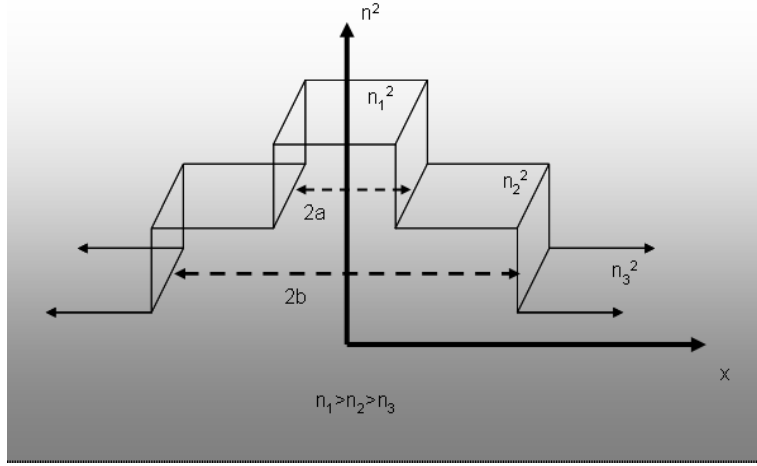


Figure 6.1: The illustration of the five layer slab waveguide.

$$\begin{aligned} -h_1 A \sin(h_1 a) &= -h_2 \frac{A \cos(h_1 a)}{\cos(h_2 a)} \sin(h_2 a) \\ \tan(h_1 a) &= \frac{h_2}{h_1} \tan(h_2 a) \end{aligned} \quad (6.11)$$

At $x = b$; $\frac{\partial \xi_{y1}(x)}{\partial x} = \frac{\partial \xi_{y3}(x)}{\partial x}$ and so

$$\begin{aligned} -h_2 \frac{A \cos(h_1 a)}{\cos(h_2 a)} \sin(h_2 b) &= -h_3 \frac{A \cos(h_1 a)}{\cos(h_2 a)} \cos(h_2 b) e^{h_3(b-b)} \\ h_2 \tan(h_2 b) &= h_3 \\ h_2 \tan(h_2 b) = h_3 &\implies h_2 = \frac{1}{b} \arctan\left(\frac{h_3}{h_2}\right) \end{aligned} \quad (6.12)$$

substituting 6.12 to 6.11.

$$\tan(h_1 a) = \frac{h_2}{h_1} \tan(h_2 a) \implies h_1 a = \arctan\left(\frac{h_2}{h_1} \tan\left(\frac{a}{b} \arctan\left(\frac{h_3}{h_2}\right)\right)\right) \quad (6.13)$$

where $h_1^2 = k^2 n_1^2 - \beta^2$; $h_2^2 = k^2 n_2^2 - \beta^2$; $h_3^2 = \beta^2 - k^2 n_3^2$

$M\pi$ is eliminated because we will study $M = 0$ mode. In addition, exponential terms have not been considered because they are cancelled in confinement factor calculation (electric field is multiplied by its conjugate).

If $kn_1 \geq \beta \geq kn_2$ then equation 6.13 will be as following:

$$\tan(h_1 a) = \frac{h_2}{h_1} \tan(h_2 a) \implies h_1 a = M\pi + \arctan\left(\frac{h_2}{h_1} \tan\left(\frac{a}{b} \arctan h\left(\frac{h_3}{h_2}\right)\right)\right) \quad (6.14)$$

where $h_1^2 = k^2 n_1^2 - \beta^2$; $h_2^2 = \beta^2 - k^2 n_2^2$; $h_3^2 = \beta^2 - k^2 n_3^2$

We have two options:

$$\begin{aligned}
\sqrt{\frac{n_1^2 - n_2^2}{n_1^2 - n_3^2}} &\leq \frac{h_1}{k\sqrt{n_1^2 - n_3^2}} \leq 1 && \text{1.condition} \\
0 &\leq \frac{h_1}{k\sqrt{n_1^2 - n_3^2}} \leq \sqrt{\frac{n_1^2 - n_2^2}{n_1^2 - n_3^2}} && \text{2.condition}
\end{aligned} \tag{6.15}$$

To understand these equations we may view at relationship equations between electric fields, refractive index, propagation constant and wavelength.

$$\Gamma = \frac{\int_0^a \xi_{y1}^2(x, z, t) dx}{\int_0^a \xi_{y1}^2(x, z, t) dx + \int_a^b \xi_{y2}^2(x, z, t) dx + \int_b^c \xi_{y3}^2(x, z, t) dx} \tag{6.16}$$

Optical confinement factor calculation can be made merely with above equation. However, electric fields are obtained from the calculations which have refractive indices analysis. These indices are dependent wavelengths and this condition causes complicated and different type solution ways.

Above calculations have all analogy about optical confinement factor. We have used an approximation which belongs to M.J.Adams to obtain simply optical confinement factor.

$$\begin{aligned}
v^2 &= a^2 k^2 (n_1^2 - n_3^2) \\
u^2 &= a^2 (k^2 n_1^2 - \beta^2) = a^2 h_1^2 \\
w^2 &= a^2 (\beta^2 - k^2 n_3^2) = v^2 - u^2 = a^2 h_3^2 \\
t^2 &= a^2 (k^2 n_2^2 - \beta^2) = u^2 - v^2 c^2 = a^2 h_2^2 \\
t'^2 &= a^2 (\beta^2 - k^2 n_2^2) = v^2 c^2 - u^2 = a^2 h_2'^2
\end{aligned} \tag{6.17}$$

$$c^2 = \frac{n_1^2 - n_2^2}{n_1^2 - n_3^2} \approx \frac{n_1 - n_2}{n_1 - n_3} \tag{6.18}$$

$$u = M\pi + \arctan\left(\frac{t}{u} \tan\left(\arctan\left(\frac{w}{t}\right) - t\left(\frac{b}{a} - 1\right)\right)\right) \tag{6.19}$$

if $t \rightarrow it'$

$$u = M\pi + \arctan\left(\frac{t'}{u} \tanh\left(\arctan h\left(\frac{w}{t'}\right) - t'\left(\frac{b}{a} - 1\right)\right)\right) \tag{6.20}$$

if $c \leq u/v \leq 1$;

$$\Gamma = \frac{u + \sin u \cos u}{u + \sin u \cos u \left(1 - \frac{u^2}{t^2}\right) + u \left(\cos^2 u + \frac{u^2}{t^2} \sin^2 u\right) \left(\frac{b}{a} - 1 + \frac{1}{w}\right)} \tag{6.21}$$

if $0 \leq u/v \leq c$;

$$\Gamma = \frac{u + \sin u \cos u}{u + \sin u \cos u \left(1 + \frac{u^2}{t'^2}\right) + u \left(\cos^2 u - \frac{u^2}{t'^2} \sin^2 u\right) \left(\frac{b}{a} - 1 + \frac{1}{w}\right)} \tag{6.22}$$

6.3 Calculation of refractive index and optical confinement factor in InGaAsN by using the analytical method

The spectroscopic ellipsometry measurements [116, 117, 118, 120][116] have shown that the refractive index of strained GaInAsN/GaAs layers increases with increasing N concentration. We now want to illustrate at this point the Adachi's model can be used to investigate the refractive index of III-V and III-N-V semiconductors due to the agreement with experimental observations. Firstly, it has been stated by Sato et. al. [117] that III-N-V semiconductors have the largest refractive index compared to III-V semiconductors. Figure 6.2 confirms this prediction by means of using Adachi's model for refractive index calculations for GaAs, InGaAs and InGaAsNs with increasing N concentration. As shown in Figure 6.2 the refractive index of InGaAsNs is greater than that of both GaAs and InGaAs. The same figure also shows clearly that the refractive index increases with increasing N concentration as has been predicted experimentally.

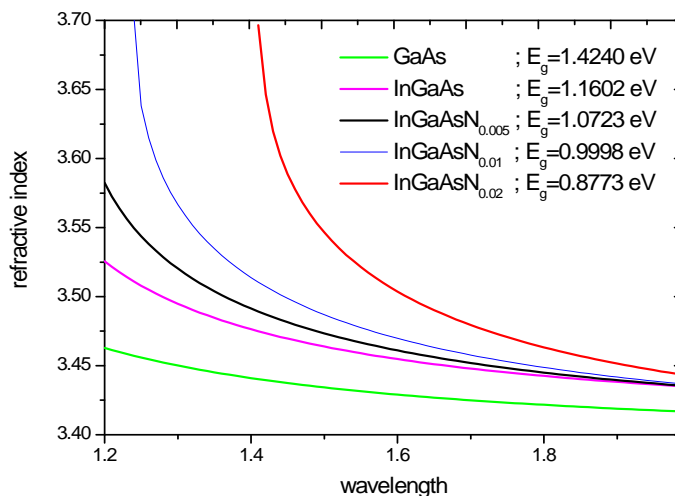


Figure 6.2: Calculated refractive index values for GaAs, InGaAs and GaInAsNs with increasing N concentration.

In the contour plot in Figure 6.3 we show the calculated nitrogen and wavelength dependence of refractive index according to Adachi's model for the GaInAsN on GaAs substrate. As can be seen from figure 6.3 that the refractive index for a fixed wavelength first increases with increasing N concentration and then reaches its maximum value when the strained band gap energy of InGaAsN

alloy becomes equal to the energy of photon (red shapes). Beyond this critical point the refractive index starts to decrease with increasing N concentration since after this point the energy of photon becomes greater than the strained band gap. Figure 6.3 also shows the variation of refractive index for a fixed N concentration as a function of wavelength of photon. The general trend is that refractive index increases with decreasing energy and reaches its peak value when the photon energy becomes comparable to the strained band gap energy and then it decreases with further decreases in energy of photon. We have calculated that the increase in In concentration has similar effect on the refractive index of InGaAsNs. Until now we have calculated the refractive indices assuming that the photons having different wavelengths are falling onto the semiconductor alloy. However, photons are produced inside the quantum well (QW) with an energy corresponding to the transition energy between conduction and valence subbands. Therefore, each In and N concentration corresponds to a photon having different energy inside a GaInAsN QW.

The contour representation showing the In and N dependence of refractive index of GaInAsN QWs in which the energy of photon is equal to the transition energy is given in Figure 6.3. As it is clear from Figure 6.4 that the refractive index of GaInAsN QWs is a complex function of In and N concentration and gets worse with an increase of In and N concentration. It gets better when the N concentration becomes greater than 3% but the light emitting devices deteriorates when N concentration reaches this value.

The optical confinement factor Γ , which is usually defined as the fraction of the squared electric field confined to active region [121, 122, 123], is an important parameter in calculating the threshold current for semiconductor lasers. The aim of this section is to compare the optical confinement factor Γ of conventional III-V semiconductors with that of the III-N-V semiconductors for separate confinement heterostructures (SCH). A five layer dielectric slab waveguide model is employed to calculate Γ . In a SCH the quantum well active region and surrounding barriers are sandwiched between optical confining layers. The advantage of this structure is that the confinement of radiation to the recombination region can be made superior to that for the conventional double heterostructure lasers, so that there is more efficient pumping of the optical field by the recombination processes. We consider three different laser structures operating around the 1.3 μm wavelength for comparison. The first type of device studied is the P-based laser, which consists of $\text{Ga}_{0.33}\text{In}_{0.67}\text{P}_{0.28}\text{As}_{0.72}$ / $\text{Ga}_{0.1}\text{In}_{0.9}\text{P}_{0.78}\text{As}_{0.22}$ / InP with unstrained QWs. The second type of device is the Al-based laser with $\text{Al}_{0.175}\text{Ga}_{0.095}\text{In}_{0.73}\text{As}$ / $\text{Al}_{0.27}\text{Ga}_{0.21}\text{In}_{0.57}\text{As}$ / InP structure parameters and the well is 1.4% compressively strained. The third type of device is the N-based laser

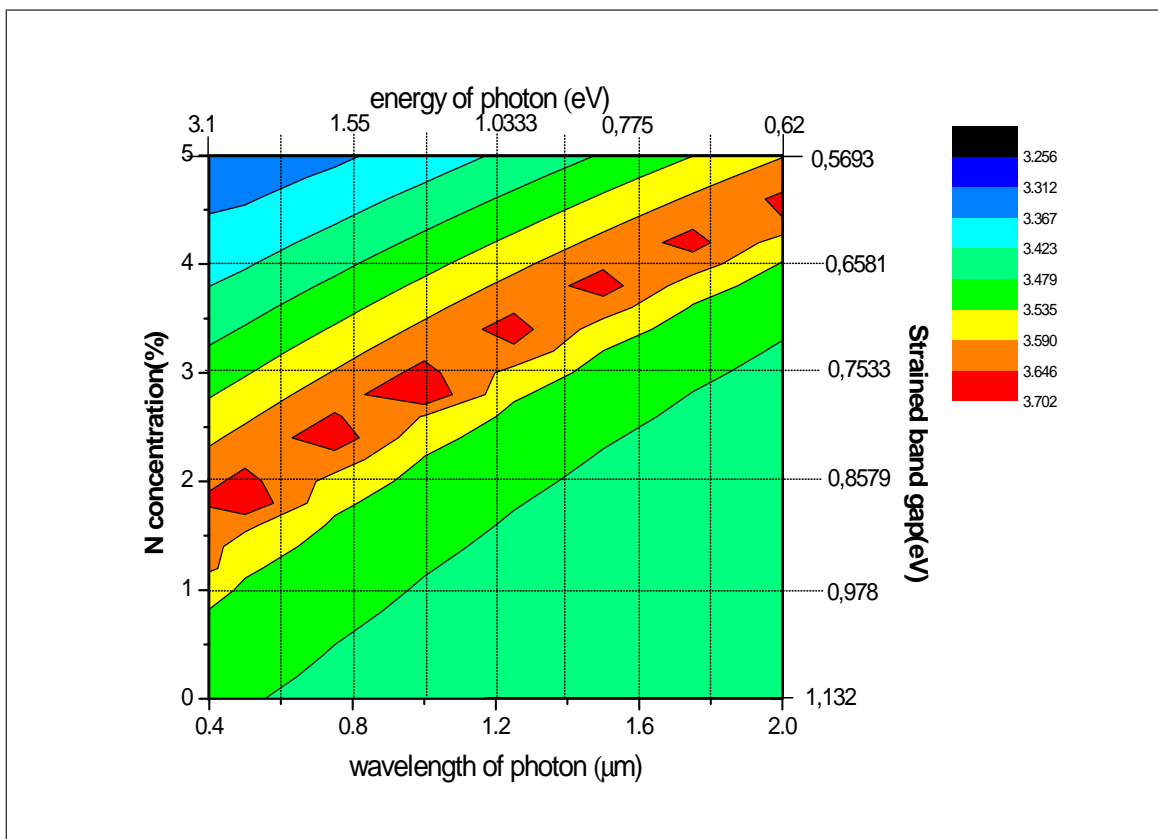


Figure 6.3: GaInNAs on GaAs substrate as a function of N concentration and wavelength of photon. The top x -axis shows the energy of photon and right y -axis shows the strained band gap of the GaInNAs on GaAs substrate for N concentrations stated on the left y -axis.

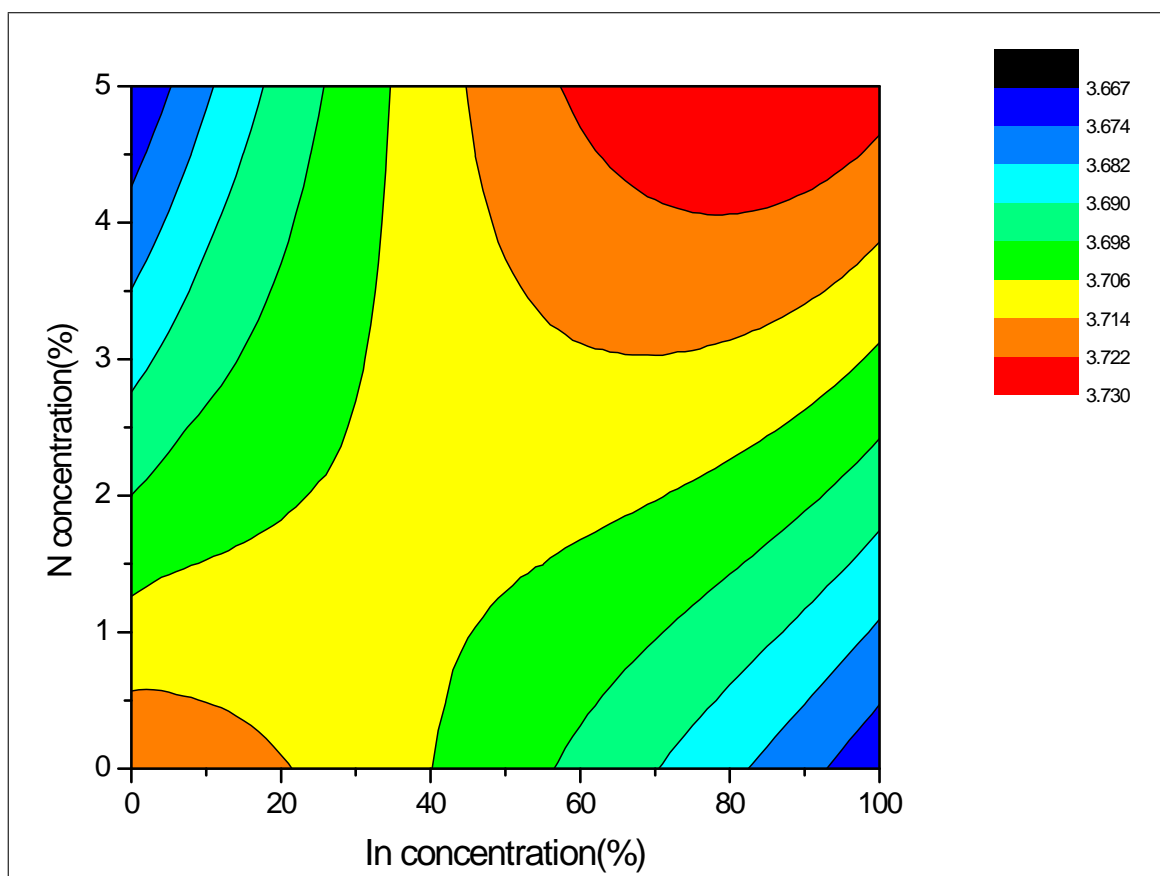


Figure 6.4: Contour maps of refractive index of GaInNAs well as a function of In and N concentration.

with 1.7% compressively strained $\text{Ga}_{0.7}\text{In}_{0.3}\text{N}_{0.022}\text{As}_{0.098}$ QWs between GaAs barriers and $\text{Al}_{0.1}\text{Ga}_{0.9}\text{As}$ cladding layers. The cavity length in all structures is taken as $610 \mu\text{m}$. As seen in figure 6.5, Γ for the three laser system increases with the thickness of the active region as expected. It is also seen from figure 6.5 that Al-based laser system has the highest Γ compared to the others. Since all the laser systems have the same emission wavelength, the difference between the Γ of the three laser system is due to the differences between the refractive indices of the barrier and cladding layers. The laser system having the largest refractive index difference between the barrier and cladding layer has the largest Γ . The refractive indices of the layers of the three laser system are tabulated in Table 6.2.

System	Well refractive index	Barrier refractive index	Cladding refractive index
InGaAsP	3,7034	3,2676	3,1906
GaInAsN	3,7036	3,4501	3,3993
AlGaInAs	3,7597	3,4518	3,1906

Table 6.2: The refractive index values of three different layers for the systems of $\text{Ga}_{0.33}\text{In}_{0.67}\text{P}_{0.28}\text{As}_{0.72}$ / $\text{Ga}_{0.1}\text{In}_{0.9}\text{P}_{0.78}\text{As}_{0.22}$ / InP, $\text{Al}_{0.175}\text{Ga}_{0.095}\text{In}_{0.73}\text{As}$ / $\text{Al}_{0.27}\text{Ga}_{0.21}\text{In}_{0.52}\text{As}$ / InP and $\text{Ga}_{0.7}\text{In}_{0.3}\text{N}_{0.022}\text{As}_{0.978}$ QWs between GaAs barriers and $\text{Al}_{0.1}\text{Ga}_{0.9}\text{As}$ cladding layers.

Therefore, one can conclude that the use of different barrier and cladding layers may improve the laser system from the standpoint of optical confinement factor. Figure 6.6 illustrates this happens indeed: the use of different barriers and cladding layers can either increase or decrease the Γ of the N-based laser system. The use of different barriers introduces strain compensated laser system and may bring benefit to the laser system. As seen in figure 6.6, the use of the tensilely strained GaAsN barrier brings improvements to the Γ , since the Γ of the N-based laser system is doubled with GaAsN barrier compared to the GaAs barrier. In addition, it is now commonly accepted [124, 125] that the introduction of N into InGaAs causes an ideal band alignment of deep conduction- and shallow valence-wells, see figure 3.1. The calculation details of the band alignments can be found in our recent papers [124, 125].

6.4 Conclusions

Our calculations confirm the experimental observations that the refractive index increases in proportion with a decrease in band gap energy both in III-V and III-N-V semiconductors. Our calculations confirm also that

- o refractive index of InGaNAs is greater than that of III-V semiconductors,
- o refractive index increases with increasing N concentration in GaInAsN alloys.

Although the band offsets of III-N-V systems are close to that of the ideal case which leads to have an improved carrier confinement, the optical confinement of III-N-V laser system is worse than that of the 1.3 μm III-V laser systems. This leads to poor optical confinement in III-N-V laser system. However, the optical confinement can be improved by means of introducing strain-compensated barrier to the III-N-V system.

As a summary, strain-compensated laser systems improves both carrier and optical confinement significantly.

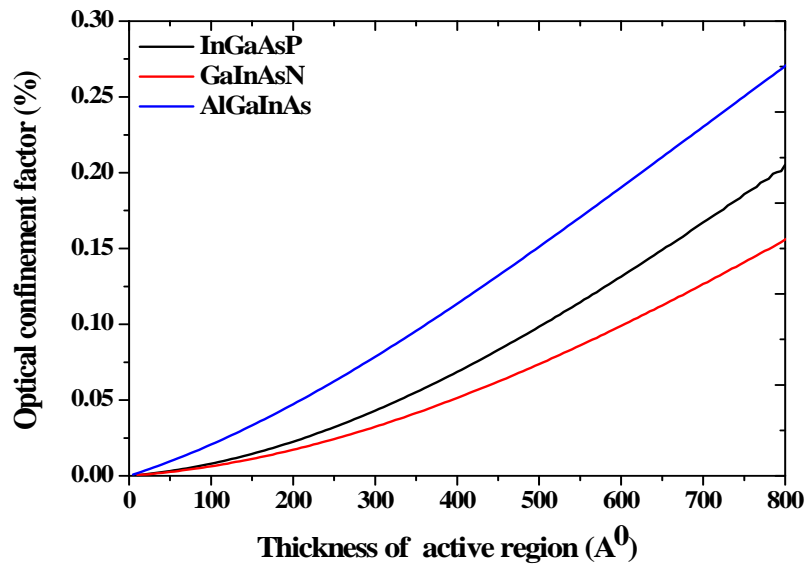


Figure 6.5: The variation of the optical confinement factor Γ versus the thickness of the active region for the laser structures of InGaAsP, AlGaInAs, and GaInAsN with an emission wavelength of $1.3 \mu\text{m}$.

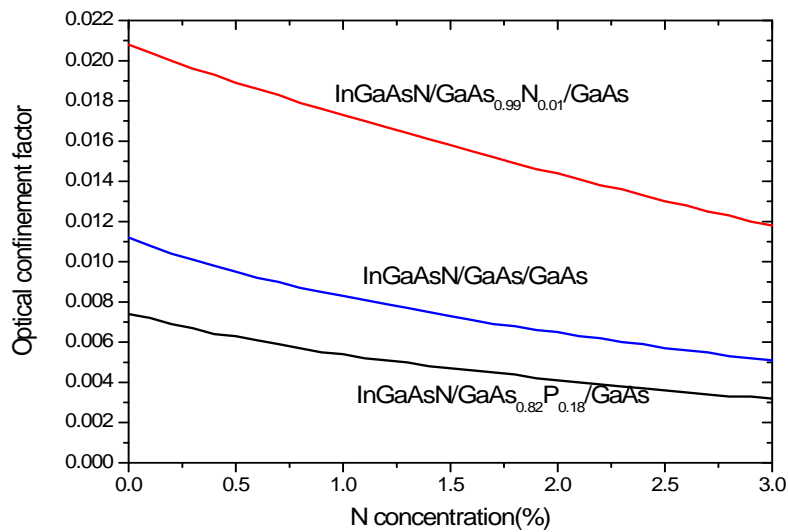


Figure 6.6: The calculated variation of Γ of N-based uncompensated (blue-line) laser system with that of the compensated laser systems with GaAsN (red-line) and GaAsP (black-line) barrier.

CHAPTER 7

CONCLUSIONS AND FUTURE WORK

The work carried out in this thesis considered the effects of nitrogen, strain, substrate and growth orientation on the band offset, critical thickness, donor binding energy and optical confinement factor of GaInAsN(Sb) bulk and QWs on GaAs and InP substrates. Conclusions have been already presented in the result part of the related chapters. In this chapter, we briefly summarize and gather together the major conclusions from the work described in this thesis.

GaInAsN alloy has superior properties compared to that of conventional III-V semiconductors. The main reason of the superiority is the incorporation of nitrogen N into GaInAs since nitrogen has a profound influence on the electronic and optical properties of the GaInAsN alloy such as

- (1) better electron confinement due to the favourable band-offset ratio,
- (2) improved density of states as a result of the matching of the electron and hole effective masses,
- (3) flexibility of tailoring the band gap allowing the extend of the wavelength of photonic device operation beyond that accessible to InGaAsP/InP and AlGaInAs/InP.

Hence, GaInAsN gives the potential to produce material lattice matched or mismatched to GaAs and InP with a wide range of band gap energies. Therefore, quaternary material system of GaInAsN has attracted a great deal of attention, both because of unusual physical properties and potential applications in a variety of electronics and optoelectronic devices like quantum well lasers, infrared detectors, high-efficiency multijunction solar cells and high speed transistors. Even if the growth stage of dilute nitride III-Vs and quaternary alloys on GaAs or InP is problematic, development in thin-film deposition have allowed these

materials to be grown with ever-improving crystalline quality, which in turn improves their optical and electronic performance.

GaInAsN heterostructure material has unusual fundamental properties which have been observed experimentally. First of all, it has the large band gap bowing parameter which causes a rapid reduction in band gap of GaInAs with incorporating small amount of nitrogen. Furthermore, new energy state E_+ has been observed in the conduction band, which is not present in a usual semiconductor. A strong increase of electron effective mass with increasing N concentration has been reported.

The physics behind the unusual characteristics of GaInAsN has been overviewed. The derivation of band anticrossing model has been introduced and the calculated band gap variation versus nitrogen and indium has been shown in the figures. We expect that to understand the physics of nitrogen incorporation and the meaning of band anticrossing provide a wide comprehension about the related calculations in other chapters.

We have shown that model solid theory is an appropriate model to perform the band offset calculations of GaInAsN QWs and band anticrossing is a model to describe the composition dependence of band gap energy of GaInAsN on GaAs and InP substrates. We have indicated that the incorporation of nitrogen into the system provide to reach the laser beam wavelengths in a range from 1.3 μm to 2.3 μm . On the other hand, the addition of nitrogen into GaInAs on GaAs and InP improves the band alignment of the system. Furthermore, the band alignment of strained GaInAsN/InP QW laser systems is better than that of the GaInAsN/GaAs. Our calculations have shown that the introduction of opposite strain to the barrier in N-based lasers on both GaAs and InP substrates not only result deep electron wells but also cause the electron wells being much deeper than that of the hole wells which is essential to have good high temperature characteristics. Our calculations have indicated that the band alignment of N-based conventionally strained QW laser systems on InP with high indium concentration (beyond 53%) compete with the ideal band alignment of GaInAsN / GaAs lasers.

In order to obtain high optical quality structures, the layer thickness must be less than the so called critical layer thickness h_c . Despite great efforts for investigation of nitrogen incorporated III-V's, there is no detailed works concerning the critical layer thickness of these structures up to our knowledge. We have presented the role of N and Sb on the critical thickness of strained GaInAsNSb QWs on GaAs and InP substrate for (001) and (111) orientations. Matheews and Blakeslee model has been used to calculate critical thickness and we have shown that its calculated results have been in agreement with experimental ones

for N (Sb) included III-V's. We have shown that the critical thickness h_c decreases with increasing In for InGaAs/GaAs and the limitation of h_c is eliminated when the compressive InGaAs wells are grown on InP substrate. We have illustrated that the effect of addition of Sb atoms is similar to that of the In atoms of both causing a reduction in h_c . Since a fixed emission wavelength can be obtained for lower concentration of Sb in GaAs_xSb_{1-x} QW than that of the In concentration in In_xGa_{1-x}As, much larger critical layer thicknesses can be obtained for GaAs_xSb_{1-x} QWs. We have noticed that nitrogen atoms have strain compensating effects in GaInAsN and so improve the h_c . Furthermore, the choice of substrate and growth orientation changes the critical thickness values of GaInAsN, completely. The calculated results have indicated that although GaInAsNSb/GaAs QW has still constraint of critical layer thickness, this problem can be eliminated by means of using InP substrate which provide improvements in critical thickness.

Incorporation of impurities into the lattice is very important in the development of semiconductors as electronic materials. It is also important to evaluate the shallow donor impurity states which influence the electronic and optical properties of the semiconductors. We have presented the effect of nitrogen on the ground state binding energy of hydrogenic donors in GaAsN. We have seen that nitrogen concentration has a strong effect on the binding energy and Bohr radius because it induces nonparabolic conduction band and causes rapid reduction in the band gap. In order to take into account the screening effect of donor concentration on binding energy, we have performed our calculations by means of analytical energy expression of screened coulomb potential which has been found in our another work. We have noticed from our calculations that intrinsic carrier density and screening parameter affect effective Bohr radius and binding energy of shallow donors on which nitrogen concentration has also a strong effect. We believe that these results are valuable for future experiments.

Finally, we have performed detailed calculations on optical confinement properties of GaInAsN QW. Optical mode confinement is one of the basic ingredients while designing the semiconductor quantum well lasers. We have presented so called Adachi's model to calculate the variation of refractive index and five-layer slab model to calculate optical confinement factor of a semiconductor quantum well laser system. We have shown that refractive indices of bulk GaInAsN varies with change of nitrogen and indium concentrations and the wavelength of the applied photon. Our calculations on nitrogen dependence of optical confinement has shown that the optical confinement of III-N-V laser system is worse than that of the 1.3 μm III-V laser systems. However, we have shown that the optical confinement can be improved by means of introducing

strain-compensated barrier to the III-N-V system.

Recent experiments and theoretical investigations have shown that nitrogen-based heterostructures have an important role in future device applications because of their unusual fundamental properties. GaInAsN and related materials is the center of great interest as QW lasers to be used in telecommunication. There are great number of studies about GaInAsN being a successful candidate for high speed transistors, high efficient solar cells, long wavelength infrared photodetectors etc. Furthermore, there are limited works on 0- and 1-dimension properties and surface characteristics of GaInAsN. As a future work, we want to deal with transport properties of GaInAsN quantum wells, wires and dots and investigate surface characteristics of N-based layers.

LIST OF REFERENCES

- [1] Kondow, M., Uomi, K., Hosomi, K. and Mozume, T. (1994). Gas-Source Molecular Beam Epitaxy of $\text{GaN}_x\text{As}_{1-x}$ using a N radical as the N source. *Japanese Journal of Applied Physics*, **33**, L1056-L1058.
- [2] Buyanova, I. A. and Chen, W. M. (2004). *Physics and Applications of Dilute Nitrides*. New York: CRC.
- [3] Aissat, A., Nacer, S., Bensebti, M. and Vilcot, J.P. (2009). Low sensitivity to temperature compressive-strained structure quantum well laser $\text{Ga}_{1-x}\text{In}_x\text{As}_{1-y}\text{N}_y/\text{GaAs}$. *Microelectronics Journal*, **40**, 10-14.
- [4] Duboz, J. Y. (2007). Energy levels and intersubband transitions in InGaAsN/AlGaAs quantum wells. *Physical Review B*, **75**, 045327-045332.
- [5] Duboz, J.Y., Gupta, J. A., Byloss, M., Aers, G. C., Liu, H. C., and Wasilewski, Z. R. (2002). Intersubband transitions in InGaAsN/GaAs quantum wells. *Applied Physics Letters*, **81**, 1836-1838.
- [6] Ma, B. S., Fan, W. J., Dang, Y. X, Cheah, W. K., Loke, W. K., Liu, W., Li, D. S., Yoon, S. F., Zhang, D. H., and Wang, H. (2007). GaInNAs double-barrier quantum well infrared photodetector with the photodetection at 1.24 μm . *Applied Physics Letters*, **91**, 051102-1-3.
- [7] Duboz, J. Y., Hugues, M., Damilano, B., Nedelcu, A., Bois, P., Kheirodin, N., and Julien, F. H. (2009). Infrared detectors based on InGaAsN/GaAs intersubband transitions. *Applied Physics Letters*, **94**, 022103-1-3.
- [8] Royalla, B. and Balkan, N. (2009). Dilute nitride n-i-p-i solar cells. *Microelectronics Journal*, **40**, 396-398.
- [9] Henini, M. (2005). *Dilute Nitride Semiconductors*. Oxford: Elsevier.
- [10] Sun, Y., Balkan, N., Erol, A., Arikan, M.C. (2009). Electronic transport in n- and p-type modulation-doped GaInNAs/GaAs quantum wells. *Microelectronics Journal*, **40**, 403-405.
- [11] Veal, T. D., Mahboob, I. and McConville, C. F. (2004). Negative Band Gaps in Dilute $\text{InN}_x\text{Sb}_{1-x}$ Alloys. *Physical Review Letters*, **92**, 136801-1-3.
- [12] Hopfield, J. J., Thomas, D. G. and Lynch, R. T. (1966). Isoelectronic Donors and Acceptors. *Physical Review Letters*, **17**, 312-315.

- [13] Trumbore, F. A., Gershenson, M., and Thomas, D. G. (1966). Luminescence due to the isoelectronic substitution of bismuth for phosphorus in gallium phosphide. *Applied Physics Letters*, **9**, 4-6.
- [14] Merz, J. L. (1968). Isoelectronic Oxygen Trap in ZnTe. *Physical Review*, **176**, 961-968.
- [15] Baldereschi, A. and Hopfield, J. J. (1972). Binding to Isoelectronic Impurities in Semiconductors. *Physical Review Letters*, **28**, 171-174.
- [16] Allen, J. W. (1971). Isoelectronic impurities in semiconductors: a survey of binding mechanisms. *J. Phys. C: Solid State Physics*, **4**, 1936-1944.
- [17] Hader, J., Koch, S. W., Moloney, J. V. and O'Reilly, E. P. (2000). Gain in 1.3 μm materials: InGaNAs and InGaPAs semiconductor quantum-well lasers. *Applied Physics Letters*, **77**, 630-632.
- [18] Zhang, Y., Ge, W. (2000). Behavior of nitrogen impurities in III-V semiconductors. *Journal of Luminescence*, **85**, 247-260.
- [19] Kent, P. R. C., Bellaiche, L. and Zunger, A. (2002). Pseudopotential theory of dilute III-V nitrides. *Semiconductor Science and Technology*, **17**, 851-859.
- [20] Klar, P. J., Grüning, H., Heimbrodt, W., Koch, J., Höhnsdorf, F., Stolz, W., Vicente, P. M. A. and Camassel, J. (2000). From N isoelectronic impurities to N-induced bands in the $\text{GaN}_x\text{As}_{1-x}$ alloy. *Applied Physics Letters*, **76**, 3439-3441.
- [21] Onabe K., Aoki D., Wu J., Yaguchi H., Shiraki Y. (1999). MOVPE Growth and Luminescence Properties of GaAsN Alloys with Higher Nitrogen Concentrations. *Physica Status Solidi(a)*, **176**, 231-235.
- [22] Perkins, J. D., Mascarenhas, A., Geisz, J. F., and Friedman, D. J. (2001). Conduction-band-resonant nitrogen-induced levels in $\text{GaAs}_{1-x}\text{N}_x$ with $x \ll 0.03$. *Physical Review B*, **64**, 121301-1-4.
- [23] Kondow, M. , Uomi, K., Niva, A., Kitatani, T., Watahiki, S., and Yazawa, Y. (1996). GaInNAs: A Novel Material for Long-Wavelength-Range Laser Diodes with Excellent High-Temperature Performance. *Japanese Journal of Applied Physics*, **35**, 1273-1275.
- [24] Höhnsdorf, F., Koch, J., Leu, S., Stolz, W., Borchert, B. and Druminski, M. (1999). Reduced threshold current densities of (GaIn)(NAs)/GaAs single quantum well lasers for emission wavelengths in the range 1.28 – 1.38 μm . *Electronics Letters*, **35**, 571-572.
- [25] Nakahara, K. , Kondow, M., Kitatani, T., Larson, M. C. and Uomi, K. (1998). 1.3 – μm continuous-wave lasing operation in GaInNAs quantum-well lasers. *IEEE Photonics Technology Letters*, **10**, 487-488.

- [26] Sato, S. and Satoh, S. (1999). 1.3 μm continuous-wave operation of GaInNAs lasers grown by metal organic chemical vapour deposition. *Electronics Letters*, **35**, 1251-1252.
- [27] Buyanowa, I. A., Chen, W. M. and Monemar, B. (2001). Electronic Properties of Ga(In)NAs Alloys. *MRS Internet Journal of Nitride Semiconductors Research*, **6**, 2.
- [28] Zaets, W. and Ando, K. (1999). Optical waveguide isolator based on non-reciprocal loss/gain of amplifier covered by ferromagnetic layer. *IEEE Photonics Technology Letters*, **11**, 1012-1014.
- [29] Takenaka, K., Proceedings of 11th International Conference on Indium Phosphide and Related Materials (1999). Davos, Switzerland, 289.
- [30] Gokhale, M. R. , Wei, J., Wang, H. and Forrest, S. R. (1999). Growth and characterization of small band gap (~ 0.6 eV) InGaAsN layers on InP. *Applied Physics Letters*, **74**, 1287-1290.
- [31] Bellaiche, L. (1999). Band gaps of lattice-matched (Ga,In)(As,N) alloys. *Applied Physics Letters*, **75**, 2578-2581.
- [32] Ubukata, A. , Dong, J., Matsumoto, K. and Ishihara, Y. (2000). Growth of $\text{Ga}_{0.46}\text{In}_{0.54}\text{N}_y\text{As}_{1-y}$ Single Quantum Wells on InP(100) Substrate by Metalorganic Chemical Vapor Deposition. *Japanese Journal of Applied Physics*, **39**, 5962-5965.
- [33] Serries, D., Geppert, T., Ganser, P., Maier, M., Köhler, K., Herres, N. and Wagner, J. (2002). Quaternary GaInAsN with high In content: Dependence of band gap energy on N content. *Applied Physics Letters*, **80**, 2448-2451.
- [34] Köhler, K., Wagner, J., Ganser, P., Serries, D., Geppert, T., Maier, M. and Kirste, L. (2004). The realization of long-wavelength ($\lambda \leq 2.3 \mu\text{m}$) $\text{Ga}_{1-x}\text{In}_x\text{As}_{1-y}\text{N}_y$ quantum wells on InP by molecular-beam epitaxy. *Journal of Physics: Condensed Matter*, **16**, S2995-S3008.
- [35] Tu, C. W. (2001). III-N-V low-bandgap nitrides and their device applications. *Journal of Physics: Condensed Matter*, **13**, 7169-7182.
- [36] Carrere, H. , Marie, X., Barrau, J., Amand, T., Bouzid, S. B., Sallet, V. and Harmand, J. C. (2004). Band structure calculation of InGaAsN//GaAs, InGaAsN//GaAsP//GaAs and InGaAsN//InGaAsP//InP strained quantum wells. *IEE Proceedings Optoelectronics*, **151**, 402-406.
- [37] Ellmers, C. , Höhnsdorf, F., Koch, J., Agert, C., Leu, S., Karaiskaj, D., Hofmann, M., Stolz, W. and Rühle, W. W. (1999). Ultrafast (GaIn)(NAs)/GaAs vertical-cavity surface-emitting laser for the 1.3 μm wavelength regime. *Applied Physics Letters*, **74**, 2271-2273.
- [38] Xin, H. P. , Tu, C. W. (1998). GaInNAs/GaAs multiple quantum wells grown by gas-source molecular beam epitaxy. *Applied Physics Letters*, **72**, 2442-2444.

- [39] Matthews, J. W. and Blakeslee, A. E. (1974). Coherent Strain in Epitaxially Grown Films. *Journal of Crystal Growth*, **24**, 188.
- [40] Ghiti, A. and Ekenberg, U. (1994). Improved laser performance due to spatial separation of heavy- and light-hole states in compressive- and tensile-strained structures. *Semiconductor Science and Technology*, **9**, 1575-1579.
- [41] Miller, B. I. , Koren, U., Young, M. G. and Chieh, M. D. (1991). Strain-compensated strained-layer superlattices for 1.5 μm wavelength lasers. *Applied Physics Letters*, **58**, 1952-1954.
- [42] Zhang, G. and Ovtchinnikov, A. (1993). Strain-compensated InGaAs/GaAsP/GaInAsP/GaInP quantum well lasers ($\lambda \sim 0.98 \mu\text{m}$) grown by gas-source molecular beam epitaxy. *Applied Physics Letters*, **62**, 1644-1646.
- [43] Silfvenius, C., Stalnacke, B., Landgren, G. (1997). MOVPE growth of strain-compensated 1300 nm $\text{In}_{1-x}\text{Ga}_x\text{As}_y\text{P}_{1-y}$ quantum well structures. *Journal of Crystal Growth*, **170**, 122.
- [44] Perkins, J. D., Mascarenhas, A., Zhang, Y., Geisz, J. F., Friedman, D. J., Olson, J. M. and Kurtz, S. R. (1999). Nitrogen-Activated Transitions, Level Repulsion, and Band Gap Reduction in $\text{GaAs}_{1-x}\text{N}_x$ with $x < 0.03$. *Physical Review Letters*, **82**, 3312-3315.
- [45] Shan, W., Walukiewicz, W., Ager, J. W., Haller, E. E., Geisz, J. F., Friedman, D. J., Olson, J. M. and Kurtz, S. R. (1999). Band Anticrossing in GaInNAs Alloys. *Physical Review Letters*, **82**, 1221-1224.
- [46] Suemune, I., Uesugi, K. and Walukiewicz, W. (2000). Role of nitrogen in the reduced temperature dependence of band-gap energy in GaNAs. *Applied Physics Letters*, **77**, 3021-3023.
- [47] Vurgaftman, I., Meyer, J. R. and Ram Mohan, L. R. (2001). Band parameters for III – V compound semiconductors and their alloys. *Journal of Applied Physics*, **89**, 5815-5875.
- [48] Gönül, B., Koçak, F., Toktamış, H. and Oduncuoğlu, M. (2004). Theoretical Comparison of the Band Alignment of Conventionally Strained and Strain-Compensated Phosphorus- Aluminum- and Nitrogen-Based 1.3 μm QW Lasers. *Chinese Journal of Applied Physics*, **42**, 764-769.
- [49] Minch, J., Park, S. H., Keating, T. and Chuang, S. L. (1999). Theory and experiment of $\text{In}_{1-x}\text{Ga}_x\text{As}_y\text{P}_{1-y}$ and $\text{In}_{1-x-y}\text{Ga}_x\text{Al}_y\text{As}$ long-wavelengthstrained quantum-well lasers. *IEEE Journal of Quantum Electronics*, **35**, 771-782.
- [50] Yong, J. C. L., Rorison, J. M. and White, I. (2002). 1.3 – μm quantum-well InGaAsP, AlGaInAs, and InGaAsN laser material gain: a theoretical study. *IEEE Journal of Quantum Electronics*, **38**, 1553-1564.

- [51] O'Reilly, E. P., Jones, G., Ghiti, A. and Adams, A. R. (1991). Improved performance due to suppression of spontaneous emission in tensile-strain semiconductor lasers. *Electronics Letters*, **27**, 1417-1419.
- [52] Thijs, P. J. A., Tiemeijer, L. F., Kuindersma, P. I., Binsma, J. J. M. and Van Dongen, T. (1991). High-performance 1.5 μm wavelength InGaAs-InGaAsP strained quantum well lasers and amplifiers. *IEEE Journal of Quantum Electronics*, **27**, 1426-1439.
- [53] Thijs, P. J. A., Tiemeijer, L. F., Binsma, J. J. M. and Van Dongen, T. (1994). Progress in long-wavelength strained-layer InGaAs(P) quantum-well semiconductor lasers and amplifiers. *IEEE Journal of Quantum Electronics*, **30**, 477-499.
- [54] Gönül, B. (1999). Influence of effective mass and energy band splittings on the radiative characteristics of QW lasers at transparency. *Physica E*, **5**, 50-61.
- [55] Sarzala, R. P. and Nakwaski, W. (2006). Physical Analysis of a Possibility to Reach the 1.30 – μm Emission from the GaAs-Based VCSELs with the InGaAs/GaAs Quantum-Well Active Regions and the Intentionally Detuned Optical Cavities. *Optical and Quantum Electronics*, **38**, 325-337.
- [56] Choquette, K. D., Geib, K. M., Ashby, C. H., Twesten, R. D., Blum, O., Hou, H. Q., Follstaedt, D. M., Hammons, B. E., Mathes, D. and Hull, R. (1997). Advances in selective wet oxidation of AlGaAs alloys. *IEEE Journal of Selected Topics in Quantum Electronics*, **3**, 916-926.
- [57] Kondow, M. and Kitatani, T. (2002). Molecular beam epitaxy of GaNAs and GaInNAs. *Semiconductors Science and Technology*, **17**, 746-754.
- [58] Jackson, A. W., Naone, R. L., Dalberth, M. J., Smith, J. M., Malone, K. J., Kisker, D. W., Klem, J. F., Choquette, K. D., Serkland, D. K. and Geib, K. M. (2001). OC-48 capable InGaAsN vertical cavity lasers. *Electronics Letters*, **37**, 355-356.
- [59] Purvis, G. (2004). GaInNAsSb by MBE. *III-Vs Review*, **17**, 43-44.
- [60] Yang, X., Jurkovic, M. J., Heroux, J. B. and Wang, W. I. (1999). Molecular beam epitaxial growth of InGaAsN:Sb/GaAs quantum wells for long-wavelength semiconductor lasers. *Applied Physics Letters*, **75**, 178-180.
- [61] Shimizu, H., Kumada, K., Uchiyama, S. and Kasukawa, A. (2001). High-performance CW 1.26 – μm GaInNAsSb-SQW ridge lasers. *IEEE Journal of Selected Topics in Quantum Electronics*, **7**, 355-364.
- [62] Gambin, V., Ha, W., Wistey, M., Yuen, H., Bank, S. R., Kim, S. M. and Harris, J. S. Jr. (2002). GaInNAsSb for 1.3 – 1.6 – μm -long wavelength lasers grown by molecular beam epitaxy. *IEEE Journal of Selected Topics in Quantum Electronics*, **8**, 795-800.
- [63] Smith, D. L., and Mailhot, C. (1988). Piezoelectric effects in strained-layer superlattices. *Journal of Applied Physics*, **63**, 2717-2719.

- [64] Anan, T., Nishi, K., Sugou, S. (1992). Critical layer thickness on (111)B-oriented InGaAs/GaAs heteroepitaxy. *Applied Physics Letters*, **60**, 3159-3161.
- [65] Blanc, S., Arnoult, A., Carrere, H., Fontaine, C. (2003). Interest of the {111} orientation for GaAsN and GaInAsN/GaAs quantum wells grown by molecular beam epitaxy. *Solid-State Electronics*, **47**, 395-398.
- [66] Volovik, B. V., Kovsh, A. R., Passenberg, W., Kuenzel, H., Grote, N., Cherkashin, N. A., Musikhin, Y. G., Ledentsov, N. N., Bimberg, D. and Ustinov, M.V. (2001). Optical and structural properties of self-organized InGaAsN/GaAs nanostructures. *Semiconductors Science and Technology*, **16**, 186-190.
- [67] Giannattasio, S., Senkader, R. J., Falster, R. J. and Wilshaw, P. R. (2003). Dislocation locking by nitrogen impurities in FZ-silicon. *Physika B: Condensed Matter*, **340**, 996-1000.
- [68] Momose, K., Yonezu, H., Fujimoto, Y., Ojima, K., Furukawa, Y., Utsumi, A., and Aiki, K. (2002). Hardening Effect of GaP_{1-x} and GaAs_{1-x}N_x Alloys by Adding Nitrogen Atoms. *Japanese Journal of Applied Physics*, **41**, 7301-7306.
- [69] Zhang, S. B., Zunger, A. (1997). Surface-reconstruction-enhanced solubility of N, P, As, and Sb in III-V semiconductors. *Applied Physics Letters*, **71**, 677-679.
- [70] Blanc, S., Arnoult, A., Carrere H., Fontaine C. (2003). GaAsN and GaInAsN/GaAs quantum wells grown on {111} substrates: growth conditions and optical properties. *Physica E*, **17**, 252-254.
- [71] Sugawara, M. (1992). Theoretical calculation of optical gain in In_xGa_{1-x}As/InP quantum wells under biaxially compressive and tensile strain. *Applied Physics Letters*, **60**, 1842-1844.
- [72] Jones, G. and O'reilly, E. P. (1993). Improved performance of long-wavelength strained bulk-like semiconductor lasers. *IEEE Journal of Quantum Electronics*, **29**, 1344-1354
- [73] Matthews, J. W. and Blakeslee, A. E. (1974). Defects in Epitaxial Multilayers: I. Misfit Dislocations in Layers. *Journal of Crystal Growth*, **27**, 118.
- [74] Van der Merve, J. H. (1963). Crystal Interfaces. Part II. Finite Overgrowths. *Journal of Applied Physics*, **34**, 123-127
- [75] Tsao, J. Y., Dodson, B. W., Picraux, S. T. and Cornelison, D. M. (1987). Critical Stresses for Si_xGe_{1-x} Strained-Layer Plasticity. *Physical Review Letters*, **59**, 2455-2458.
- [76] People, R. and Bean, J. C. (1985). Calculation of critical layer thickness versus lattice mismatch for Ge_xSi_{1-x}/Si strained-layer heterostructures. *Applied Physics Letters*, **47**, 322-324.

- [77] Ekenstedt, M. J., Andersson, T. G. and Wang, S. M. (1993). Temperature-dependent relaxation and growth phenomena in strained $\text{In}_x\text{Ga}_{1-x}\text{As}$ layers grown on GaAs. *Physical Review B*, **48**, 5289-5299.
- [78] Wang, S. M., Andersson, T. G., Vladimir, K. D. and Yao, J. Y. (1991). Critical layer thickness in $\text{In}_x\text{Ga}_{1-x}\text{As}/\text{GaAs}$ quantum wells studied by photoluminescence and transmission electron microscopy. *Superlattices Microstructure*, **9**, 123-126.
- [79] Fritz, I. J. (1987). Role of experimental resolution in measurements of critical layer thickness for strained-layer epitaxy. *Applied Physics Letters*, **51**, 1080-1082.
- [80] Grillo, V., Albrecht, M., Remmele, T., Strunk, H. P., Yu, A., Egorov and Riechert, H. (2001). Simultaneous experimental evaluation of In and N concentrations in InGaAsN quantum wells. *Journal of Applied Physics*, **90**, 3792-3798.
- [81] Fitzgerald, E. A. (1991). Dislocations in strained-layer epitaxy : theory, experiment, and applications. *Material Science Reports*, **7**, 87-142.
- [82] Goddard, L. *Ph. D. Thesis* (2005). Stanford University.
- [83] Jiang, D. S., Qu, Y. H., Ni, H. Q., Wu, D. H., Xu, Y. Q., Niu, Z. C. (2006). Optical properties of $\text{InGaAs}/\text{GaAs}$ quantum wells grown by Sb-assisted molecular beam epitaxy. *Journal of Crystal Growth*, **288**, 12-17.
- [84] Sung, L. W., Lin, H. H. (2003). Highly strained $1.24 - \mu\text{m}$ $\text{InGaAs}/\text{GaAs}$ quantum-well lasers. *Applied Physics Letters*. **83**, 1107-1109.
- [85] Ni, H. Q., Niu, Z. C., Xu, X. H., Zhang, W., Wei, X., Bian, L. F., He, Z. H., Han, Q., Wu, R. H. (2004). High-indium-content $\text{In}_x\text{Ga}_{1-x}\text{As}/\text{GaAs}$ quantum wells with emission wavelengths above $1.25 \mu\text{m}$ at room temperature. *Applied Physics Letters*, **84**, 5100-5102.
- [86] Kageyama, T., Miyamoto T., Ohta M., Matsuura T., Matsui Y., Furuhata T., Koyama F. (2004). Sb surfactant effect on $\text{GaInAs}/\text{GaAs}$ highly strained quantum well lasers emitting at 1200 nm range grown by molecular beam epitaxy. *Journal of Applied Physics*, **96**, 44-48.
- [87] Andersson, T. G., Chen, Z. G., Kulakovskii, V. D., Uddin, A. and Vallin, J. T. (1987). Variation of the critical layer thickness with In content in strained $\text{In}_x\text{Ga}_{1-x}\text{As}-\text{GaAs}$ quantum wells grown by molecular beam epitaxy. *Applied Physics Letters*, **51**, 752-754.
- [88] Temkin, H., Gershoni, D. G., Chu S. N. G., Vandenberg, J. M., Hamm, R. A. and Panish, M. B. (1989). Critical layer thickness in strained GaInAs/InP quantum wells. *Applied Physics Letters*, **55**, 1668-1670.
- [89] Ustinov, V. M. and Zhukov, A. E. (2000). GaAs-based long-wavelength lasers. *Semiconductor Science and Technology*, **15**, 41-54.

- [90] Anan, T., Nishi, K., Sugou, S., Yamada, M., Tokutome, K. and Gomyo, A. (1998). GaAsSb: A novel material for 1.3 μm VCSELs. *Electronics Letters*, **34**, 2127-2129.
- [91] Cunningham, J. E., Dinu, M., Shah, J., Quochi, F., Kilper, D. and Jan, W. Y., Williams, M. D., Mills, A., and Henderson, W. E. (2001). Growth and optical properties of GaAsSb quantum wells for 1.3 μm VCSELs. *The Journal of Vacuum Science and Technology B*, **19**, 1948-1952.
- [92] Tian, Y. and Wang, H. (2006). Analysis of DC characteristics of GaAs double heterojunction bipolar transistors (DHBTs) with a pseudomorphic GaAsSb base. *Microelectronics Journal*, **37**, 38-43.
- [93] Peter, M., Serries, D., Herre, N., Fuchs, F., Klefer, R., Winkler, K., Bachem, K. H. and Wagner, J. (1999). *International Physics Conference Series*, **156**, Ch:2.
- [94] Harmand, J-C., Caliman, A., Rao, E. V. K., Largeau, L., Ramos, J., Teissier, R., Travers, L., Ungaro, G., Theys, B. and Dias, I. F. L. (2002). GaNAsSb: how does it compare with other dilute III-V-nitride alloys? *Semiconductor Science and Technology*, **17**, 778-784.
- [95] Uesugi, K., Morooka, N., Suemune, I. (1999). Strain effect on the N composition dependence of GaNAs bandgap energy grown on (001) GaAs by metalorganic molecular beam epitaxy. *Journal of Crystal Growth*, **201/202**, 355-358.
- [96] Dmochowski, J. E. (2007). Donors in Semiconductors-are they Understood in Electronic Era? *Journal of Physics: Conference Series*, **79**, 012010.
- [97] Janotti, A., Reunchan, P., Limpijumnong, S. and Van de Walle, C. G. (2008). Mutual Passivation of Electrically Active and Isovalent Impurities in Dilute Nitrides. *Physical Review Letters*, **100**, 045505-1-4.
- [98] Rogers, F. J., Graboske, H. C. Jr. and Harwood, D. J. (1970). Bound Eigenstates of the Static Screened Coulomb Potential. *Physical Review A*, **1**, 1577-1586.
- [99] Lam, C. S. and Varshni, Y. P. (1971). Energies of s Eigenstates in a Static Screened Coulomb Potential. *Physical Review A*, **4**, 1875-1881.
- [100] McEnnan, J., Kissel, L. and Pratt, R. H. (1976). Analytic perturbation theory for screened Coulomb potentials: Nonrelativistic case. *Physical Review A*, **13**, 532-559.
- [101] Patil, S. H. (1984). Energy levels of screened Coulomb and Hulthén potentials. *Journal of Physics A: Mathematical and General*, **17**, 575-593.
- [102] Yukalov, V. I., Yukalova, E. P. and Oliveria, F. A. (1998). Renormalization-group solutions for Yukawa potential. *Journal of Physics A: Mathematical and General*, **31**, 4337-4348.

- [103] Chatterjee, A. (1986). $1/N$ expansion for the Yukawa potential revisited: II. *Journal of Physics A: Mathematical and General*, **19**, 3707-3710.
- [104] Lee, C. (2000). *Physics Letters A*, **267**, 101-108.
- [105] Chakrabarti, B. and Das, T. K. (2001). Analytic superpotential for Yukawa potential by perturbation of the Riccati equation. *Physics Letters A*, **285**, 11-16.
- [106] Gönül, B. (2004). Exact Treatment of $\ell \neq 0$ States. *Chinese Physics Letters*, **21**, 1685-1688.
- [107] Gönül, B., Köksal, K. and Bakır, E. (2006). An alternative treatment for Yukawa-type potentials. *Physica Scripta*, **73**, 279-283.
- [108] Cooper, F., Khare, A. and Sukhatme, U. P. (1995). Supersymmetry and Quantum Mechanics. *Physics Reports*, **251**, 267-385
- [109] Sze, S. M. (1981). *Physics of Semiconductor Devices*, (Wiley, New York, 1981) 2. Edition
- [110] Harrison, P. (2005). *Quantum Wells, Wires and Dots*, (2nd ed.). New York: Wiley.
- [111] Wu, J., Walukiewicz, W. and Haller E. E. (2001). Calculation of the ground state of shallow donors in $\text{GaAs}_{1-x}\text{N}_x$. *Journal of Applied Physics*, **89**, 789-791
- [112] Chadi, D. J. and Cohen, M. L. (1974). Correlation between the static dielectric constant and the minimum energy gap. *Physics Letters A*, **49**, 381-382
- [113] Kwon, Y. D. (2006). Theory of the screened Coulomb field generated by impurity ions in semiconductors. *Physical Review B*, **73**, 165210-1-9.
- [114] Koumetz, S. D., Pesant, J. C. and Dubois, C. (2008). A computational study of ion-implanted beryllium diffusion in gallium arsenide. *Computational Materials Science*, **43**, 902-908.
- [115] Singh, J. (2003). *Electronic and Optoelectronic Properties of Semiconductor Structures*. Cambridge: Cambridge University Press.
- [116] Kitatani, T., Kondow M., Shinoda K., Yazawa Y. and Okai M. (1998). Characterization of the Refractive Index of Strained GaInNAs Layers by Spectroscopic Ellipsometry. *Japanese Journal of Applied Physics*, **37**, 753-757.
- [117] Sato, S., Osawa Y. and Saitoh T. (1997). Room-Temperature Operation of GaInNAs/GaInP Double-Heterostructure Laser Diodes Grown by Metalorganic Chemical Vapor Deposition. *Japanese Journal of Applied Physics*, **36**, 2671-2675.

- [118] Li, P. W., Guang H. C. and Li N. Y. (2000). Ellipsometric Study of the Optical Properties of InGaAsN Layers. *Japanese Journal of Applied Physics*, **39**, L898-L900.
- [119] Casey, Jr. H. C., Panish, M. B., Schlosser, W. O. and Paoli, T. L. (1974). GaAs-Al_xGa_{1-x}As heterostructure laser with separate optical and carrier confinement. *Journal of Applied Physics*, **45**, 322-333.
- [120] Jin, S. R. (2003). Wavelength dependence of the modal refractive index in 1.3 μm InGaAsP, AlGaInAs and GaInNAs lasers using high pressure. *Physica Status Solidi (b)*, **235**, 491-495.
- [121] Anderson, W. W. (1965). Mode confinement and gain in junction lasers. *IEEE Journal of Quantum Electronics*, **1**, 228-236.
- [122] Hakki, B.W. and Paoli, T.L. (1975). Gain spectra in GaAs double-heterostructure injection lasers. *Journal of Applied Physics*, **46**, 1299-1307.
- [123] Botez, D. (1978). Analytical approximation of the radiation confinement factor for the TE mode of a double heterojunction laser. *IEEE Journal of Quantum Electronics*, **14**, 230-232
- [124] Gönül, B., Köksal, K. and Bakır, E. (2006). Comparison of the band alignment of strained and strain-compensated GaInNAs QWs on GaAs and InP substrates. *Physica E*, **31**, 148-154.
- [125] Gönül, B., Bakır, E. and Köksal, K. (2006). Analysis of the band alignment of highly strained indium-rich GaInNAs QWs on InP substrates. *Semiconductor Science and Technology*, **21**, 876-880.
- [126] Loehr, J. P. (1998). *Physics of Strained Quantum Well Lasers*. London: Kluwer Academic Publishers.
- [127] Tomic, S., O'Reilly, E. P., Fehse, R., Sweeney, S. J., Adam, A. R., Andreev, A. D., Choulis, S. A., Hosea, T. J. C. and Riechert, H. (2003). Theoretical and experimental analysis of 1.3-μm InGaAsN/GaAs lasers. *IEEE Journal of Selected Topics in Quantum Electronics*, **9**, 1228-1238.
- [128] Skierbiszewski, C. (2002). Experimental studies of the conduction-band structure of GaInNAs alloys. *Semiconductor Science and Technology*, **17**, 803-814.
- [129] Skierbiszewski, C., Perlin, P., Wisniewski, P., Knap, W., Suski, T., Walukiewicz, W., Shan, W., Yu, K. M., Ager, J. W., Haller, E. E., Geisz, J. F. and Olson, J. M (2000). Large, nitrogen-induced increase of the electron effective mass in In_yGa_{1-y}N_xAs_{1-x}. *Applied Physics Letters*, **76**, 2409-2412.
- [130] Lindsay, A., Tomic, S., O'Reilly E. P. (2003). Derivation of a 10-band k-p model for dilute nitride semiconductors. *Solid state electronics*, **47**, 443-446.

CURRICULUM VITAE

The author was born in Istanbul, in January, 1980. He graduated from Süreyyapaşa Elementary and Secondary, Haydarpaşa Anatolian Technical Schools in Istanbul, in 1991, 1994, 1998, respectively. He received his B.S. degree in Engineering Physics Department from University of Gaziantep in January 2004. Then he has started his PhD program on solid state physics in Engineering Physics Department in University of Gaziantep in 2004. During the PhD, he was supported by TUBITAK. He is married.

PUBLICATIONS

- [1] Gönül, B., Köksal, K. and Bakir, E. (2006). Comparison of the band alignment of strained and strain-compensated GaInNAs QWs on GaAs and InP substrates. *Physica E*, **31**, 148-152.
- [2] Gönül, B., Bakir, E. and Köksal, K. (2006). Analysis of the band alignment of highly strained indium-rich GaInNAs QWs on InP substrates. *Semiconductor Science and Technology*, **21**, 876-879.
- [3] Gönül, B., Köksal, K. and Bakir, E. (2006). An alternative treatment for Yukawa-type potentials. *Physica Scripta*, **73**, 279-283.
- [4] Gönül, B. and Köksal, K. (2006). Equivalence of two alternative approaches to Schrödinger equations. *Physica Scripta*, **73**, 629-631.
- [5] Gönül, B. and Köksal, K. (2007). *Physica Scripta*, A search on the Nikiforov-Uvarov formalism. **75**, 686-690.
- [6] Gönül, B. and Köksal, K. (2007). Solutions for a generalized Woods-Saxon potential. *Physica Scripta*, **76**, 565-570.
- [7] Gönül, B., Köksal, K. and Bakir, E. (2007). A theoretical investigation of carrier and optical mode confinement in GaInNAs QWs on GaAs and InP substrates. *Physica Status Solidi C*, **4**, 671-673.
- [8] Gönül, B., Bakir, E. and Köksal, K. (2008). Two electrons in a quantum dot: a unified approach. *International Journal of Physics*, **4** (2008) 671-673.
- [9] Köksal, K., Gönül, B. and Oduncuoglu M. (2009). The critical layer thickness of InGaAsSb QWs on GaAs and InP substrates for (001) and (111) orientations, *European Physical Journal B*, **69**, 211-218.